TRIUMF

ANNUAL REPORT
SCIENTIFIC ACTIVITIES
2003

ISSN 1492-417X

CANADA'S NATIONAL LABORATORY
FOR PARTICLE AND NUCLEAR PHYSICS

OPERATED AS A JOINT VENTURE

MEMBERS:

THE UNIVERSITY OF ALBERTA
THE UNIVERSITY OF BRITISH COLUMBIA
CARLETON UNIVERSITY
SIMON FRASER UNIVERSITY
THE UNIVERSITY OF VICTORIA

ASSOCIATE MEMBERS:

THE UNIVERSITY OF GUELPH
THE UNIVERSITY OF MANITOBA
McMASTER UNIVERSITY
L'UNIVERSITÉ DE MONTRÉAL
QUEEN'S UNIVERSITY
THE UNIVERSITY OF REGINA
THE UNIVERSITY OF TORONTO

UNDER A CONTRIBUTION FROM THE
NATIONAL RESEARCH COUNCIL OF CANADA

DECEMBER 2004

The contributions on individual experiments in this report are outlines intended to demonstrate the extent of scientific activity at TRIUMF during the past year. The outlines are not publications and often contain preliminary results not intended, or not yet ready, for publication. Material from these reports should not be reproduced or quoted without permission from the authors.

Experiment 715
Weak interaction symmetries in β^+ decay of optically trapped ^{37,38m}K

(D. Melconian, SFU; J.A. Behr, M.R. Pearson, TRIUMF; K.P. Jackson, TRIUMF/SFU)

We present here an update on our progress in testing the standard model using optically trapped ^{38m}K and ^{37}K. The pure Fermi β^+ decay of ^{38m}K is a sensitive probe of scalar contributions to the weak interaction, while the decay of polarized ^{37}K can be used to search for right-handed currents and time-reversal symmetry violating interactions. The background and experimental set-ups for these experiments have been described elsewhere [TRIUMF 2002 Annual Report, p.34], so we provide here only a brief report on recent progress.

Status on the scalar search

A great deal of progress has been made in accurately understanding all possible sources of systematic error, and their effect on our measurement of the $\beta^+-\nu$ correlation parameter, $a_{\beta\nu}$. For example, by careful comparison of our three measurements of the electric field (fastest recoil TOF, fastest "wrong-way" recoil TOF, and photoionized atoms) we can now constrain our field nonlinearity to be less than 1.0 V/cm/cm and the resulting error in $a_{\beta\nu}$ to be <0.0011. We can also constrain the angle dependence of the efficiency of the microchannel plate and assign an error of 0.0008 to this effect.

Our experiment can uniquely constrain one potential source of systematic error from the atomic physics. Dependence of the probability of electron shakeoff on the recoil ion energy has been demonstrated in ^{6}He β^- decay [Carlson *et al.*, Phys. Rev. **129**, 2220 (1963)]. A recent simple atomic physics calculation relates this effect to atomic oscillator strengths and suggests that it could be larger in β^+ decay [Scielzo *et al.*, Phys. Rev. **A68**, 022716 (2003)]. The recoil energy spectrum to lowest order is distorted by $(1+sE_{\rm rec})$. We are able to constrain this effect experimentally by fitting s and $a_{\beta\nu}$ simultaneously in our TOF[E_β] fit for $Ar^{+1,+2,+3}$. We only include s in the Ar^{+1} spectrum because the model suggests that s for Ar^{+2} (or Ar^{+3}) would be 0.11 (or 0.05) the size of s for Ar^{+1}. We find $s = 0.007 \pm 0.017$, producing a change in $a_{\beta\nu}$ of 0.0002 ± 0.0020. A similar simultaneous fit to Ar^{+1} using our reconstructed angular distribution gives consistent result and error (see Fig. 43). We can constrain s and $a_{\beta\nu}$ simultaneously because the greatest sensitivity to $a_{\beta\nu}$ is at the null in the angular distribution, and because we fit as a function of E_β. A fit to the total TOF spectrum summed over all E_β would be more strongly correlated to the recoil momentum spectrum.

We have gone through our error budget in a similar fashion and have determined all systematic effects on $a_{\beta\nu}$. The plastic scintillator energy calibration is the one last source of systematic error we have yet to thoroughly define. Once this is done, the analysis will be completed. Alexandre Gorelov presented a preliminary result at the DNP03 meeting in Tucson: $\tilde{a}_{\beta\nu} \equiv a/(1 + b_F \Gamma m_e/E_\beta) = 0.9978 \pm 0.0030(\text{stat}) \pm 0.0045(\text{syst})$.

Polarized measurements

We continue to analyze the data set of our experiment on the decay of polarized ^{37}K taken in the fall of 2002. The results, described below, include an atomic measurement of the polarization and a 3% measurement of the neutrino asymmetry. We have also made very preliminary measurements of the D coefficient and an observable we call $R_{\rm slow}$, which will require greater statistical accuracy to be competitive.

Our measurement cycle starts by accumulating and confining ≈2000 radioactive ($T_{1/2}$ = 1.23 s) ^{37}K in a magneto-optic trap (MOT). The MOT provides a

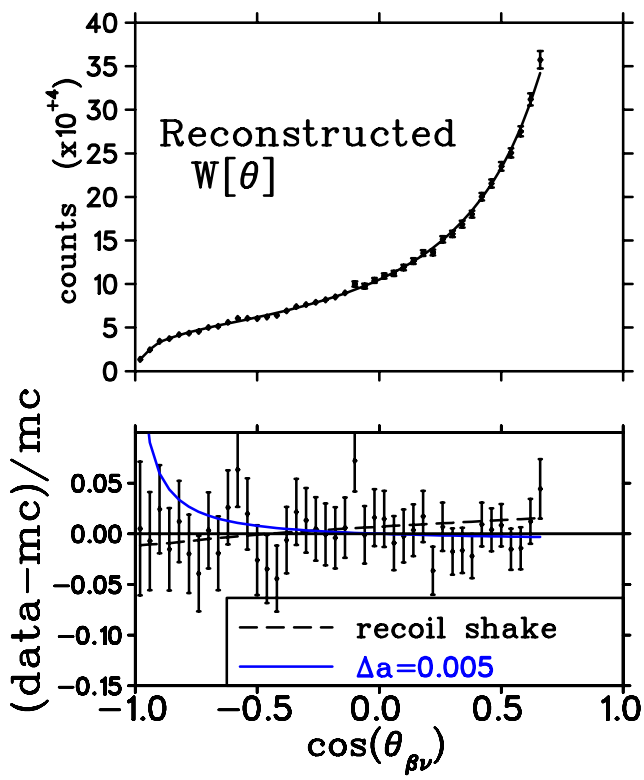

Fig. 43. Constraint of the recoil shake-off dependence on its momentum. The top plot shows the reconstructed angular distribution and comparison to a MC simulation. The lower plot shows the effect of a 0.5% change in $a_{\beta\nu}$ from the fit value, and the effect of a change in recoil shake-off dependence of $s = 0.03$ (the size predicted by Scielzo *et al.*). The functional dependence is quite different, so we can constrain both effects simultaneously.

nearly ideal source of atoms. They are well-localized in space ($\sim$1 mm^3) and are cold enough ($\sim$1 mK) to have a negligible contribution to the recoil momentum spread. The β^+ and daughter recoil freely escape the shallow trap with negligible perturbations to their momenta. We have shown from β asymmetry measurements that the MOT completely depolarizes the atoms, so we turn the MOT off and use optical pumping techniques to highly polarize the atoms. We make our nuclear measurement during the time the MOT is off, and so the cloud of atoms is expanding due to their small (yet finite) thermal motion. Therefore, we turn off the optical pumping after 1.4 ms and reactivate the MOT in order to re-trap atoms that have not decayed, and then we start the cycle again.

Atomic measurement of the polarization An important aspect of our polarized experiment is that we can measure the atom cloud polarization *in situ* and *non-destructively* using atomic techniques. We use a pulsed 355 nm laser which only photoionizes atoms from the excited $4P_{1/2}$ state. The resulting ^{37}K$^+$ ions are collected by the electric field and detected by the MCP detector. The photoions not only serve to image the cloud of atoms, but also provide an extremely sensitive and clean measure of the excited state population, which is directly proportional to the fluorescence. This is a much cleaner method than looking for the fluorescence directly, because our geometry is optimized for particle (not light) collection efficiency, and we can use the TOF and position information to minimize and correct for the background from β decays.

Atoms that are fully polarized can no longer absorb the optical pumping light (because there is no higher $m_{F'}$ level to get excited to), so the degree to which the fluorescence vanishes is related to the polarization. This relationship has been modelled using the rate equations and we can fit the decay of the fluorescence as a function of the optical pumping time to deduce the polarization. This is shown in the left panel of Fig. 44. The background (dashed line) is determined from events which do not hit the MCP in the same place as the photoions. The right panel of Fig. 44 shows the χ^2 map for various values of the nuclear polarization input into the model. The results are consistent for σ^+ and σ^- light, and average to $\langle P\rangle = 0.965\pm0.004$. To account for the model dependence of the deduced polarization, we assign a systematic uncertainty of 1.5% so that the nuclear polarization is determined to be $P = (96.5 \pm 1.5)\%$.

Angular correlations: B_ν and D The β-telescope and MCP recoil detectors are very well understood from the in-depth analysis done in extracting our value of $\tilde{a}_{\beta\nu}$. Considering the kinematics of the decay of ^{37}K polarized perpendicular to the telescope-MCP detection axis, one can show that the recoil asymmetry, apparent as an asymmetry in the $\hat{x}$ direction, is directly related to the neutrino asymmetry, B_ν. Thus using the polarization deduced from the photoion data and analyzing the position dependence of the clean $\beta-$Ar coincidences, we can measure B_ν. The data (points) and fit to a detailed MC simulation (line) of projections of the MCP position spectrum are shown in the top panel of Fig. 45. The bottom panel shows the asymmetries in $\hat{x}$ (left) and $\hat{y}$ (right), which are proportional to PB_ν and PD, respectively.

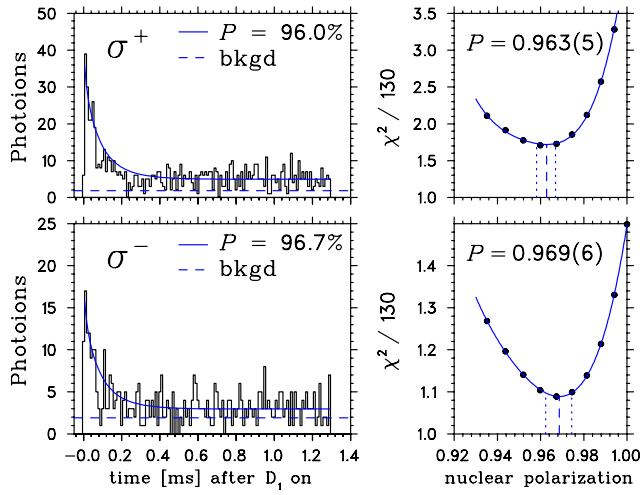

Fig. 44. Fit of the vanishing of the fluorescence for various values of the nuclear polarization for $\sigma^\pm$ (left) and the χ^2 map (right) whose minima yield $\langle P_{\rm nucl}\rangle = 0.966 \pm 0.015$.

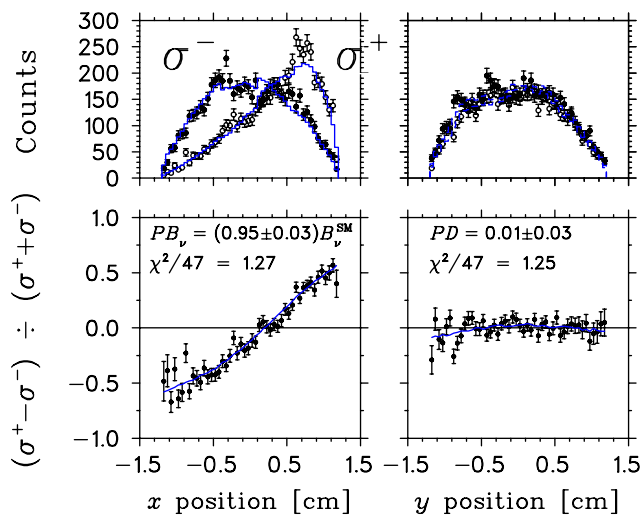

Fig. 45. MCP position spectra for $\beta-$Ar^{+1} coincidences in the back-to-back geometry. The polarization axis is along $\hat{x}$ and so the asymmetry along that direction is proportional to PB_ν. Shown is the data (points) and the fit to a MC simulation (solid line). A $\hat{y}$ asymmetry would arise from the time-reversal violating D term; we do not see an asymmetry and so we limit D to be less than 0.04.

We obtain SM predictions for the correlation parameters based on the measured value of the ratio of matrix elements, $\lambda \equiv g_V M_F / g_A M_{GT} = -0.5754(16)$ [Hagberg, private communication; Ball, private communication]. The result of fitting the $\hat{x}$ asymmetry and dividing out the measured nuclear polarization is $B_\nu = (0.986 \pm 0.029)\ B_\nu^{\rm SM} = -0.758 \pm 0.022$, with analysis on systematic effects ongoing (see below and Table V). Similarly, by fitting the $\hat{y}$ asymmetry (or lack thereof), we can search for a non-zero D coefficient which violates time-reversal symmetry; final state effects which mimic T-violating interactions have been estimated [Holstein, Phys. Rev. **C5**, 1529 (1972)] and should be half as large as those in ^{19}Ne which measured $D < 1.6 \times 10^{-3}$ (90% CL) [Hallin *et al.*, Phys. Rev. Lett. **52**, 337 (1984)]. Our result, currently limited by statistics, is $D < 0.06$ (90% CL).

We have investigated a few of the larger systematic effects in the polarized experiment, the results of which are listed in Table V. The two most significant sources are from the atomic measurement of the polarization, and the position of the thermally expanding cloud of atoms. Upon turning off the magnetic field for trapping the atoms, the cloud centroid changes. This is difficult to characterize because the photoion techniques are effective on trapped atoms, but are relatively poor on the optically pumped atomic cloud. Instead we probe the polarized atom cloud position by varying its input to the MC and making χ^2 maps of the resulting fits to the projections in the top panel of Fig. 45. This gave an $\hat{x} - \hat{y}$ centroid with ± 0.5 mm uncertainty. The variation in the fit to PB_ν over this same range gives us the systematic uncertainty due to the cloud position: $\delta(PB_\nu) = \pm 0.012$. In the same manner, we estimate for each source listed in Table V the systematic uncertainty on our $B_\nu = -0.758$ measurement.

Our measurement of the ν asymmetry is in agreement with the standard model value of $B_\nu^{\rm SM} = -0.7564(15)$ and so we interpret our result as a limit.

Table V. Error budget for the neutrino asymmetry measurement. We are still in the process of identifying additional systematic sources and assigning their systematic uncertainty.

Source of uncertainty	δB_ν
Statistical	0.022
Polarization	0.015
Direction of OP axis	0.002
Cloud $\hat{x} - \hat{y}$ position	0.012
Cloud size	0.003
MCP position efficiency	0.001
Others (in progress)	–
Systematic	$\gtrsim 0.020$
Total	$\gtrsim 0.030$

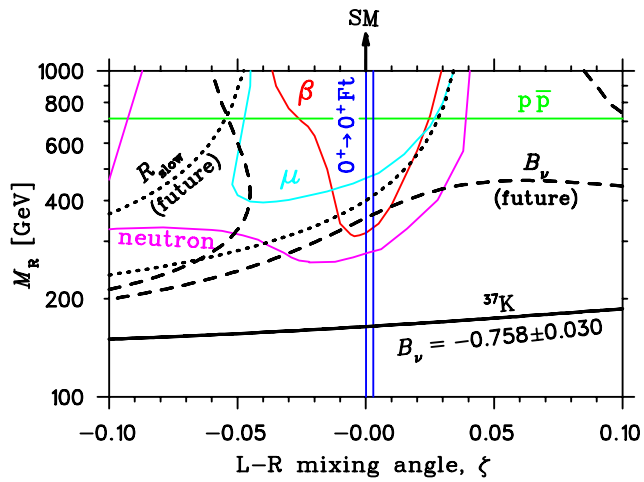

Fig. 46. 90% confidence level limits on the right-handed current parameters M_R and ζ in the manifest left-right symmetric model, including our ν asymmetry measurement. Also shown as dashed (dotted) lines are the limits obtained with measurements of B_ν ($R_{\rm slow}$) with an accuracy of $\sigma = 0.001$.

A comparison of our 90% CL limit to other experiments that constrain right-handed currents in the manifest left-right symmetric models is given in Fig. 46. In the standard model, there is no right-handed boson, so these limits exclude regions of lower M_R and finite mixing angle, ζ. Our result excludes right-handed masses of <150 GeV/c^2. Shown as a dashed line is the limit one would obtain with a $\sigma_{B_\nu} = 0.001$ measurement in agreement with the SM.

As described in last year's Annual Report, we have added two phoswich β detectors along the optical pumping axis with the intent of measuring the β asymmetry. The β singles measurement was found to have unacceptably large backgrounds due to atoms implanting and depolarizing on the mirrors in front of the phoswiches. However, by requiring a recoil coincidence with the MCP, we obtain clean spectra of polarized atoms that decayed directly from the optically pumped cloud. The physics that can be extracted from such correlations is discussed below.

Angular correlations continued: $R_{\rm slow}$ The geometry of the phoswich and MCP detectors, depicted in Fig. 47, is such that fast Ar$^+$ recoil events are supressed because the electric field of -810 V/cm is not large enough to significantly alter the ion trajectory, so recoils with large momenta along $-\hat{x}$ will miss the MCP. For slow recoils, however, the field is able to focus the ions within the active area of the MCP. In this way, the kinematics and geometry of these events help to pick out slow recoil events. In the purely back-to-back geometry depicted in Fig. 47, this translates to events where the β alone goes along $\hat{x}$ into the phoswich, while the ν and recoil are both emitted in the opposite

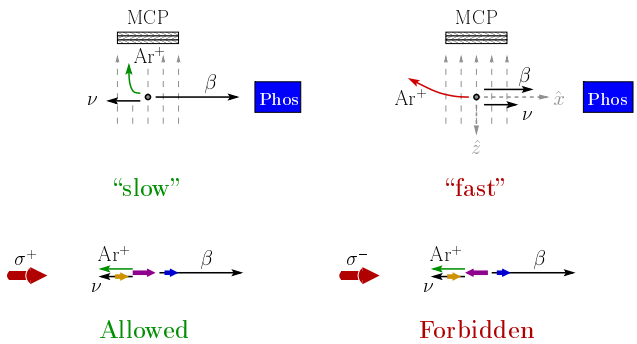

Fig. 47. Geometry (not to scale) and kinematics of phoswich-MCP coincidences. The top panel depicts how the experimental set-up and kinematics of the decay accept slow recoils, while fast Ar^+ will not fire the MCP. The bottom panel shows how angular momentum can only be conserved for the slow recoils if the initial nuclear spin is aligned with the β direction.

direction. In reality, however, the Ar^+ and ν are not constrained to be along $-\hat{x}$ and the differentiation of fast to slow recoils becomes less precise. We have shown that we can enhance selectivity of slow recoils based on the TOF. At the present time with current statistics this cut is not practical, however, this can be employed in the future when we have more events.

Continuing to consider the back-to-back geometry for simplicity, it is easy to show that helicity arguments require that, for a purely $V-A$ interaction, the initial nuclear spin of the ^{37}K must be aligned with the β direction. If it were opposite, the initial spin projection of $m_I = -I$ could not equal the sum of the final state spins: $m_{I'} + m_{\text{leptons}} = m_{I'} + 1 > m_I$. We therefore define a vanishing observable, R_{slow}, to be the ratio of phoswich-MCP coincidences with $\hat{i} \cdot \hat{p}_\beta = -1$ over $\hat{i} \cdot \hat{p}_\beta = +1$. We measure R_{slow} by looking at the $\hat{x}$-MCP asymmetry as per the B_ν measurement, except this time requiring that a β fired the phoswich detector instead of the (back-to-back) β-telescope.

Noting that the lepton spins are aligned in back-to-back decay, one can see that the Fermi component (i.e. where $a_{\beta\nu} = +1$) of this mixed F/GT decay is supressed. To the extent that we measure only slow recoils, the Gamow-Teller part of the decay is singled out, making us much less sensitive to the value of λ. The dependence of R_{slow} on right-handed current (RHC) parameters goes like $(\delta + \zeta)^2$, where $\delta \equiv (M_L/M_R)^2$. This can be understood by considering how a $V+A$ interaction couples to left-handed neutrinos: 1) directly through a new right-handed boson exchange, or 2) weak eigenstate mixing of the left- and right-handed bosons. In the first case, the matrix element with a W_R exchange is supressed relative to the W_L by the $1/M_W^2$ mass-dependence of the propagator, resulting in a M_L^2/M_R^2 dependence. For the second case, the mixing goes like $\sin\zeta$ which, for small admixtures, is linear in ζ. The overall probability of having a right-handed current goes like the square of the sum of these two terms, namely $(\delta + \zeta)^2$.

The R_{slow} observable is therefore a sensitive probe of the RHC parameters and will depend only weakly on the accuracy of the measurement of λ. The drawback is in the number of events: there are approximately 4 times fewer events than our B_ν measurement due to kinematics and detector acceptances, and so R_{slow} is highly statistics limited. Our current data set yields a 10% measurement of the $\hat{x}_{\text{MCP}}$-asymmetry which translates into roughly similar limits as obtained by the 3% measurement of B_ν. We plan to continue analyzing this observable, in particular checking how much sensitivity can be gained by making the additional TOF cut to help pick slow recoil events.

These preliminary results are quite promising, and we expect to be able to make great improvements by resolving some simple detector problems and utilizing increased yield expected not only from ISAC, but also from the MBR laser upgrade described below.

Experiment 956 developments

Experiment 956, limits on tensor interactions from recoil singles spin asymmetry, has had experimental planning progress. This observable vanishes for Gamow-Teller transitions in the absence of tensor interactions, so our present level of polarization is more than good enough to make a competitive measurement.

We have realized that a coincidence between γ-ray and recoil will still produce a vanishing observable, but make the experiment cleaner as well as give the recoil momentum dependence. We are pursuing this with a plan to make a measurement in ^{80}Rb as an M.Sc. project.

Experiment 925 developments

Initial tests of Expt. 925, isospin mixing in ^{36}Ar from polarized observables in ^{36}K decay, form the bulk of Ofer Aviv's M.Sc. thesis, Tel Aviv University. Modelling of the rather complex recoil TOF spectrum to explore sensitivity to $a_{\beta\nu}$ is proceeding well. The higher-energy 9.8 MeV β^+ Q-value produces higher-momentum neutral recoils than ^{37}K, and the MCP detects them with good efficiency, a surprising result. Plans on completing the hyperfine splitting and quadrupole moment measurement are proceeding.

Off-line developments

We have moved the contents of the TRINAT off-line lab in the main office building to the on-line lab.

MOPA efficiency We have improved the output power from our tapered amplifier system by placing one of the frequency-shifting AOM's before it instead

of after it. There is still sufficient pump power to saturate the tapered amplifier.

MBR-110 upgrade After much effort, we were unable to adapt the lower-model MBR-PE ring laser to frequency lock it to a potassium line. The design, which replaces the 899-21 thick and thin etalons with a single higher-finesse etalon, requires very subtle control of that etalon with multiple feedback loops. We are commercially upgrading the unit to a full MBR-110. We can project that this will increase the number of trapped atoms by a factor of three.

CFORT On the polarization front, we are working to develop a circularly-polarized far-off resonance trap (CFORT) which promises extremely high polarizations because only the $M_F = F$ state is trapped and all others are repelled. It is expected that we can achieve >99.9% polarization. This type of trap was developed and loaded efficiently with Rb atoms by JILA [Miller *et al.*, Phys. Rev. **A66**, 023406 (2002)]. Adapting this to our requirements and to potassium atoms is the M.Sc. project of Erika Prime. A ring laser adapted from an existing standing-wave cavity will provide the light for the trap. We have characterized this laser to have very good spatial mode quality.

405 nm probe We hope to use the 405 nm laser to measure the magnetic sublevel populations directly by scanning our laser over the Zeeman-shifted transition frequencies. This is necessary to further calibrate the measurement of the vanishing of fluorescence to remove its model dependence, and also allow the measurement of the tensor alignment term in addition to the vector polarization. The 405 nm diode laser is presently limited by its frequency linewidth. In the meantime, we have measured the specific mass isotope shift of the potassium $5P_{1/2}$ state between stable ^{39}K and ^{41}K atoms. In the probing, we can distinguish between $4P$ and $5P$ populations because our 532 nm pulsed laser can only photoionize the latter. As part of this effort, we are measuring the absolute photoionization cross section of the $5P_{1/2}$ state as the senior thesis project of Lorraine Courneyea at UBC.

Photoionization If we are able to photoionize atoms directly from the ground state, we would be able to sensitively probe the cloud expansion once the MOT is off and the atoms are fully optically pumped. Presently the photoions vanish as the atoms polarize and so we have very weak statistics on the cloud parameters (size, position, temperature). Photoionization from the ground state, though destructive, could be used to image both the trapped *and* untrapped atoms.

Coherent population trapping Coherent population trapping is a subtle quantum mechanical interference effect in the laser-atom system that could in principle limit polarization from optical pumping. Atoms can be stalled in a dark superposition of sublevels. Our work on creation and destruction of this effect in our apparatus has now been published [Gu *et al.*, Optics Comm. **220**, 365 (2003); *ibid.*, Phys. Rev. **A68**, 015804 (2003)].

Experiment 744
A kinematically complete study of $\pi^- p \rightarrow e^+ e^- n$
(M.A. Kovash, Kentucky)

TRIUMF Expt. 744 is a kinematically complete study of the inverse pion photoproduction reaction, $\pi^- p \rightarrow e^+ e^- n$. In the one photon exchange approximation this proceeds through the production and decay of a single virtual photon. In the low-energy region the amplitudes for the generalized process of charged pion photoproduction include the well-known contact Kroll-Ruderman interaction which is determined by gauge invariance at threshold, and which dominates the near-threshold region for real photons. An analogous set of diagrams also contributes to the yield of virtual photons in radiative pair production, although at values of $q^2 \neq 0$. A description of this process in terms of Feynman amplitudes then uses form factors to describe the coupling of the virtual photon to the hadrons. It is the Kroll-Ruderman term, through the combined requirements of gauge invariance and PCAC, which is sensitive to the nucleon axial and pseudoscalar form factors, G_A and G_P. Radiative pair production thus offers a *unique* opportunity to probe the axial structure of the nucleon at small time-like values of q^2.

As in the case of pion electroproduction, the hadronic component of the cross section for radiative pair production is of the general form

$$\frac{d\sigma_{\gamma^*}}{d\Omega} = \frac{d\sigma_T}{d\Omega} + |\epsilon|\frac{d\sigma_L}{d\Omega} + A\epsilon cos(2\phi) + B\sqrt{\frac{|\epsilon|(1+\epsilon)}{2}} cos(\phi)\,.$$

The kinematic variables are the polar angle of the virtual photon, the azimuthal angle between the leptonic and hadronic planes, and the photon polarization. The various terms in this equation are the transverse and longitudinal cross sections, and the transverse-transverse and transverse-longitudinal interference cross sections. The ϕ and ϵ dependences shown in this equation can be exploited to experimentally determine the individual response functions. For example, the ϕ-averaged cross section contains only the longitudinal and transverse components, which are themselves individually determined via the usual Rosenbluth separation. Conversely, a harmonic analysis of the azimuthal dependence of the measured cross section allows one to determine

the transverse-transverse and longitudinal-transverse interference terms from the data. Of course, to do this decomposition requires knowledge of the variables $(\theta_\gamma, \phi_\gamma, \epsilon_\gamma)$ for each event.

We study the reaction $\pi^- p \rightarrow e^+e^-n$ using the RMC pair spectrometer to detect the e^+e^- pairs. The pion beam enters the detector along the axial field lines (with $B = 2.4$ kG) and interacts with the liquid hydrogen target at the detector centre. The target is surrounded by an array of inner scintillators (A, A′), and the 12-segment C scintillator array. The e^+e^- pairs are tracked from the target through a dual-coordinate inner wire chamber (IWC) providing both z and azimuthal coordinates of the hits. The IWC is surrounded by a large-volume 4-layer drift chamber. Layers 1, 2 and 4 provide both x and y track coordinates. The wires in the third chamber have a 7° stereo angle with respect to the drift chamber axis, with which the z position of the track crossing can be determined. An outer layer of scintillators (D) is segmented into 16 sectors and provides a second component of the hardware trigger for e^+e^- events.

Study of the reaction $\pi^- p \rightarrow e^+e^-n$ requires that both the electron and positron momentum vectors are determined at their point of origination in the target. From this information the five kinematic variables which characterize this 3-body final state can be determined: the photon mass, its polarization, and its polar angle of emission, as well as the angle between the e^+e^- plane and the plane containing the virtual photon and recoil neutron. The trajectories are individually recorded in the IWC and drift chambers. From these hit positions the tracking algorithm determines the magnitudes of the individual momenta and the coordinates of the centres of the helical trajectories.

During the summer we collected first production data for the capture in flight of 160 MeV/c pions in a liquid hydrogen target, using the RMC spectrometer to detect the e^+e^- pairs. For each event, the 3-momentum of each lepton was determined from the measured track direction and curvature, thus defining the energy, momentum and polarization of the virtual photon as well as its polar and azimuthal angles of emission. The large angular coverage of the RMC detector ($\Omega \sim 3\pi$) provides us with excellent acceptance for e^+e^- pairs emitted from photons produced at all angles.

Unfortunately, at about the mid-point of the data collection the power connections to the first quadrupole magnet on the M9A channel failed and the run had to be terminated. This equipment has been repaired and the final production run has been tentatively scheduled for the summer of 2004. In the meantime, the data from the 2003 run are being analyzed in Kentucky.

Experiment 766
The ortho-para transition rate in muonic molecular hydrogen
(D. Armstrong, College of William & Mary)

Muon capture has long been recognized as a useful probe of the semileptonic weak interaction. The elusive pseudoscalar coupling g_p for the proton, in particular, can be measured using μ^- capture. While the theoretical expectation for the value of g_p appears robust (chiral perturbation theory results match the older current algebra predictions), the experimental situation is not as clear. The two most recent and most precise measurements for the proton appear to disagree with each other significantly. The radiative muon capture (RMC) experiment (TRIUMF Expt. 452) [Wright *et al.*, Phys. Rev. **C57**, 373 (1998)] yields a much larger value for g_p than does the late-1970s measurement from Saclay [Bardin *et al.*, Phys. Lett. **104B**, 320 (1981)], which used ordinary, non-radiative muon capture (OMC). However, both experiments used liquid hydrogen targets, and their interpretation in terms of weak couplings requires knowledge of the relative population of the muonic atomic and molecular states. In particular, λ_{op}, the transition rate between the ortho and para states of the $p\mu p$ molecule needs to be known with precision. The extracted value of g_p is changed drastically (especially for the case of the OMC experiment) depending on the value of λ_{op} assumed – see Fig. 48.

The $p\mu p$ molecule is formed almost entirely in the (excited) ortho-molecular state, and can (if the muon doesn't itself decay, or get absorbed by the proton) decay to the para-molecular ground state. This decay rate (λ_{op}) is expected to be rather slow; the best

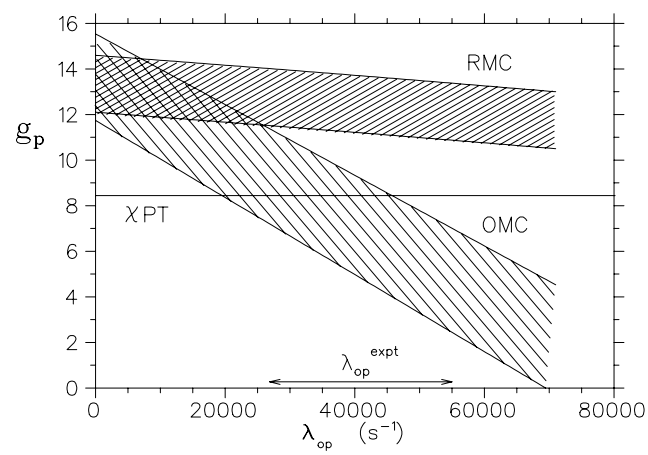

Fig. 48. The pseudoscalar coupling g_p from radiative (RMC) and ordinary (OMC) muon capture experiments vs. λ_{op}. The chiral perturbation theory (χPT) prediction for g_p is indicated. The horizontal arrows indicate the single previous measurement of λ_{op}.

theoretical prediction $\lambda_{op} = (7.1 \pm 1.2) \times 10^4$ s^{-1} [Bakalov *et al.*, Nucl. Phys. **A384**, 302 (1982)] is not in good agreement with the only previous measurement which yielded [Bardin *et al., op. cit.*] $\lambda_{op} = (4.1 \pm 1.4) \times 10^4$ s^{-1}. Thus, a new measurement of λ_{op} is needed to resolve this dilemma.

Note that the RMC and OMC values could be reconciled if a sufficiently small value of λ_{op} is found (for example, they agree happily for $\lambda_{op} = 0$), however, this would imply serious problems with our theoretical understanding of g_p. Conversely, if λ_{op} is found to be significantly larger than the previous measurement, the RMC result would then be in reasonable agreement with theory for g_p, but doubt would be cast on the OMC result (OMC measurements previous to that of Bardin *et al.* had larger errors, and don't provide significant constraints on g_p).

Experimental technique

Our experiment accesses λ_{op} by measuring the time distribution of neutrons following μ^- capture in the target ($\mu^- + p \rightarrow \nu_\mu + n$). Due to the different combinations of hyperfine muonic atomic states that make up the ortho and para molecules, and the spin-dependence of the weak interaction, muon capture proceeds more rapidly from the ortho state ($\lambda_o \sim 600$ s^{-1}) than the para state ($\lambda_p \sim 200$ s^{-1}). Thus the time-dependence (relative to the arrival of the μ^- in the target) of the neutrons produced is not a simple exponential, but is modified by the ortho-para conversion. A fit to the time distribution allows λ_{op} to be extracted, and avoids the difficulty of determining the absolute neutron detection efficiency.

Five liquid scintillation detectors were used to detect the monoenergetic 5.2 MeV neutrons from μ^- capture on the proton. These detectors surrounded the liquid hydrogen target; the hydrogen is isotopically enriched protium to eliminate complications due to muon transfer to heavier isotopes. Plastic scintillators placed between the detectors and target allowed discrimination between neutrons and electrons from muon decay. Two independent levels of pulse-shape discrimination (PSD) in hardware and software were applied to separate neutrons from photons in the liquid scintillators. A pair of plastic scintillators in a telescope identified muons incident on the target.

The combination of TRIUMF's high duty factor and the use of multihit electronics allows us to avoid having to reject "pileup" muons. The arrival time was digitized for every muon arriving in a 32 μs window before the time of the neutron. Thus muon pileup causes a perfectly flat background to the time spectrum, and cannot cause a distortion to the time fit. Similarly, the (large) cyclotron-induced background of neutrons produced elsewhere than the target also creates a flat background, since they are uncorrelated with a muon passing through the beam scintillators.

Data were taken in two periods (June and November, 1999) for a total of 3 weeks of beam. The analysis of these data is nearing completion.

Results

The only backgrounds that can produce anything other than a flat contribution to the time spectrum are 1) muon capture on the target walls, 2) muons that pass through the beam telescope but fail to enter the target, and 3) photons from the target that either sneak through the PSD or produce real neutrons through (γ, n) reactions. The target walls are made of Au and Ag so μ^-s stopped there are rapidly captured, thus the background is eliminated by a cut rejecting the first ~500 ns of the time spectrum. The second background (primarily muon capture in the final beam scintillator) was measured via empty-target runs and found to be manageable. The final background was measured by separate runs with a μ^+ beam. The primary source of photons from the target (aside from muonic X-rays, which are rejected via a prompt timing cut) is from bremsstrahlung of decay electrons, so the background remains the same for a μ^+ beam while the signal (muon capture) disappears. Again, the background was found to be small.

The 5.2 MeV neutron signal from a typical liquid scintillator is shown in Fig. 49. Electron rejection and PSD cuts have been applied, and an out-of-time background subtraction has been performed. The characteristic "box" shape of the liquid scintillator response to a monoenergetic neutron is clearly seen. The time distribution of events in the correct energy window is shown in Fig. 50, after the 500 ns wall-background cut

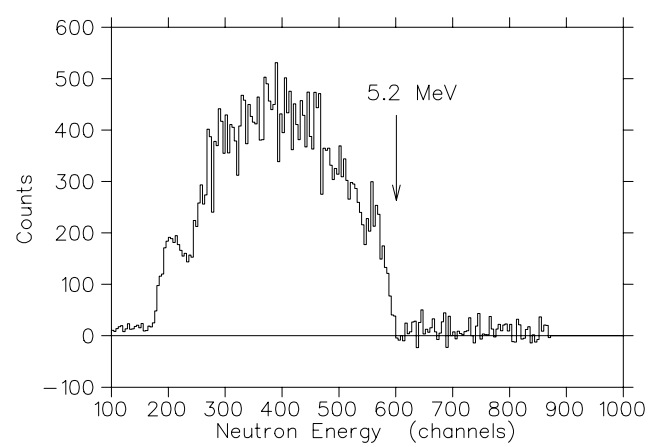

Fig. 49. Typical neutron energy spectrum, after neutron PSD cuts and subtraction of out-of-time background. The 5.2 MeV endpoint of the OMC neutron from hydrogen is indicated.

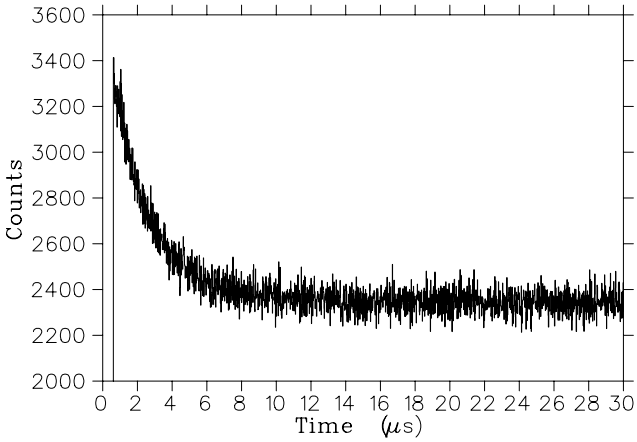

Fig. 50. Time spectrum of neutrons from μ^- capture on protium, after PSD, neutron energy, and wall-background cuts.

has been applied. The ~2 μs lifetime hydrogen muon capture component is seen, superimposed on a time-independent background, as described above.

Figure 51 shows the neutron time spectrum after the flat background is subtracted. For clarity, the muon decay lifetime has been divided out. Clear evidence of the ortho-para transition is seen. The extracted value of λ_{op} is not quoted here, pending completion of careful checks of the systematic errors; final results should be available in a few months. All indications are that the result will be sufficiently precise to have a major impact in resolving the dilemma in our knowledge of the proton's pseudoscalar coupling.

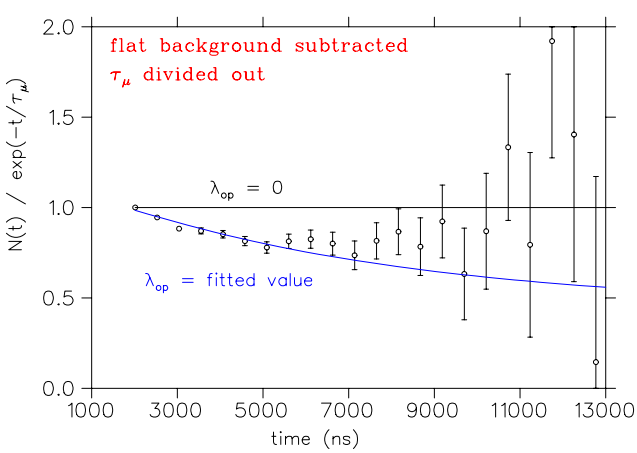

Fig. 51. Neutron time spectrum, with time-independent background subtracted, and the free muon lifetime divided out. A fit showing the functional form expected for a non-zero λ_{op} is shown, compared with the expectation for no ortho-para transfer.

Experiment 778
Pion proton cross sections in the Coulomb-nuclear interference region
(H. Denz, R. Meier, Tübingen; E.L. Mathie, Regina)

A number of quantities fundamental to the strong interaction, such as the πNN coupling constant and the sigma-term of the proton, may be extracted from pion nucleon phase shift analyses. The values of some of these quantities remain in dispute, due in part to the status of the πp database, in particular at low energies.

Cross section measurements at forward angles are typically problematic due to the overlap of scattered pions and muons arising from decays upstream. In addition the energy of recoil protons is such that they do not generally escape the target or survive out to the radius of detectors. Experiment 778 was specifically designed to determine differential cross sections of pion proton elastic scattering at low energies, in particular at small scattering angles in the so-called Coulomb-nuclear interference (CNI) region. This experiment is a complement to measurements of the πp analyzing power previously made in CHAOS Expt. 560, and recently in Expt. 862 (at higher energy).

This experiment received beam time in 1998 through 2000, using the CHAOS detector. In the interest of a well defined target thickness of high areal density protons, a planar liquid hydrogen target (developed at TRIUMF) was used. For each event, the incoming particle and the scattered pion were detected in CHAOS. The forward going proton, coincident with pions scattered to large angles, was also detected. In order to separate scattered pions at small angles from the beam halo of decay muons, forward going particles were tracked through the CHAOS wire chambers and then detected in an auxiliary detector array. A neural net, trained at each energy using multiple runs at different momenta with incident pion or muon triggers, was used to interpret the information from this array.

In total, data were taken for $\pi^{\pm}p$ differential cross sections at 8 energies between 15 and 67 MeV, in an angular range from 8° to 180°, with all of the low energy data obtained in M13 and the higher energy data obtained in M11. In earlier stages of the data analysis, the raw data (4.7 TB) were reduced by a factor of 10 by removing obvious decay events.

Enough disk space and computer power has been available at Tübingen to keep all of the remaining information for the M13 data sets on disk and to simultaneously analyze and simulate these data. In 2003 it became clear that the angular resolution was not sufficiently improved with tracking algorithms based upon GEANT to justify the factor of 10 penalty in analysis speed. A true 3D scattering angle determination was implemented. This is particularly important for

the forward angle results.

Studies of systematic effects, acceptance determinations and data analysis for the M13 data are virtually complete and final results for this important data set are expected in 2004. The simultaneous measurement of μp scattering with acceptances determined in the same Monte Carlo simulations gives an independent evalution of the normalization uncertainty. Preliminary results from the analysis of the larger angle data show generally good agreement of the shape of angular distributions with current phase shift analyses at the higher measured energies, but deviate at very backward angles and low energies, more so for π^+p than for π^-p.

Experiment 823
Pure Fermi decay in medium mass nuclei
(G.C. Ball, TRIUMF)

Precise measurements of the intensities for superallowed Fermi $0^+ \rightarrow 0^+$ β-decays have provided a demanding test of the CVC hypothesis at the level of 3×10^{-4} and also led to a result in disagreement with unitarity (at the 98% confidence level) for the CKM matrix. Since this would have profound implications for the minimal standard model, it is essential to address possible "trivial" explanations for this apparent non-unitarity, such as uncertainties in the theoretical isospin symmetry-breaking correction. Uncertainties in the calculated Coulomb corrections can be studied by extending the precision β-decay measurements to heavier ($A \geq 62$, $T_z = 0$) odd-odd nuclei where these corrections are predicted to be much larger [Towner and Hardy, Phys. Rev. **C66**, 035501 (2002)]. The primary goal of the Expt. 823 experimental program is to measure the half-lives and branching ratios for the superallowed β-decay of these radioactive nuclei produced at ISAC. The early measurements have focused on ^{74}Rb (see 1999–2002 Annual Reports).

High precision measurement of the half-life of the superallowed β-emitter ^{62}Ga

A preliminary measurement of the half-life of ^{62}Ga, the first in the series of ($A \geq 62$, $T_z = 0$) odd-odd superallowed β-emitters, was carried out in the spring. A ^{62}Ga beam of ~800/s was produced from the surface ion source using a ZrC target. Beam time was allotted near the end of the running period with this target for a preliminary half-life measurement for ^{62}Ga. By this time the target had deteriorated and the yield for the short-lived β-emitter ^{62}Ga had decreased by about a factor of 4. However, the yield was still sufficient to obtain a measurement of the half-life of ^{62}Ga with a precision of ~0.16%. The experiment was carried out at GPS1 using the fast tape transport system. Details of this method have been described previously (see 1999 Annual Report). A total of 50 runs each with a statistical uncertainty of ~1.5 ms was obtained. The results are shown in Fig. 52. The long-lived (9.74 m) isobar ^{62}Cu was a significant contaminant that limited the precision of these measurements. The ratio of ^{62}Ga/^{62}Cu was increased by about a factor of two by operating the mass separator in high-resolution (m/Δm ~5000) mode. However, this also resulted in a decrease in the intensity of ^{62}Ga and therefore resulted in no real gain in the precision that could be achieved in a reasonable length of time. A preliminary analysis of these data gives a value of 116.10 ± 0.19 ms. This result is statistically consistent with all three previous measurements: 115.95 ± 0.30 ms [Alburger, Phys. Rev. **C18**, 1875 (1978)], 116.34 ± 0.35 ms [Davids *et al.*, Phys. Rev. **C19**, 1463 (1979)], and 115.84 ± 0.25 ms [Hyman *et al.*, Phys. Rev. **C68**, 015501 (2003)]. It should be possible to substantially improve the precision of the present measurement to the required precision of 0.05% once the ISAC laser ion source is operational.

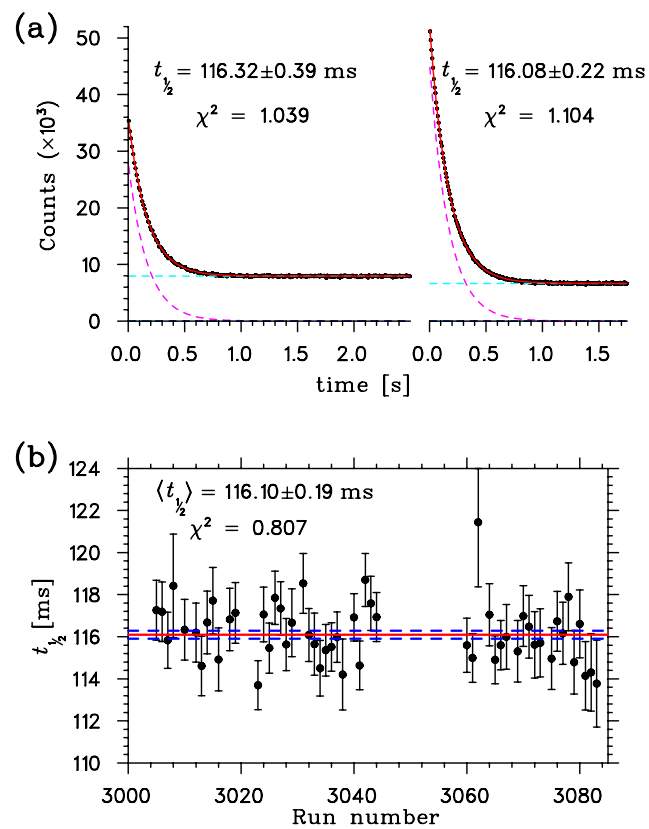

Fig. 52. a) Decay curves obtained for ^{62}Ga by summing and fitting the data obtained for all runs while operating the mass separator in low (left) and high (right) resolution modes; the long-lived background is ^{62}Cu and b) the half-life results obtained by fitting the data for each separately.

Measurement of the non-analogue $0^+ \rightarrow 0^+$ transition in ^{38m}K

The determination of the transition strengths for non-analogue $0^+ \rightarrow 0^+$ decays provides a critical test of the model predictions for superallowed β-decays. In particular, they provide a direct measurement of the isospin-mixing component of the Coulomb correction. Recently, Towner and Hardy [*op. cit.*] have recalculated the nucleus-dependent corrections for the nine well-known superallowed β-emitters for several shell model effective interactions. The values of the square of the Fermi matrix element (δ^1_{C1}) to the first excited 0^+ state in ^{38m}K range from 0.062 to 0.186%.

An experiment designed to measure this weak decay branch was carried out in October, 2002. The fast tape transport system was used to collect and move the ^{38m}K samples out of the vacuum chamber and position them between two thin plastic scintillator paddles each backed by a Compton suppressed (∼25%) HPGe detector from the 8π spectrometer. As a result, the sensitivity for detecting the 1209 keV γ-ray following the β-decay of ^{38m}K($t_{1/2} = 0.925$ s) to the first excited $0_2{}^+$ state in ^{38}Ar at 3377 keV was enhanced by the reduction in the background coming from the decay of the long-lived isobaric contaminant $^{38}K_{gs}$($t_{1/2} = 7.64$ min) which emits a 2168 keV γ-ray with a branching ratio of 99.8%. For more details see the 2002 Annual Report. The $^{38}K_{gs}$ contaminant was minimized by collecting the ^{38m}K samples for only 0.3 s. Unfortunately, with the ISAC TiC target used to produce the ^{38m}K beam, the yield of the short-lived ^{38m}K isomer was found to be two orders of magnitude smaller than the intensity of the long-lived $^{38}K_{gs}$. As a consequence, the ratio of the $^{38m}K/^{38}K_{gs}$ initial activities was only ∼4:1 and no γ-ray peak was observed at 1209 keV. Nevertheless, from a preliminary analysis of these data the upper limit for the non-analogue $0^+ \rightarrow 0^+$ decay was found to be <15–20 ppm at the 90% confidence level, corresponding to $\delta^1_{C1} < 0.22$–0.29%.

This experiment will be repeated using the full 8π spectrometer and SCEPTAR which will give an increased β-γ coincidence efficiency of a factor of 10 and substantially improved Compton suppression since the HPGe detectors will be a factor of two further away from the source. In addition, a Ta production target operating at ≥40 μA will be used since recent yield measurements have shown that the ratio of beam intensities for $^{38}K_{gs}/^{38m}$K is only ∼10:1.

Experiment 824

Further measurement of the rate of the ^{21}Na$(p,\gamma)^{22}$Mg reaction

(J.M. D'Auria, SFU, for the DRAGON Collaboration)

While the main goal of Expt. 824 was completed in 2002, nevertheless, it was of interest to continue studies of the astrophysically important ^{21}Na$(p,\gamma)^{22}$Mg reaction. As described in some detail in the 2002 TRIUMF Annual Report, this reaction plays an important role in the production of the radionuclide, ^{22}Na. This isotope with a lifetime of 3.77 years, emits a γ-ray of 1.274 MeV, which should be observable by present gamma-ray telescopes. In the NeNa nuclear reaction cycle that occurs during an ONe novae stellar explosion, there should be sufficient ^{22}Na produced for such an observation according to present models of such explosive scenario. Knowledge of the various reactions, and in particular the ^{21}Na$(p,\gamma)^{22}$Mg reaction, that play a role in this cycle is quite important as this isotope has not yet been observed.

Beam time was provided in 2003 to allow a more complete study of the rate of this reaction over a wider stellar temperature range. In fact the DRAGON facility was used to study this reaction from $E_{cm} = 200$ to 1103 keV, a range covering both novae and a significant part of X-ray bursts in exploding stars. Figure 53 shows our present understanding of the levels of ^{22}Mg based primarily upon studies performed here and/or by the TRIUMF-DRAGON group elsewhere.

As was described previously, the experiment was carried out at ISAC using DRAGON. A beam of pure ^{21}Na ($q = 5^+$) with intensities up to 1×10^9 s^{-1} was delivered to the DRAGON hydrogen gas target (∼4.6 torr). Incident beam energies were varied from ∼215 keV/u to ∼1.15 MeV/u to study directly radiative proton capture on states with $E_{cm} = 206$ keV to 1.101 MeV (see Fig. 53). As both the technique and some of these studies have been described in great detail elsewhere [Hutcheon *et al.*, Nucl. Instrum. Methods **A498**, 190 (2003); Bishop *et al.*, Phys. Rev. Lett. **90**, 162501 (2003); 2002 TRIUMF Annual Report; D'Auria *et al.* (submitted to Phys. Rev.)], only some of the results will be presented in this report.

Displayed in Fig. 54 are the ion energies observed with the DSSSD (double sided silicon strip detector) located at the focal plane of DRAGON. The incident ^{22}Na beam energy into the gas target was set to excite the level resonance at $E_{cm} = 738$ keV. This is a single spectra and switching on a coincidence with the prompt reaction gammas indicated that the few events above channel 2100 were due to beam pulses (leaky beam) transmitted through the separator. A total of 216 ^{22}Mg recoil events was observed for a total integrated beam on target of $1.67 \pm 0.07 \times 10^{12}$. The resulting thick target yield is $3.18 \pm 0.21_{stat} \pm 0.29_{syst} \times 10^{-10}$ per incident ^{21}Na ion, corresponding to a resonance strength, $\omega\gamma$, for the $E_{cm} = 738$ keV state in ^{22}Mg of $219 \pm 15_{stat} \pm 20_{syst}$ meV. The measured stopping cross section of ^{21}Na energies was determined as $8.74 \pm 0.39 \times 10^{-14}$ eV/(atom/cm^2).

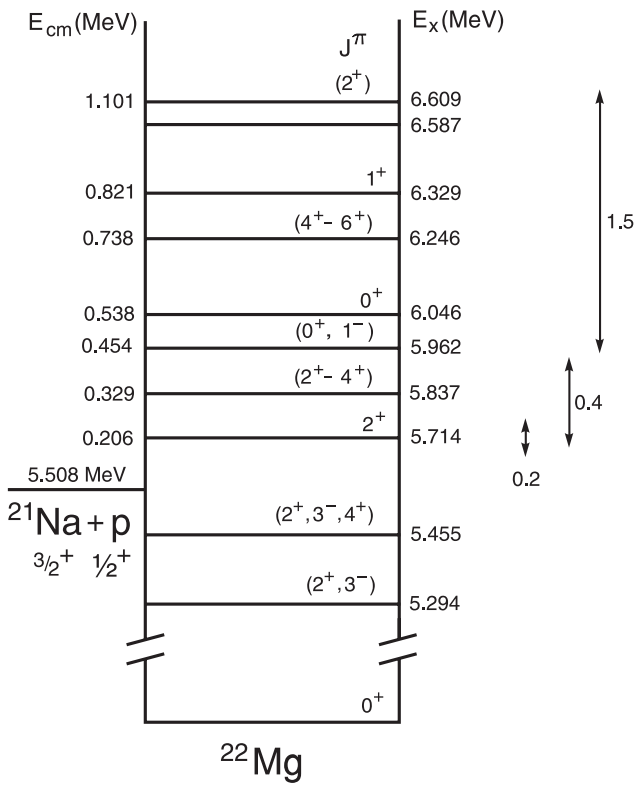

Fig. 53. Level scheme of ^{22}Mg in energy region for states of astrophysical interest.

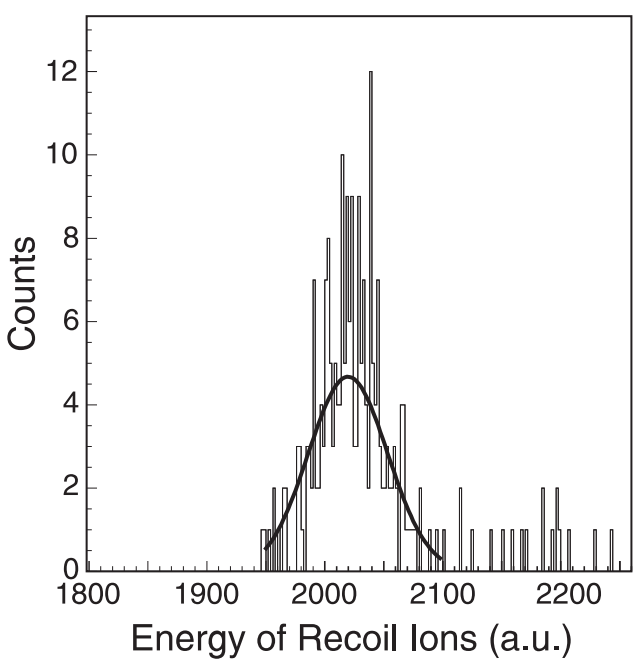

Fig. 54. DSSSD singles data for the ^{22}Mg resonance level at $E_{\rm cm} = 738$ keV. The events above channel 2100 are from "leaky beam" events.

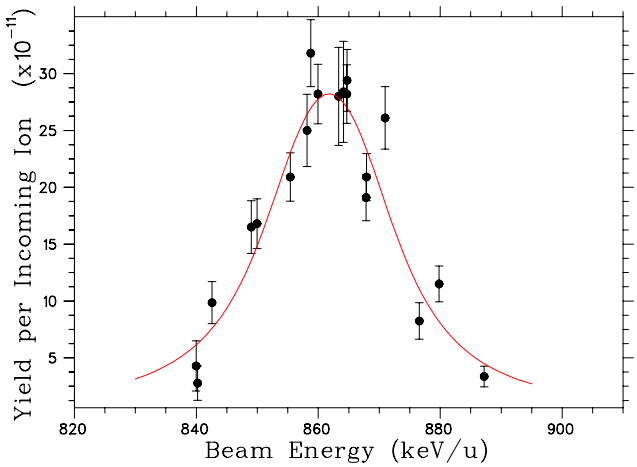

Fig. 55. Measured yield of ^{22}Mg recoils as a function of beam energy for the level resonance at $E_{\rm cm} = 821$ keV.

The resonance at $E_{\rm cm} = 821$ keV was studied over a range of 20 keV above and below the resonance energy. Data were analyzed in singles mode as the EMS provided suppression by a factor of $\sim 10^{11}$ of the ^{21}Na beam with respect to the recoiling reaction products. The experimental yield curve obtained for this resonance is displayed in Fig. 55 along with a least-squares fit of the thick target yield function for a wide resonance to the data. While $E_{\rm beam}$, dE/dx and ΔE were measured, $E_{\rm cm}$, Γ, and $\omega\gamma$ were set as free parameters in the fit. The error bars are statistical and were convoluted with an $\sim$0.2% error due to the uncertainty in the incoming beam energy. To deduce the resonance widths from the fit parameter Γ, several contributions to the measured width had to be subtracted. These contributions are the (assumed) Gaussian energy spread of the beam, the broadening of the resonance due to energy straggling in the target and the zero point motion of the H_2 target molecules. The quadratic sum (3.0 keV/u) of these functions was linearly subtracted from the fitting parameter to deduce the Lorentz-shaped natural width. This result was validated through simulation calculations which included beam energy uncertainty and straggling. From the resulting fit, the resonance strength was found to be $\omega\gamma = 556 \pm 41_{\rm stat} \pm 65_{\rm syst}$ meV, the resonance energy $E_{\rm cm} = 821.3 \pm 0.9$ keV, and the natural width $\Gamma = 16.1 \pm 2.8$ keV, with a reduced chi-squared value of 2.3.

The data for the 1101 keV resonance in ^{22}Mg were taken in the energy range of $E_{\rm cm} = 1090$ to 1135 keV and were analyzed in singles mode in a manner similar to that for the 821 keV resonance. Figure 56 shows the experimental yield curve for the 1101 keV resonance in ^{22}Mg, plotted as a function of incoming beam energy. As before, a least squares fit to the thick target yield function was performed, allowing the extraction

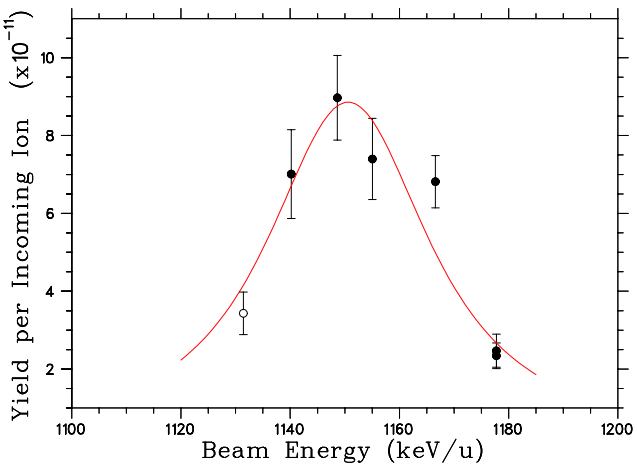

Fig. 56. The yield curve of the 1101 keV resonance as a function of incident beam energy. The lowest point is believed influenced by a neighbouring resonance and was not included in the fit.

of $\omega\gamma$, Γ, and $E_{\rm cm}$. The displayed error bars arise from statistics and a similar 0.2% error in beam energy. In earlier studies of Ruiz et al. [Phys. Rev. **C65**, 042801 (2002)] there is another resonance about 20 keV lower that is believed to overlap with the low-energy tail of the 1101 resonance. Since the data were incomplete in this region, it was not possible to include this contribution. Ignoring the lowest energy yield point, the reduced chi-square for the final fit was 1.44 and the resonance strength was found to be $\omega\gamma = 368 \pm 47_{\rm stat} \pm 41_{\rm syst}$ meV at a resonance energy of 1101.1 ± 2.5 keV. A Γ of 30.1 ± 6.5 keV was deduced after subtracting experimental contributions.

Table VI summarizes the results of Expt. 824 with values of the energies and resonance strengths of seven resonances above the proton threshold in ^{22}Mg which are believed to play a role in novae and X-ray bursts. Errors on $\omega\gamma$ are the combined (in quadrature) statistical and systematic errors.

Figure 57 displays the respective resonant rates for each of the seven ^{22}Mg states populated in the ^{21}Na$(p,\gamma)^{22}$Mg reaction for temperatures consistent with ONe novae and X-ray bursts; an upper limit is shown for the possible resonance at 329 keV. Also

Table VI. Resonance strengths and level energies for ^{21}Na$(p,\gamma)^{22}$Mg reaction.

$E_{\rm x}$ (MeV)	$E_{\rm cm}$ (keV)	Γ (keV)	$\omega\gamma$ (meV)
5.714	205.7 ± 0.5		1.03 ± 0.21
5.837	329		≤ 0.29
5.962	454 ± 5		0.86 ± 0.29
6.046	538 ± 13		11.5 ± 1.36
6.246	738.4 ± 1.0		219 ± 25
6.329	821.3 ± 0.9	16.1 ± 2.8	556 ± 77
6.609	1101.1 ± 2.5	30.1 ± 6.5	368 ± 62

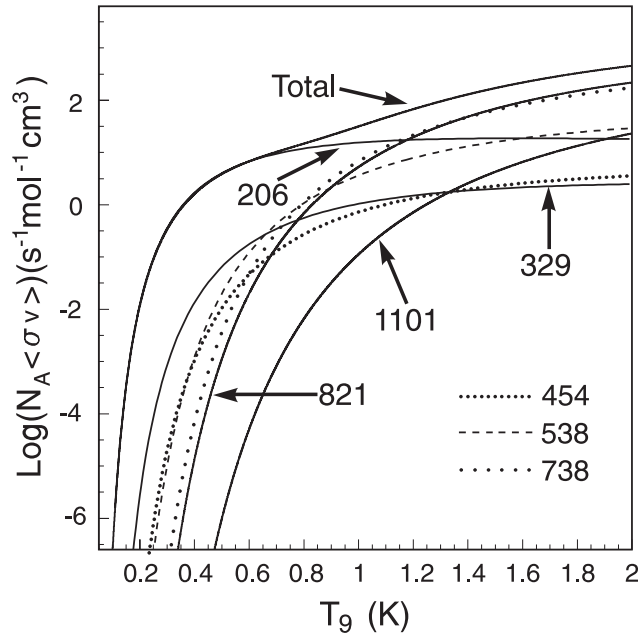

Fig. 57. Estimated reaction rate as a function of temperature based upon the resonances observed in this study. An upper limit for the possible resonance at $E_{\rm cm} = 329$ keV was plotted.

included in the figure is the total ^{21}Na$(p,\gamma)^{22}$Mg reaction rate.

It is evident from our resonance strength measurements that the ^{22}Mg state at $E_{\rm x} = 5.714$ MeV ($E_{\rm cm} = 206$ keV) is the dominant contributor to the ^{21}Na$(p,\gamma)^{22}$Mg rate for the entire span of ONe novae temperatures ($\lesssim 0.4$ GK) and also up to temperatures of $\sim$1.1 GK (X-ray burst range). The states at $E_{\rm x} = 5.837$ (if it exists) and 5.962 MeV are wholly insignificant for ^{22}Na production in an ONe nova. Beyond 1.1 GK, other higher states start to play a role.

The strength of the 206 keV resonance, as determined in these studies, was used as an input into nuclear reaction network calculations of an ONe nova for purposes of the production of ^{22}Na. Abundance calculations were compared to those performed previously and it was found that the final mass fraction was reduced by 50%. This resulted from the fact that the measured $\omega\gamma_{206}$ is higher than used previously. A higher reaction rate indicates that the ^{22}Na is produced sufficiently quickly in the nova that it has time to react further, leading to its reduced presence at the end of the explosion. This could explain the lack of an observation of this radionuclide, ^{22}Na, using the discarded COMPTEL satellite. It also gives some criteria for searches with the new satellite, INTEGRAL.

In addition full hydrodynamic calculations were performed in which the role of the ^{21}Na$(p,\gamma)^{22}$Mg reaction was assessed in X-ray bursts. Basically two different models were used, one of which assumed that

the rate of the ^{21}Na$(p,\gamma)^{22}$Mg reaction was zero. The results of this calculation indicated that individual reactions do not play a critical role in X-ray burst models, except for specific rates related to potential waiting points. X-ray bursts occur at such high relative temperatures that different pathways to heavier masses are found.

Experiment 838
Double radiative capture on pionic hydrogen
(RMC Collaboration)

Introduction

When negative pions are stopped in hydrogen they form pionic hydrogen atoms. These atoms can disintegrate via several modes that include the well-known processes of charge exchange $\pi^- p \to \pi^0 n$, radiative capture $\pi^- p \to \gamma n$, and pair production $\pi^- p \to e^+ e^- n$. However, an additional mode involving double radiative capture is expected also

$$\pi^- p \to \gamma\gamma n \quad .$$

The predicted branching ratio for double radiative capture is 5.1×10^{-5} [Beder, Nucl. Phys. **B156**, 482 (1979)], with a mechanism that is dominated by the annihilation of the stopped, real π^- on a soft, virtual π^+, i.e. $\pi\pi \to \gamma\gamma$.

The underlying dynamics of $\pi\pi$ annihilation are rather intriguing. It led Ericson and Wilkin [Phys. Lett. **57B**, 345 (1975)] to suggest the reaction as a probe of the pion field in the nucleus, and Gil and Oset [Phys. Lett. **346B**, 1 (1995)] to suggest the reaction as a window on the $\pi\pi \to \gamma\gamma$ vertex. The possible sensitivity to the pion's polarizability of double radiative capture $\pi^- p \to \gamma\gamma n$ or radiative pion photoproduction $\gamma p \to \gamma\pi n$ reaction is also of interest (see Wolfe *et al.* [Int. J. Mod. Phys. **E5**, 227 (1996)] and Drechsel and Filkov [Z. Phys. **A349**, 177 (1994)]).

Set-up

In Expt. 838 we have performed the first measurement of this rare mode of radiative capture. Our experiment was performed on the M9A beam line using the RMC spectrometer (see Fig. 58). The incoming pions were counted in a plastic scintillator beam telescope and stopped in a 2.7 l liquid hydrogen target. The outgoing photons were detected by $\gamma \to e^+ e^-$ pair production in a cylindrical Pb converter and electron-positron tracking in cylindrical multiwire and drift chambers. An axial magnetic field was used for momentum analysis. The two-photon trigger was based on the hit multiplicities and the hit topologies in the trigger scintillator rings and the drift chamber cells.

A typical $\pi^- p \to \gamma\gamma n$ event is shown in Fig. 59. During our four week running period we collected

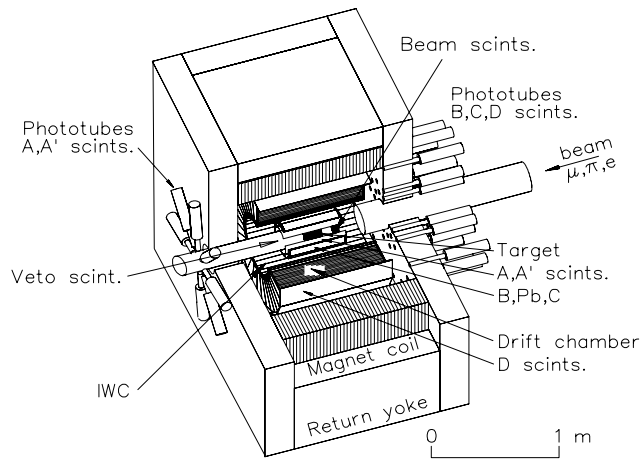

Fig. 58. The RMC spectrometer showing the hydrogen target, lead converter, cylindrical multiwire and drift chambers, trigger scintillators and spectrometer magnet.

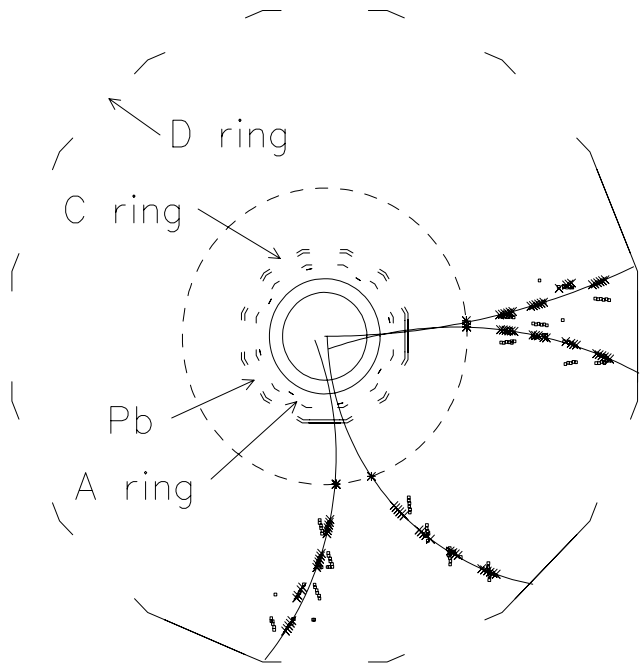

Fig. 59. A typical $\pi^- p \to \gamma\gamma n$ event. The plot shows the fit in the plane perpendicular to the beam axis. The electron-positron pairs converge at the lead converter and the reconstructed photon pairs originate from the hydrogen target located at the centre. The trigger pattern of zero hits in the A-counter ring, two hits in the C-counter ring, and four hits in the D-counter ring is also displayed.

$\pi^- p \to \gamma\gamma n$ data from 3.1×10^{11} pion stops in liquid hydrogen.

Analysis

One source of background was real γ-γ coincidences arising from $\pi^0 \to \gamma\gamma$ decay following $\pi^- p \to \pi^0 n$ charge exchange. The π^0s are produced by either at-rest or in-flight pion charge exchange. The at-rest source yields photon pairs with opening angles $\cos\theta < -0.91$, while the in-flight source yields photon pairs

with $\cos\theta < -0.76$. Thus a photon pair opening angle cut was necessary to separate the double radiative capture signal from the pion charge exchange background.

Another source of background was accidental γ-γ coincidences from simultaneous multiple π^- stops. Multiple pion stops in one beam bucket can yield a γ-ray pair by the accidental coincidence of one photon from the first pion and another photon from the second pion (via either single radiative capture or pion charge exchange). Thus a beam counter pulse height cut was necessary to separate the single pion stops from multi pion stops.

In addition, a tracking cut imposed minimum values for the number of points on the tracks and maximum values for the chi-squared of fits to the tracks, and a photon cut required that the electron-positron pairs intersect at the Pb converter and that the reconstructed photon pairs originate from the H_2 target. A total of 2.3×10^6 photon pairs passed both the tracking cuts and photon cuts, and a total of 635 events survived the opening angle cut and beam counter cut. After subtraction of residual backgrounds from $\pi^0 \to \gamma\gamma$ decay and multi-π stops, we obtained a total of 482 ± 42 $\pi^- p \to \gamma\gamma n$ events with summed energies $E_{\rm sum} > 80$ MeV and opening angles $\cos\theta > -0.1$.

Results

To obtain the branching ratio for double radiative capture on pionic hydrogen we used the equation

$$B.R. = \frac{N_{\gamma\gamma}}{N_{\pi^-} \cdot \epsilon\Omega \cdot F \cdot c_{\rm bm} \cdot c_{\rm stop}}$$

where N_{π^-} is the number of livetime-corrected pion stops, $N_{\gamma\gamma}$ is the number of background-subtracted $\pi^- p \to \gamma\gamma n$ events, and $\epsilon\Omega \cdot F$ is the detector acceptance. Note that the appropriate acceptance was obtained using Monte Carlo [Wright *et al.*, Phys. Rev. **C57**, 373 (1998); Wright *et al.*, Nucl. Instrum. Methods **A320**, 249 (1992)], with the $\pi^- p \to \gamma\gamma n$ kinematical distributions taken from Beder [*op. cit.*]. The factor $c_{\rm stop} = 0.85 \pm 0.01$ accounts for the fraction of incident pions that stopped in hydrogen (see Wright *et al.* [*op. cit.*] for details) and the factor $c_{\rm bm} = 0.99$ accounts for the efficiency of $\pi^- p \to \gamma\gamma n$ events passing the beam telescope cut. Using the equation above we obtained a branching ratio of $(3.05 \pm 0.27(\text{stat}) \pm 0.31(\text{syst})) \times 10^{-5}$. Note that the quoted uncertainty contains a statistical error of $\pm8\%$ from $N_{\gamma\gamma}$ and a systematic error of $\pm10\%$ in total. The systematic error is completely dominated by the $\pm10\%$ uncertainty in the determination of the acceptance $\epsilon\Omega \cdot F$. The uncertainties in N_{π^-}, $c_{\rm stop}$ and $c_{\rm bm}$ were each $\leq2\%$ and entirely negligible. We stress that the result we quote is the total $\pi^- p \to \gamma\gamma n$ branching ratio for all photon energies ($0 < E_\gamma < m_\pi$) and all opening angles ($-1.0 < \cos\theta < +1.0$).

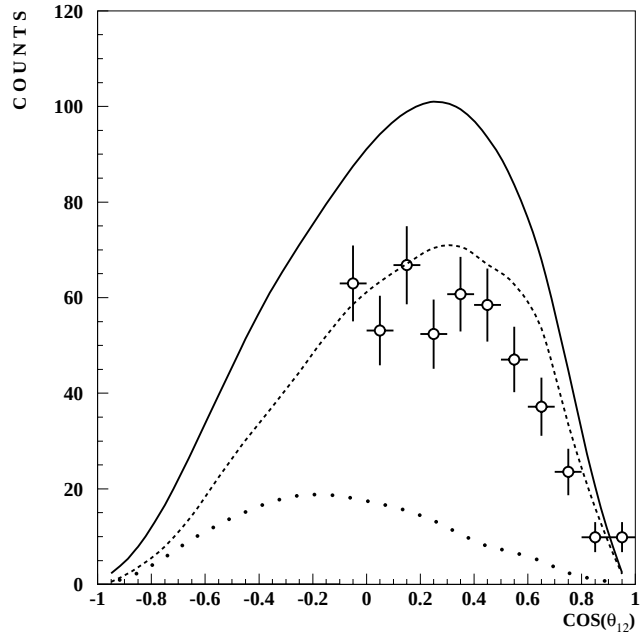

Fig. 60. Comparison of the opening angle distributions from the background subtracted experimental data (open circles) and the theoretical calculation (curves). The dashed curve is the $\pi\pi$ annihilation process, the dotted curve is the NN bremsstrahlung process, and the solid curve is the full calculation. These curves are convoluted with the response function of the RMC spectrometer.

In Fig. 60 we compare our measured data with Beder's calculation [Beder, *op. cit.*]. The dashed curve assumes the $\pi\pi$ annihilation mechanism only, the dotted curve assumes the NN bremsstrahlung mechanism only, and the solid curve is the full calculation. Note that the curves have been convoluted with the response function of the RMC spectrometer. The figure shows that the $\pi^- p \to \gamma\gamma n$ branching ratio and opening angle distributions from experiment and theory are in reasonable agreement. The general consistency of experiment and theory supports the theoretical prediction of a dominant $\pi\pi$ annihilation mechanism.

However, our measured branching ratio is somewhat smaller than the theoretical branching ratio. We note that Beder's calculation was performed at tree-level and neglects contributions from pion loops, etc. We therefore speculate that higher order terms may explain the remaining difference between experiment and theory.

Significance

In summary, in Expt. 838 we have made the first measurement of double radiative capture on pionic hydrogen by recording γ-ray coincidences from π^- stops in liquid H_2. We found the branching ratio to be $(3.05 \pm 0.27(\text{stat}) \pm 0.31(\text{syst})) \times 10^{-5}$ by assuming the

kinematical distributions from Beder [*op. cit.*]. Moreover, the measured branching ratio and opening angle distribution support the theoretical hypothesis of a $\pi\pi$ annihilation mechanism.

Experiment 862
Analyzing powers in the $\vec{p}(\pi, \pi\pi)$ reactions with CHAOS
(E.L. Mathie, Regina)

In this experiment, an attempt to use the Canadian High Acceptance Orbit Spectrometer, CHAOS, to observe at least two charged reaction products from 280 MeV negative pion interactions with polarized protons in the CHAOS polarized proton target was made. Cross section measurements for $\vec{p}(\pi, \pi\pi)$ reactions such as determined in the related CHAOS Expt. 624, have provided the best tests of the predictions of chiral perturbation theory (ChPT) in a fundamental interaction. Experiment 862 was the first (and only) attempt to measure a polarization observable in a kinematic regime which is a compromise between energies where the $\vec{p}(\pi, \pi\pi)$ cross sections are large enough and where the theory is best understood.

The polarization observable is sensitive to the spin orientation of the target proton and is defined in terms of the differential cross sections σ^+ (σ^-) for positive (negative) target polarization according to

$$A = \frac{1}{P_{\rm tgt}} \frac{\sigma^+ - \sigma^-}{\sigma^+ + \sigma^-}$$

where $P_{\rm tgt}$ refers to the magnitude of target polarization and σ refers to any one of several differential cross sections which may be determined.

The polarized target was first developed for CHAOS Expt. 560. The control system was extensively changed to operate in a more modern control environment. The orientation of the proton spins is accomplished in an external, high homogeneity magnetic solenoid. The target material is first cooled to low temperatures using a helium 3-4 dilution refrigerator. Bombardment with suitably tuned microwaves induces polarization of the electron system, which is subsequently transferred to the proton system. Upon completion of this dynamic phase, the microwaves are turned off, leading to a rapid drop in temperature and the proton spin relaxation time to increase suddenly, effectively freezing the proton spin polarization. Once frozen, the target was physically moved from the polarizing solenoid above CHAOS into the spectrometer, where the normal magnetic field serves to preserve the polarization for days. During the actual movement of the target, a third small superconducting magnet, local to the target cryostat, was used to preserve the polarization. The target polarization was determined by calibration of the NMR with the signal due to the small natural polarization arising from thermal equilibrium.

In previous pion production experiments, limitations to the maximum data acquisition rate meant the trigger had to discriminate against the prolific pion proton elastic scattering reaction. However, improvements to the CHAOS data acquisition before this experiment meant that this was no longer required, and new data for pion proton elastic scattering were simultaneously obtained. Experiment 862 received beam in the summer of 2002, however, a critical beam element degenerated and then failed completely before a significant data set of the relatively low rate $\vec{p}(\pi, \pi\pi)$ was accumulated.

During the brief period of running, data were collected for three cycles of the target polarization (both spin orientations form a cycle) and for one series of measurements with the background target configuration. This was sufficient time to produce a useful analyzing power distribution for the elastic scattering reaction, which was published in 2003; however, to date, all attempts to extract meaningful two pion distributions have failed.

Experiment 863
Ground state magnetic moments of ^{75,77,79}Ga (LTNO)
(P. Mantica, Michigan State)

Experiment 863 continued data-taking in 2003 with the goal of improving the statistical significance of the radiofrequency sweeps in the search for the nuclear magnetic resonance of ^{75}Ga. The experimental apparatus was improved by increasing the solid angle subtended by the β particle detectors, which consist of two plastic scintillator ΔE-E telescopes. In order to increase the count rate further, the low energy beam of ^{75}Ga was produced at the TRIUMF-ISAC facility using a 30 μA proton beam current on the Ta production target equipped with a surface ion source. The ^{75}Ga nuclei were implanted into an iron foil mounted on the cold finger inside the ^{3}He/^{4}He dilution refrigerator of the LTNO, which was held near 10 mK. The temperature of the cold finger was monitored by observing the γ-ray anisotropy from a ^{54}Mn thermometer sandwiched with the iron foil on the cold finger. Three HPGe detectors were placed at 0°, 180°, and 270° relative to the applied magnetic field to detect thermometer γ-rays as well as to detect γ-rays emitted from levels populated by the ^{75}Ga β-decay and subsequent decay of the daughter, ^{75}Ge. In this run as in previous runs there was no evidence of other $A = 75$ isobaric contaminants in the radioactive beam.

Polarization of ^{75}Ga was observed by detecting an

asymmetry in the emitted β particles at 0° and 180°. The polarization of ^{75}Ga was confirmed by observing an equal and opposite β asymmetry upon reversing the externally-applied magnetic field. The observed β particle asymmetry of 15% was of the same magnitude as that observed in previous runs.

Radiofrequency scans over the range 90 to 140 MHz were completed. Scans from a previous run indicated the possibility of an effect near the centre of this range and thus a major goal of the 2003 run was to look for resonant destruction of β asymmetry at a level better than 1%. The scans were performed to high precision due to the high implantation rate of ^{75}Ga and the high detection efficiency for β particles. The frequency range that was swept by the applied rf covered nuclear magnetic moment values from 1.6 to 2.5 μ_N. These data are currently under analysis.

Experiment 864
Measurement of the two-photon capture mode of the pionic deuterium atom
(P. Zolnierczuk, T. Gorringe, Kentucky)

To date, the only established system with a baryon number B = 2 is the deuteron. The experimental discovery of another dibaryon would certainly provide new insight into hadron dynamics at the GeV scale.

A recent claim for a dibaryon with mass 1956 ± 6 MeV and width ≤ 8 MeV has been published by the Di2γ collaboration [Khrykin *et al.*, Phys. Rev. **C64**, 4002 (2001)], where they hypothesized that d^* dibaryons were first produced via the two-body process $pp \to d^*\gamma$ and then decayed via the three-body process $d^* \to pp\gamma$. Khrykin *et al.* have argued that $(J^\pi, T) = (1^+, 1)$ is the most natural choice for the d^*'s quantum numbers, being the lowest spin-isospin pp-decoupled state with zero orbital angular momentum.

Gerasimov [arXiv.org:nucl-th/9808070] suggested that double-radiative capture of pionic deuterium

$$\pi^- d \to nn\gamma\gamma$$

is an excellent candidate for further investigations of the dibaryon's existence. The $d^*(T_z = -1)$ dibaryon is first produced via radiative capture $\pi^- d \to d^*\gamma$ and then disintegrates via radiative decay $d^* \to nn\gamma$. Using a simple model, Gerasimov estimated that the branching ratio for the d^* mediated process might be as large as 0.5% exceeding by 2 orders of magnitude the expected two-photon branching ratio for non-resonant double-radiative capture in pionic deuterium.

We have found a total of 370 two-photon events (see Fig. 61) with a small opening angle between the two photons ($\cos\theta_{12} > -0.2$). This number of events should be compared to 580 ± 110 events from the non-resonant pion double-radiative capture on deuterium

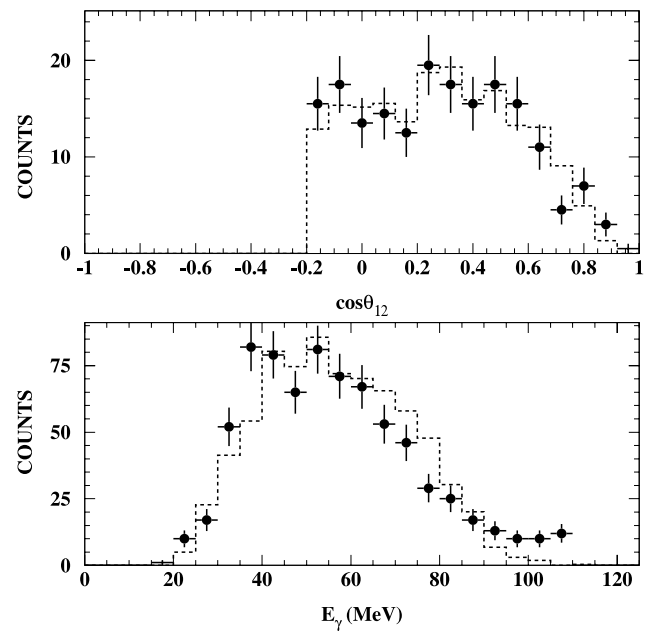

Fig. 61. The photon opening angle $\cos\theta_{12}$ (top) and summed photon energy spectra (bottom) for events passing the tracking cuts and photon cuts.

estimated using the measured branching ratio for non-resonant double radiative capture on hydrogen and assuming the ratio of single radiative capture to double radiative capture to be identical on a hydrogen target and a deuterium target. In addition, the opening angle distribution of the experimental data is consistent with the Monte Carlo simulations assuming non-resonant capture. The expected signature of dibaryon events, a monoenergetic peak from the production process $\pi^- d \to d^*\gamma$ and a three-body continuum from the decay process $d^* \to nn\gamma$, is not seen.

The resulting branching ratio upper limit on d^* production in π^-d capture was obtained by determining the limits on the production γ-ray yield It was found to be smaller than 6.7×10^{-6} (90% C.L.) for d^*s in the mass range of 1920 to 1980 MeV and width of < 10 MeV (see Fig. 62).

We have found no evidence for narrow dibaryon production in $\pi^- d$ capture and in particular, we observed no evidence for a narrow dibaryon of mass $M = 1956$ MeV as claimed by Khrykin *et al.* Our upper limit on dibaryon production is several orders of magnitude below the yield estimate of Gerasimov and our null result is consistent with the null result of the WASA collaboration [Calen *et al.*, Phys. Lett. **B427**, 248 (1998)]. However, above and below the 1920–1980 MeV mass range, our experimental sensitivity rapidly deteriorates due to the energy cut-off in the spectrometer acceptance.

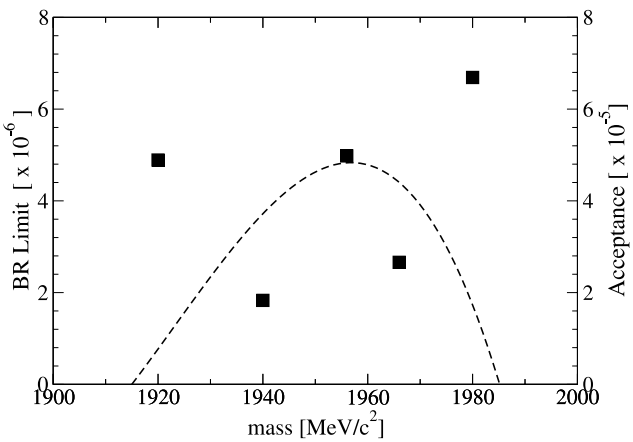

Fig. 62. The 90% C.L. dibaryon branching ratio upper limit versus the d^* mass (full squares and left-hand scale) and the Monte Carlo acceptance versus the d^* mass (dashed line and right-hand scale).

Experiment 871
Meson and quark effects in nuclear β decay of ^{20}Na

(K. Minamisono, JSPS/TRIUMF; K. Matsuta, T. Minamisono, Osaka)

In order to study the G-parity irregular term in the weak nucleon current, the alignment correlation term in the β-ray angular distribution from nuclear-spin aligned ^{20}Na ($I^\pi = 2^+$, $T_{1/2} = 449.7$ ms) has been measured for the first time. A large enhancement of the present result over the value calculated by the impulse approximation (IA) was preliminarily obtained and a discrepancy between the present result and β-γ angular correlation experiments was observed, which implies the importance of the contribution from higher order terms. In order to extract the very small G-parity violating induced tensor term, the alignment correlation term of the mirror partner, ^{20}F, has to be measured. In the process of measuring the alignment correlation term, we developed the technique of polarizing Na isotopes by the colinear laser pumping method and studied the hyperfine interaction of Na isotopes in several materials and measured the quadrupole moments of ^{20,21}Na, which are also reported here.

Atomic polarization of Na isotopes

For the measurement of the alignment correlation term, we first developed the method of polarizing Na isotopes. The experiment was performed at the ISAC radioactive beam facility. For the production of ^{20,21}Na (^{26,28}Na) ions, the 500 MeV proton beam from the TRIUMF cyclotron was impinged on a thick SiC (Ta) production target, which was coupled to the surface ionization source. Na ions were extracted at an energy of 40.8 keV, mass separated, and transported to the polarizer beam line where they were polarized by the colinear laser pumping method. The atomic polarization of neutralized Na atom passing through Na vapour cell was produced by pumping Na atoms on the D_1 transition ($3s\ 2S_{1/2} \leftrightarrow 3p\ 2P_{1/2}$) with circularly polarized laser light. Both ground state hyperfine levels ($3s\ 2S_{1/2}$ $F = I \pm 1/2$) were pumped to achieve high polarization using electro-optic modulators (EOM). Essentially the same technique was used as that developed for other experiments [Levy, Proc. 9th Int. Workshop on Polarized Source and Targets (World Scientific, 2002) p.334]. The optical pump laser was a Coherent 899-21 frequency stabilized dye ring laser pumped by a 7 W argon-ion laser. In order to compensate for the Doppler shift, the beam energy was scanned by changing the bias voltage of the Na vapour cell.

The atomic polarization was not measured, but we measured the nuclear polarization of Na isotopes by implanting Na ions into single-crystal NaF (cubic), which is known to keep the polarization well under a strong magnetic field. The nuclear polarization was checked by comparing the β-ray asymmetric angular distribution, $W(\theta) \sim 1 + A\mathcal{P}\cos\theta$, obtained with positive-helicity laser light compared to that with negative helicity. Here, θ is the angle between the direction of the β-rays and the orientation axis, A the asymmetry parameter, and $\mathcal{P}$ the polarization. A typical result of laser pumping for ^{20}Na is shown in Fig. 63. In the

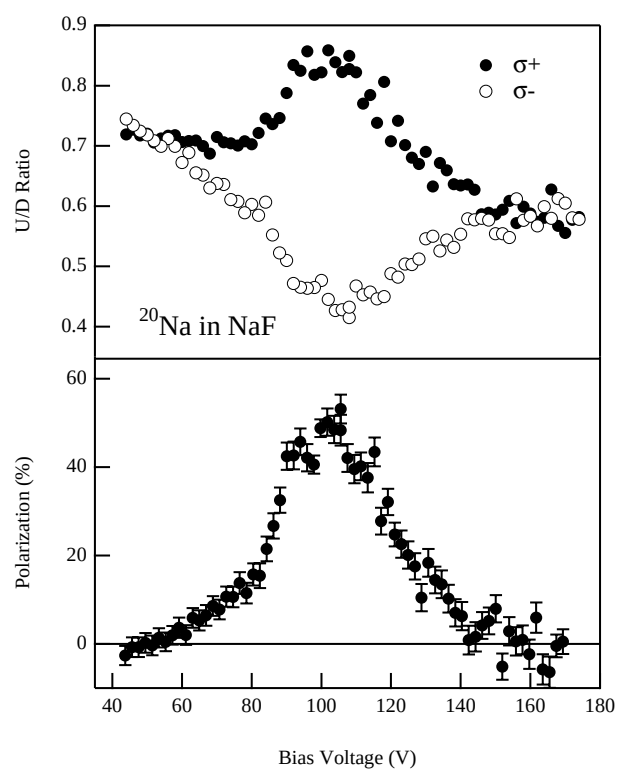

Fig. 63. Result of laser pumping method for ^{20}Na in NaF. In the upper part, the β-ray counting ratio between counters placed 0°(U) and 180°(D) relative to the polarization direction is shown. In the lower part, the deduced polarizations are shown, where $A = 1/3$ was assumed.

upper part, the β-ray counting ratio between counters placed 0°(U) and 180°(D) relative to the polarization direction is shown for the positive (σ^+) and negative (σ^-) laser helicities. In the lower part, the deduced polarizations are shown, where the asymmetry parameter $A = 1/3$ was assumed. A large polarization (∼50%) has been achieved.

Hyperfine interaction

For the creation of a nuclear alignment to measure the alignment correlation term, the spin manipulation technique was applied; an artificial interchange and/or equalization of the population of the magnetic sub-levels, which is described below. For the spin manipulation, the Na atoms were implanted into a single crystal which has a proper electric field gradient q, under a strong magnetic field H_0. The quadrupole interaction between q inside the crystal and the quadrupole moment Q of the nucleus, superposed on the magnetic interaction between the magnetic moment μ of the nucleus and H_0, changes the energy of each magnetic sub-level as

$$E_m = -h\nu_L m + \frac{h\nu_Q}{12}\left(3\cos^2\beta - 1\right)\left\{3m^2 - I(I+1)\right\},$$

so that the single NMR frequency splits into $2I$ lines depending on the nuclear spin I, which correspond to the energy intervals of the magnetic sub-levels. Here, m is the magnetic sub-level, ν_L the Larmor frequency, $\nu_Q = 3eqQ/\{2I(2I-1)h\}$, and the asymmetry parameter of q is assumed to be symmetric. Under these conditions, a transition between two adjacent magnetic sub-levels can be selectively induced by applying an rf field (NMR).

An accurate knowledge of the quadrupole interaction is required for a reliable spin manipulation and thus the selection of the catcher, particularly for ^{20}Na, was one of the important keys for the measurement of the alignment correlation term. For this purpose, we tested several catchers and measured the polarization retained in the catcher and the relaxation time of the polarization. A typical result for the relaxation of ^{20}Na polarization is shown in Fig. 64. We found that ZnO and Mg, which have a proper electric field gradient for the spin manipulation of ^{20}Na, can retain the polarization with long relaxation times and that Pt can retain the polarization even better. The polarization of Na isotopes measured at ISAC is summarized in Table VII.

Quadrupole moments of ^{20,21}Na

Introduction In the process of developing the spin manipulation technique for ^{20}Na, the electric quadrupole coupling constant was measured, from which the quadrupole moment can be extracted.

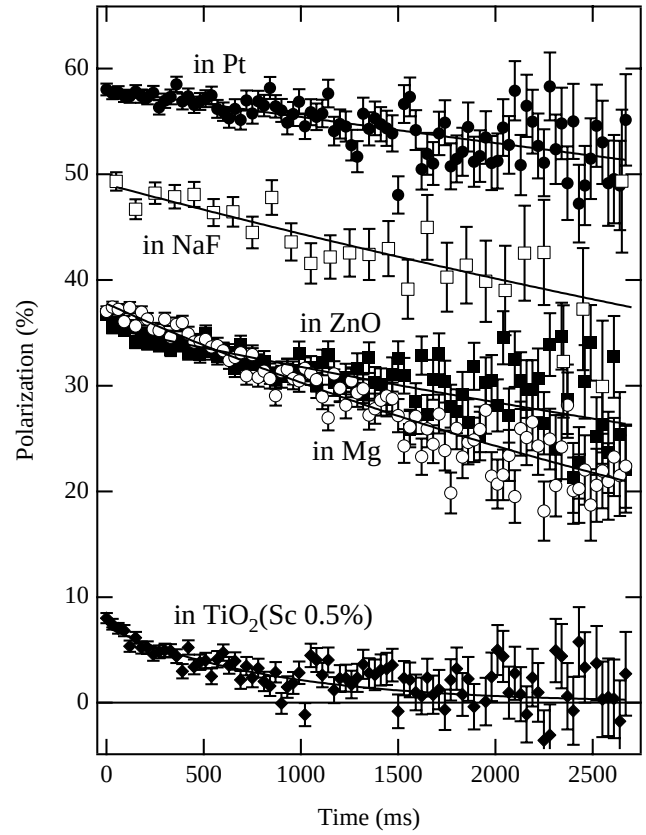

Fig. 64. Relaxation of ^{20}Na polarization in several catchers. The lines are the results of fits.

The quadrupole moments of long chains of Na isotopes have been measured in the experiment of on-line laser spectroscopy of hyperfine structure of the $3p$ $^2P_{3/2}$ state (D_2 line) [Touchard *et al.*, Phys. Rev. **C25**, 2756 (1982)] and in the β-NMR experiment [Keim *et al.*, Eur. Phys. J. **A8**, 31 (2000)]. However, some of the quadrupole moments have not been measured or have been measured with poor statistics. Since the quadrupole moment is very sensitive to a halo structure outside the spherical core, it is very important to have reliable values of the quadrupole moments. In the present study, the electric quadrupole coupling constants, eqQ/h, of ^{20,21}Na in single-crystal ZnO(hcp) were measured. Previously their quadrupole moments have been known only preliminarily or with poor statistics.

Results and discussion By applying the spin manipulation technique, nuclear quadrupole resonance (NQR) spectra of ^{20,21}Na in ZnO were measured as shown in Fig. 65. Here full circles are the data of ^{20}Na and open circles of ^{21}Na. The solid line is the result of a fit to the ^{20}Na data and the broken line for ^{21}Na. In the experiment, the crystalline c-axis was set perpendicular to the external magnetic field. Through the adiabatic fast passage method in NMR, the direction

Table VII. Measured polarization of Na isotopes at ISAC. The catchers indicated by stars were newly tested since last year's Annual Report. Here A is the asymmetry parameter, which is the integrated value of all measured decay branches, AP the typical measured asymmetry, T_1 the spin-lattice relaxation time, P_0 the initial polarization corrected for A and T_1, eqQ/h the electric quadrupole coupling constant, and η the asymmetry parameter of the electric field gradient. For ZnO and Mg, $\eta = 0$ is assumed because of the symmetric crystal structure.

Catcher		^{20}Na	^{21}Na	^{26}Na	^{28}Na
	$T_{1/2}$	447.9 (ms)	22.49 (s)	1.072 (s)	30.5 (ms)
	I^π	2^+	$3/2^+$	3^+	1^+
	A	0.33	0.81	–0.94	–0.76
NaF	AP (%)	16.0 ± 0.4	20.8 ± 0.2	–46.6 ± 1.1	–35.9 ± 2.5
(cubic)	T_1 (s)	9.9 ± 3.1	9.0 ± 0.2	24.6 ± 4.2	–
	P_0 (%)	51.0 ± 1.3	33.5 ± 0.5	52.8 ± 1.3	47.3 ± 3.3
TiO_2	AP (%)	5.3 ± 0.3	13.7 ± 0.3	–44.8 ± 0.5	–34.1 ± 2.5
(rutile)	T_1 (s)	3.4 ± 1.3	13.0 ± 0.5	32 ± 11	–
	P_0 (%)	18.3 ± 1.5	24.0 ± 0.5	46.8 ± 0.9	44.9 ± 3.3
	$\lvert eqQ/h\rvert$ (MHz)	–	5.20 ± 0.03	–	–
	η	0.33 ± 0.03		–	–
$LiNbO_3$	AP (%)	4.3 ± 0.3	5.3 ± 1.6	–40.4 ± 0.6	–26.3 ± 3.0
(ilmenite)	T_1 (s)	1.8 ± 0.5	1.3 ± 0.3	5.3 ± 0.5	–
	P_0 (%)	17.0 ± 1.7	56 ± 28	51.8 ± 1.5	34.7 ± 4
MgF_2*	AP (%)	–	–	–18.6 ± 0.6	–
(rutile)	T_1 (s)	6 ± 3	–	7.4 ± 2.0	–
	P_0 (%)	8.4 ± 0.6	–	22.3 ± 1.3	–
ZnO*	AP (%)	–	–	–	–
(hcp)	T_1 (s)	9.0 ± 0.5	9.63 ± 0.09	–	–
	P_0 (%)	35.5 ± 0.2	22.0 ± 0.1	–	–
	$\lvert eqQ/h\rvert$ (kHz)	683.7 ± 2.7 ± 5.3	939.3 ± 1.9 ± 8.2	–	–
	η	0		–	–
Mg*	AP (%)	–	–	–	–
(hcp)	T_1 (s)	4.5 ± 0.1	–	–	–
	P_0 (%)	37.8 ± 0.2	–	–	–
	$\lvert eqQ/h\rvert$ (kHz)	36.75 ± 0.06	–	–	–
	η	0		–	–
Pt*	AP (%)	–	–	–14.5 ± 0.4	–
(ccp)	T_1 (s)	22 ± 2	–	0.78 ± 0.08	–
	P_0 (%)	58.0 ± 0.1	–	55.0 ± 5.9	–

of polarization was reversed by applying a set of rf values, with both frequency (±20 kHz and ±50 kHz for ^{20}Na and ^{21}Na, respectively) and amplitude modulated. Since we measured the NQR spectra both with the positive-helicity laser light (σ^+) and with the negative helicity (σ^-) for the laser pumping method to produce the atomic polarization, we define the effective asymmetry change as the difference between the measured asymmetry change with σ^+ and that with σ^- as effective $AP \equiv AP(\sigma^+) - AP(\sigma^-)$, in order to maximize the NMR signal so that a reliable measurement was performed.

At first, a two component gaussian was fitted to the NQR spectrum of ^{21}Na in ZnO. We found two resonances, which may be caused by two final locations of Na isotopes in ZnO or other reasons. We call the larger resonance main and the smaller one sub. A constant asymmetry change was observed because the transition between $m = -1/2 \leftrightarrow 1/2$ was always induced ($I = 3/2$) owing to the multi-rf technique. In the analysis of ^{20}Na in ZnO, the ratio of the main and sub resonances of ^{21}Na in ZnO was used because the measurement of the sub resonance of ^{20}Na in ZnO was not completed. The results are summarized in Table VIII together with a theoretical prediction and the quadrupole moments reported before. The second errors in the present results are the systematic errors owing to the unknown origin of the sub resonances. Here, one tenth of the width of the main resonance is considered as the systematic error and the error for the ratio $R \equiv Q(^{20}\mathrm{Na})/Q(^{21}\mathrm{Na})$ is a total error. The theoretical values are calculated by the shell model code OXBASH [Brown *et al.*, MSUCL Rep. N. 524] with *sd* model space, which reproduces the present experimental

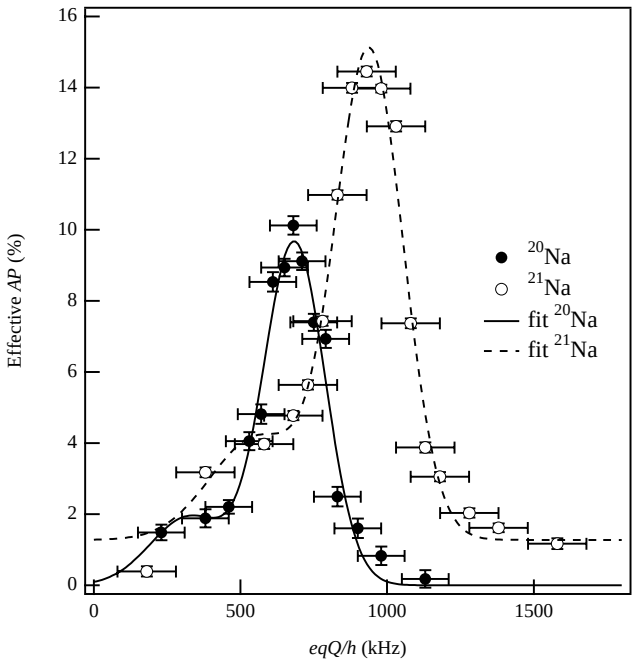

Fig. 65. Electric quadrupole resonance spectra of ^{20,21}Na in ZnO. The full circles are the data of ^{20}Na and open circles of ^{21}Na. The solid line and broken line are the results of fits.

Table VIII. Electric quadrupole coupling constants of ^{20,21}Na in ZnO. R is defined by the ratio between quadrupole moments of ^{20,21}Na as $R \equiv Q(^{20}\mathrm{Na})/Q(^{21}\mathrm{Na})$. The theoretical values were calculated by OXBASH. For experimental values see the text.

	^{20}Na	^{21}Na
$\lvert eqQ/h \rvert$ (kHz)	683.7 ± 2.7	939.3 ± 1.9
	± 5.3	± 8.2
R	0.728 ± 0.009	
$Q_{\mathrm{theor.}}$ (mb)	+84	+110
R	0.76	
$Q_{\mathrm{exp.}}$ (mb)	90 ± 10	61 ± 39
R	1.48 ± 0.96	

ratio of the quadrupole moments. Since the experimental quadrupole moment of ^{20}Na was taken from a figure in Keim *et al.* [ENAM98 (AIP **445**, 1998) p.50], it should be considered as preliminary data. The quadrupole moment of ^{21}Na was measured in Touchard *et al.* [Phys. Rev. **C25**, 2756 (1982)]. In Table VIII, a reanalyzed value of $Q(^{21}\mathrm{Na})$ by the latest reference value of the hyperfine coupling constant $A(^2P_{3/2})$ and the quadrupole moment of ^{23}Na [Wo Yei *et al.*, Phys. Rev. **A48**, 1909 (1993); Jonsson *et al.*, Phys. Rev. **A53**, 4021 (1996)] is listed. For the first time, we determined the ratio of $Q(^{20}\mathrm{Na})/Q(^{21}\mathrm{Na})$ within ∼1% relative error. In order to extract the quadrupole moment from the present electric quadrupole coupling constant, the reference value of the electric quadrupole coupling constant, with well known quadrupole moment, will be measured.

Alignment correlation term of ^{20}Na

Introduction G parity is one of the important symmetries to be tested in the parity violating weak nucleon current. G operation is a product of the charge conjugation and the charge symmetry. It is a parity operation in the charge space. Many experimental and theoretical works have been performed and it was shown that there is no large G parity violation in the weak nucleon current. However, there still remains a possible small violation caused by the mass difference between the proton and neutron, or more fundamentally, between the up and down quarks inside the nucleon, or other reasons. A recent review can be found in the paper [Wilkinson, Eur. Phys. J. **A7**, 307 (2000)]. For this purpose, a high measurement experiment of the alignment correlation terms in the mass $A = 12$ system was performed by the Osaka group [Minamisono *et al.*, Phys. Rev. **C65**, 015501 (2002)]. In order to search for such a small G parity violating term, we need to extend the experiment to a variety of mass systems so that possible nuclear structure effects are eliminated. In the present study, the alignment correlation term of ^{20}Na in the $A = 20$ system was measured for the first time.

The β-ray angular distribution from an oriented nucleus is given by $W(E,\theta) \sim 1 + \mathcal{P}\hat{B}_1(E)\mathrm{P}_1(\cos\theta) + \mathcal{A}\hat{B}_2(E)\mathrm{P}_2(\cos\theta)$, where E is the β-ray energy, θ the angle between the direction of the β-ray and the orientation axis, $\mathcal{P}$ the polarization, $\mathcal{A}$ the alignment, $\hat{B}_1(E)$ the polarization correlation term and $\hat{B}_2(E)$ the alignment correlation term given by $\hat{B}_2(E) = -2\hat{H}_2(E,0)/3$ [Holstein, Rev. Mod. Phys. **46**, 789 (1972)], where

$$\hat{H}_2(E,s) = \frac{E}{2M}\left(1 - \frac{d \pm d_{\mathrm{II}}}{c} \pm \frac{b}{c} + (-1)^s\delta(E)\right).$$

Here ± is for the electron and positron decays, respectively, M the nuclear mass, b the weak magnetism, c the Gamow-Teller matrix element, d the time component in the main axial vector current, d_{II} the G parity irregular induced tensor term and $\delta(E)$ the contribution from higher order matrix elements. Taking advantage of the symmetry between mirror β-decays, d_{II} can be extracted from the difference of the alignment terms as $\hat{B}_2(E)_{^{20}\mathrm{F}} - \hat{B}_2(E)_{^{20}\mathrm{Na}} = -2E(b - d_{\mathrm{II}} - \Delta\delta(E))/(3Mc)$, where $\Delta\delta(E) = (\delta(E)_{^{20}\mathrm{F}} - \delta(E)_{^{20}\mathrm{Na}})/2$.

The angular correlation between the β-ray and subsequent γ-ray from the first excited state in ^{20}Ne to its ground state has also been used to test G symmetry. If we express the β–γ angular correlation as $W(\theta_{\beta\gamma}) = 1 + a(E)\cos\theta_{\beta\gamma} + p(E)\cos^2\theta_{\beta\gamma}$, the counterpart of the alignment correlation term is given by

$p(E) = \hat{H}_2(E,1)/2$. Thus, these two experiments have different contributions from higher order terms, which provide us a chance to cancel the higher order term.

Spin manipulation In the present experiment, a single crystal ZnO (hcp) was used as a catcher. The polarized ^{20}Na were implanted into ZnO placed at the centre of an NMR magnet made of permanent magnet material (5250 Oe at the centre and parallel to the polarization). In ZnO, (35.5 ± 0.2)% polarization and T_1 = 9.0 ± 0.5 s were observed, as seen in Fig. 64. The spin manipulation and the measurement of the β-ray energy spectrum from the aligned nucleus were performed in accordance with a timing program. A typical result of the spin manipulation is shown in Fig. 66. A pulsed beam method was employed. After the beam was chopped, the polarization in counting section named I was converted into alignment in section III and back again to polarization in section V. Because we can't directly measure the degree of alignment, we calculated it from the polarization in sections I, II, IV, V and the efficiency of the spin manipulation, which was measured in a separate run. In section VIII, the alignment was created, which has an opposite sign to the alignment created in section III. The vertical lines in the figure are to guide the eye. The full circles are the beam cycle named 1, in which the alignments were created in an order of minus to plus in sections III and VIII, respectively. In order to compensate for the relaxation of the polarization and alignment, the alignments were created in a different order in beam cycle 2, which is shown by the open circles. They constitute one cycle and the cycle was repeated until the required statistics were achieved.

Results and discussion From the ratio of β-ray counts between these positive and negative alignments, the alignment correlation terms were extracted as

$$\hat{B}_2(E) \sim \frac{1}{\hat{\mathcal{A}}}\left(\frac{N(\mathcal{A}_1^+,E)}{N(\mathcal{A}_2^-,E)}\frac{N(\mathcal{A}_2^+,E)}{N(\mathcal{A}_1^-,E)} - 1\right)$$

with

$$\hat{\mathcal{A}} = \mathcal{A}_1^+ - \mathcal{A}_2^- + \mathcal{A}_2^+ - \mathcal{A}_1^-.$$

Here, $\mathcal{A}_i^\pm$ is the degree of positive or negative alignment in beam cycle i and $N(\mathcal{A}_i^\pm, E)$ the β-ray counts from the aligned nucleus. By extracting the alignment correlation term from the ratio, we do not need to normalize the β-ray counts by the beam current so that the systematic error could be reduced. The obtained alignment correlation terms are shown in Fig. 67, where systematic corrections were applied for each data point.

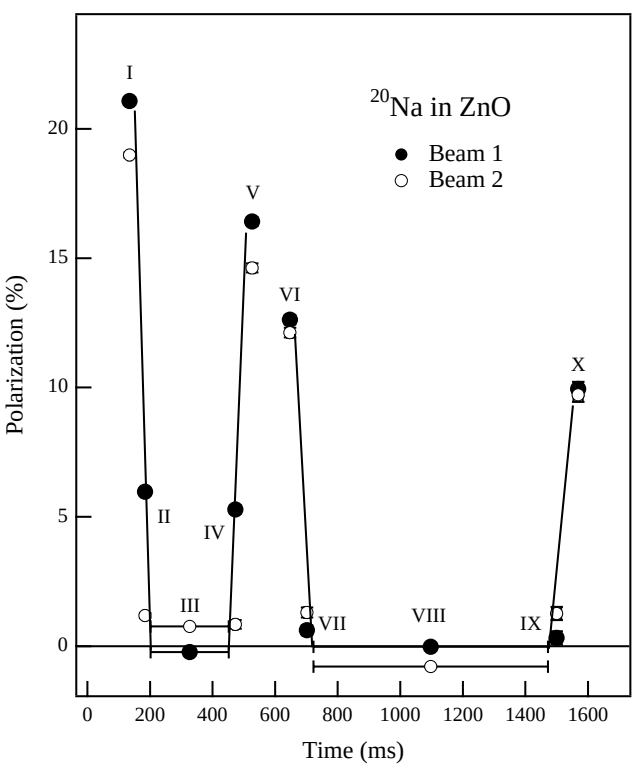

Fig. 66. Result of the spin manipulation of ^{20}Na in ZnO. The polarization change as a function of time is shown. At time zero, the beam was stopped. Roman numerals are the names of counting sections. The vertical lines are to guide the eye.

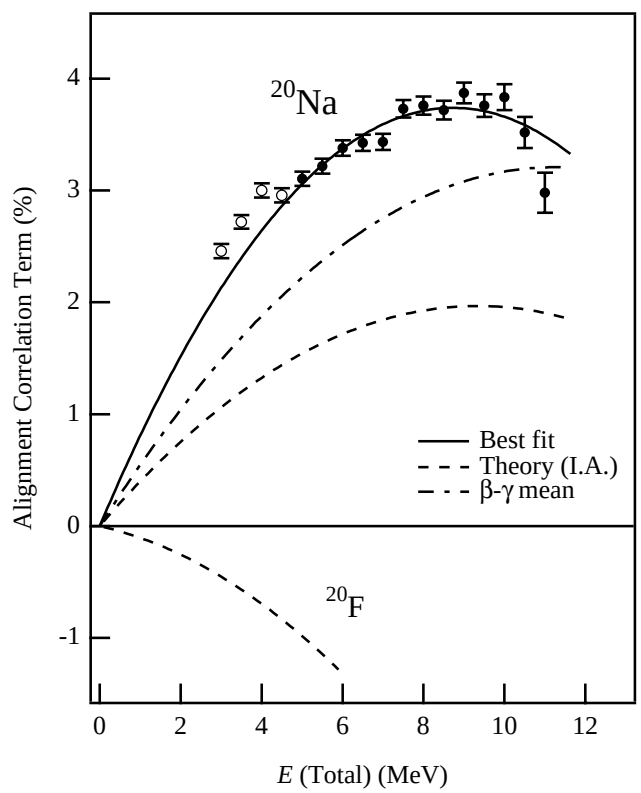

Fig. 67. Alignment correlation terms of ^{20}Na. The full circles were used for the fit and open circles were not. The solid line is the fit, the broken lines are theory(IA) and the dotted broken line is the result of β-γ angular correlation experiments.

In the figure, full circles were used for the fit and open circles were not because of a large scattering effect on the surface of the catcher. The solid line is the result of the fit and the broken lines are the theoretical predictions based on the IA [Calaprice *et al.*, Phys. Rev. **C15**, 2178 (1977)]. Together with the present result, the result of a fit of three existing β-γ angular correlation experiments [Dupuis-Rolin *et al.*, Phys. Lett. **79B**, 359 (1978); Tribble *et al.*, Phys. Rev. **C23**, 2245 (1981); Rosa *et al.* Phys. Rev. **C37**, 2722 (1988)] is shown by the dotted broken line, where the original β-γ angular correlation data were multiplied by $-4/3$ to plot the result of the fit in the figure. We found a huge enhancement in the present data compared with the theoretical calculation based on the IA, which might be explained by including meson exchange effects inside the nucleus as indicated in the result of the experiment on the alignment correlation term in the $A = 12$ system [Minamisono *et al.*, Phys. Rev. **C65** 015209 (2002)]. We also found a discrepancy between the present result and the result of β-γ angular correlation experiments. The contribution from higher order terms $\delta(E)$ should be considered in the analysis. Detailed analysis of systematic corrections and errors is now in progress. In order to reduce the scattering effect on the surface of the catcher, which has one of the largest contributions to the systematic errors, a new run with thin single crystal Mg is planned. For the extraction of very small f_T, the alignment correlation term of the mirror partner, ^{20}F, has to be measured.

Experiment 875
MuScat: muon scattering in low Z materials for muon cooling studies

(R. Edgecock, RAL)

Introduction

An important requirement of the Neutrino Factory accelerator complex is the ability to cool the muons in the transverse plane. Without this, it is likely the neutrino intensity will be considerably smaller than required for the physics program. Due to the muon lifetime, such cooling needs to be fast and the currently preferred technique is ionization cooling. In the case of the transverse cooling required for a Neutrino Factory, this involves passing the muons through an absorber in which they lose both longitudinal and transverse momentum. The lost longitudinal momentum is then restored using rf cavities following the absorber.

As well as a cooling effect coming from the ionization energy loss, there is heating coming from multiple scattering and the final cooling achieved is a balance between these. Theory suggests this balance is most favourable for elements with low atomic number, in particular, liquid hydrogen. However, an extensive literature search has failed to find any measurements of the muon scattering distribution in light elements. The most relevant data found come from the scattering of 2.7 MeV/c electrons on Al, Be and Li. These data show a clear trend: as Z decreases, the agreement with Moliere theory gets worse. If this trend continues to hydrogen, there will be two effects:

- The level of cooling achieved would be less than expected.
- Due to the increased scattering in the tails, the fraction of muons scattered out of the cooling channel could be much bigger than expected.

Due to the importance of this to ionization cooling, the MuScat experiment has been created to measure the scattering of muons of various momenta in a number of low atomic number materials, in particular liquid hydrogen. As well as checking these observations, MuScat will compare a range of muon scattering models with the data.

A four week test period was allocated to the MuScat experiment in the M11 beam line at TRIUMF in June and July, 2000 and much was learnt about the experiment during this time. As a result, a number of changes were made and an improved version of the experiment was constructed. This was tested with cosmic rays and a proton beam at RAL at the end of 2002 and then sent to TRIUMF at the beginning of 2003. Time was allocated in the M20 beam line in April and May, 2003.

The following sections will describe the improved version of the experiment, the running in TRIUMF and the status of the analysis of the data. The aim is to have the analysis finished for NuFact'04 in Japan.

M20 beam line

The M20 beam line is a quadrupole muon decay channel, employing two bending magnets with quadrupole transport between them. This allows a dramatic reduction in the background to muons by selecting different momenta for the two bends and using a momentum slit in the quadrupole channel. By using forward decay pions, a muon beam up to almost 180 MeV/c is possible and this is how the beam line was used by MuScat. It should be noted that it is normally used for "surface" muons and was not used in the forward decay mode for 20 years before MuScat arrived!

The experiment

As the aim of the experiment is to make a precise measurement of the multiple scattering of muons, the amount of material that the muons must pass through has to be kept to a minimum. For this reason, it is not possible to do any tracking before the target and a collimation system is employed to reduce the beam

dimensions so that the incoming particle position is known accurately enough. In addition, the measurement of the position of the scattered muon relies on the first tracking detector as all subsequent detectors are affected by scattering in the first. Any additional detectors are only used to aid in noise rejection and for checking systematics. To minimize scattering in air, as much of the experiment as possible is mounted in vacuum. Finally, to eliminate particles other than muons, a good time-of-flight system is required.

The detector designed to satisfy these requirements and used in the M20 beam in 2003 is shown in Fig. 68. The most upstream parts are a veto shield and veto scintillator to eliminate beam halo. These are followed by the first trigger counter, which also acts as the TOF start. This is built from two fingers of scintillator, each 1 mm thick, 28 mm long and 3 mm high. These overlap by 20 mm in length and 3 mm in height. The timing resolution is about 250 ps. The TOF stop comes from the following rf-bucket of the cyclotron. This is almost a square-wave of length 1.9 ns, the smearing of the edges corresponding to a resolution of about 500 ps.

This trigger scintillator is followed by a 1 m long vacuum tube containing the collimation system. This consists of a 40 mm thick lead block at the front and a 160 mm lead block at the back, with two 10 mm disks behind the front collimator and another two in front of the back collimator. The first block has a slit 20 mm long by 2 mm high cut in it, while the slit in the second block is tapered to prevent large angle scatters off the internal face. With this arrangement, the scattering distribution is measured vertically, in the narrow direction of the slot. The second dimension is longer to increase the particle intensity. There are also two pairs of intermediate blocks each 10 mm thick with larger slits in them to prevent scattering off the internal faces and an active collimator in front of the back block. The latter consists of a strip of scintillator above and below the slit in the collimator. Finally, the whole collimator tube is wrapped in about 6 mm of lead.

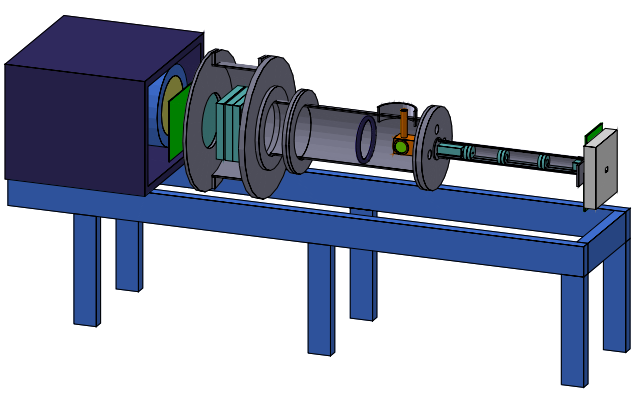

Fig. 68. The MuScat experiment in 2003.

The vacuum tube is connected to the main vacuum vessel, which contains the targets. These are:

- liquid hydrogen, 100 mm and 150 mm thick
- lithium, 12.7 mm and 6.3 mm thick
- beryllium, 3.7 mm and 1.0 mm thick
- carbon, 2.5 mm thick
- aluminum, 1.5 mm thick
- CH2, 4.8 mm thick
- iron, 0.2 mm and 5.1 mm thick

The "thick" iron sample is used simply to blow the beam up to give a better coverage of the detectors and improve the measurement of the efficiency. The liquid hydrogen targets were built by the Targets group at TRIUMF. The two lengths were achieved in the same structure simply by rotating it through 90° in the horizontal plane.

The solid targets are mounted on a target wheel that can be controlled from outside the vacuum so it is unnecessary to break this each time a target is changed. The wheel has 12 slots, the last of which has no target mounted and is used to measure the intrinsic properties of the beam. These are monitored on a regular basis. In addition, two sets of lithium targets are used to allow systematic checks.

Three detectors built from scintillating fibres are used for tracking. These consist of two offset planes of 1 mm thick fibres in each dimension, to give a uniform efficiency and two dimensional readout. There are a total of 1024 fibres per chamber. The light from the scintillating fibres is transmitted to photomultipliers using clear fibres. The PMTs used are Hamamatsu R5900 L16s and contain 16 anodes, each 16 mm long and 0.8 mm wide. Bundles of 16 × 16 clear fibres are formed to match these anodes, thus giving a 16-fold multiplexing. To ensure that signals can be de-convoluted, the scintillating fibres are read out at both ends and the PMTs at each end are rotated by 90° with respect to each other. The detectors are mounted inside the vacuum vessel to minimize the amount of material between them and the target. The PMTs, on the other hand, must sit outside and this means the fibre arrays form the vacuum seal. The leak rate from these is sufficiently small, however, that a vacuum of less than 5×10^{-6} torr was achieved. The last of three detectors is shown mounted on the back plate of the vacuum vessel in Fig. 69.

A second scintillator for use in the trigger sits behind the tracking detectors, outside the vacuum. The final part of the detector is TINA, a NaI calorimeter of 460 mm diameter and 510 mm depth. It has a measured energy resolution (fwhm) of 3.6% at 90 MeV for electrons, with an energy dependence of $E^{-0.55}$. As it is not big enough to cover the full area of the tracking

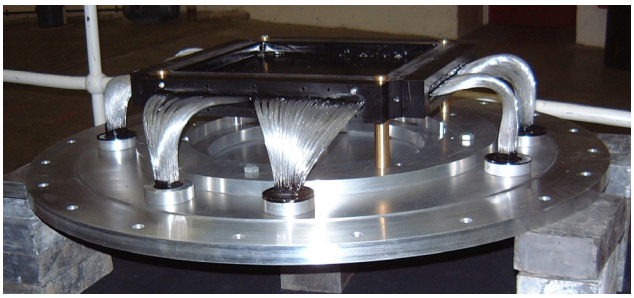

Fig. 69. The third Scifi detector mounted on the experiment end-flange.

detectors after extrapolation of the tracks, it is used offset from the centre of the experiment. Nevertheless, it is valuable for both a muon energy measurement and to check the beam composition.

Initial results from 2003

In 2003, MuScat had about 16 days of data-taking in the M20 beam line and recorded a total of 57 M triggers, as shown in Table IX. The analysis of these data so far has focused on three main areas: understanding the beam, understanding the detector and developing a full GEANT4 simulation of the detector. It should also be noted that theoretical work is being undertaken in Oxford University that will directly predict the scattering distributions that MuScat will measure. A strong collaboration has been created with the authors of this work. In this section, only a few aspects of the work done so far will be summarized.

Beam composition The time-of-flight distribution measured with the two bending magnets in M20 set to the same momentum and the momentum slit wide open is shown in Fig. 70(a) and under normal running conditions, with the bends set for forward decays and a narrow momentum slit in Fig. 70(b). In the former it is possible to identify peaks due to electrons, muons and

Table IX. Number of triggers recorded in 2003.

Target type	Number of events
Liquid hydrogen 15 cm full	3.1 M
Liquid hydrogen 15 cm empty	3.9 M
Liquid hydrogen 10 cm full	7.9 M
Liquid hydrogen 10 cm empty	8.5 M
Lithium 1.3 cm	6 M
Lithium 0.6 cm	6 M
Beryllium 0.4 cm	3 M
Beryllium 0.1 cm	3 M
Carbon 0.3 cm	2 M
Aluminum 0.2 cm	3 M
Polythene 0.5 cm	2 M
Iron 0.02 cm	2 M
Iron 0.5 cm	2 M
Empty	5 M
Total	57 M

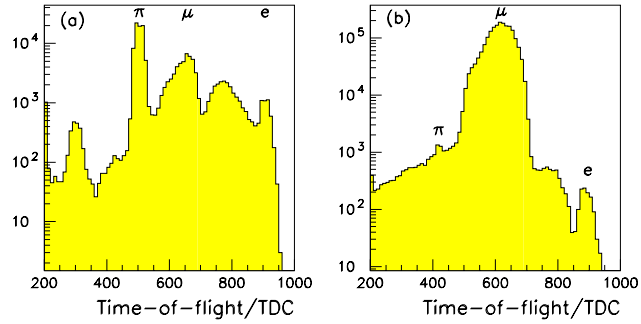

Fig. 70. Time-of-flight distributions.

taus. There are a number of other peaks which correspond to earlier rf pulses of the cyclotron and these are believed to be due to the protons. There are more than one of these because the protons do not penetrate all the way through the detector to the second trigger scintillator plane. Thus a "proton" trigger actually results from a proton signal in the first trigger counter and an accidental coincidence with another particle, pion, muon or electron, hitting the second trigger counter.

In normal running conditions, using forward muon decays and a narrow momentum slit, it can be seen that the backgrounds from particles other than muons are essentially eliminated. The shoulder on the muon peak is currently being understood, but is believed to be due to pion decays after the momentum slit.

Additional particle identification is possible with TINA. Although the details are still being understood, Fig. 71 shows the energy deposition of muons that strike the calorimeter well away from the edges. The tail to higher energies is believed to be due to electrons

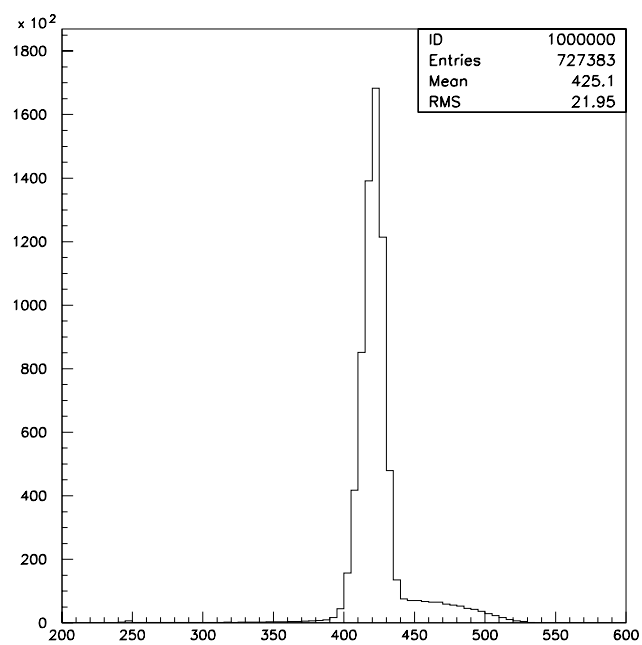

Fig. 71. Energy distribution of muons in TINA.

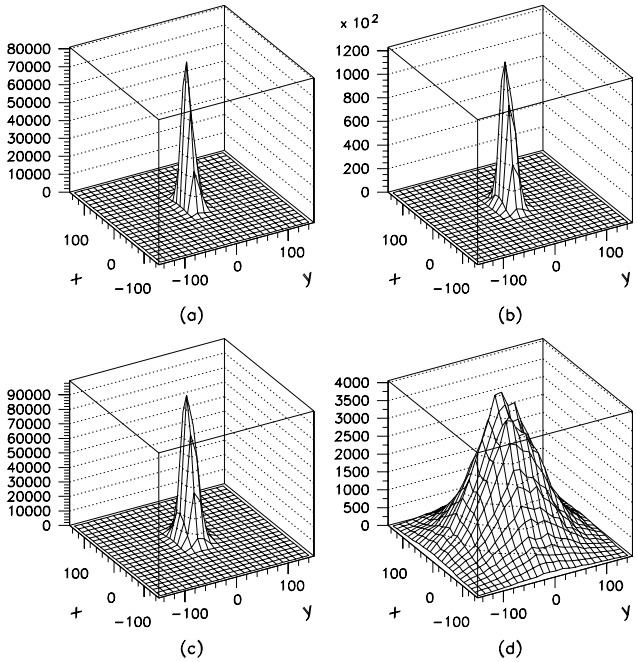

Fig. 72. Raw hit distributions in the first scintillating fibre detector with (a) no target, (b) thin lithium, (c) thick lithium and (d) thick iron. The distributions are broader in x as this is the long dimension in the collimator slits. The scattering will be measured in y.

which come from muon decays during the integration time of the electronics.

Beam momentum As M20 has not been used for forward muon decays for a long period, it is very important to have an independent measurement of the beam momentum. This is possible in two ways: (1) using the time of flight of a number of particle types and (2) using the kinetic energy depositions in TINA for these particle types. Both of these have been investigated and give a preliminary measurement consistent with expectations from the M20 magnet settings.

Tracking The tracking detectors are clearly the most important element of the experiment and a lot of work has been done to understand them. In particular, the pedestals and gains have been determined and the alignment, hit identification and error determination are almost final. Tests of the tracking algorithm are also almost complete. As an example, Fig. 72 shows very preliminary raw hit distributions, without tracking requirements, for running with solid targets. The algorithm for deconvoluting the real muon scattering distribution from these raw distributions has been developed and is also under test.

In addition, a detailed GEANT4 simulation of the whole experiment has been written. Much work has gone into comparing this with data, down to fine details, and this has brought many improvements to the simulation and a better understanding of the experiment. An example is shown in Fig. 73. A method of using a number of scattering algorithms as input to GEANT4 for comparison with the raw scattering distributions from the data is also under development.

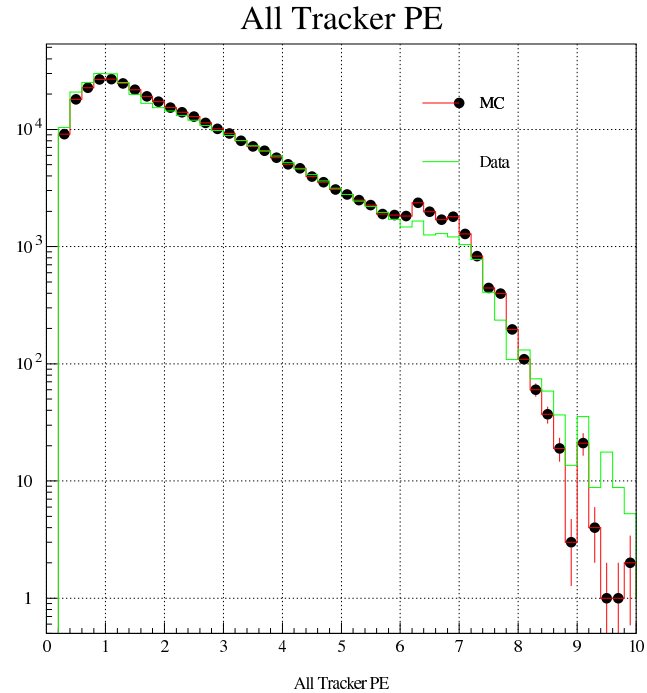

Fig. 73. Comparison of total signals from clusters found in the tracking detector, measured in photo-electrons, between data (solid line) and Monte Carlo (points). Note the differences above 6 pe are because a single saturation value for the electronics is used in the Monte Carlo, while there are variations for the real data.

Experiment 880
Ortho-para effect of muon catalyzed fusion in solid deuterium
(K. Ishida, K. Nagamine, RIKEN/KEK)

We measured the dependence of the rate of muon-catalyzed fusion in D_2 (dd-μCF) on the ortho-para state of deuterium molecules. In the dd-μCF process, the resonant formation of $dd\mu$, $d\mu + D_2 \rightarrow [(dd\mu)dee]$, is one of the most important processes determining the overall efficiency of producing fusions. Since this process requires an energy matching between the initial state and the final state, the rate is very sensitive to the states of $d\mu$ (hyperfine states $F = 3/2$ or $1/2$, kinetic energy etc.) and D_2 (vibrational and rotational molecular states, kinetic energy etc.). Although the system had been experimentally investigated by changing various parameters such as the temperature and the density, full understanding was not achieved yet. In order to obtain further understanding of this process, we started to investigate the effect of another parameter, namely the ortho-para state of the D_2 molecule.

The measurement was performed at the M9B channel in June, 2000. We prepared two deuterium targets, one the "normal" D_2 (67% ortho and 33% para) and the other was an "ortho" D_2 (99.7% ortho and 0.3% para). A detailed explanation of the gas preparation procedure as well as the experimental set-up is given in references [Toyoda *et al.*, Phys. Lett. **B509**, 30 (2001); *ibid.*, Phys. Rev. Lett. **90**, 243401 (2003)]. The deuterium gas was solidified on a thin silver foil maintained at 3.5 K to make a solid D_2 target of 40 mm in diameter and 0.3 mm in thickness. To detect protons from fusion events, we used silicon surface barrier (SSB) detectors in pairs so that the "ΔE vs. E" particle identification method was applied. The fusion proton emission time spectrum after muon stopping as shown in Fig. 74 was analyzed to extract various parameters such as the effective $dd\mu$ formation rate from $d\mu(F{=}3/2)$ state, $\tilde{\lambda}_{\frac{3}{2}}$, and the hyperfine transition rate from $d\mu(F{=}3/2)$ to $d\mu(F{=}1/2)$ state, $\tilde{\lambda}_{\frac{3}{2}\frac{1}{2}}$. The obtained values are shown in Table X for normal D_2 and ortho D_2. It was found that the effective $dd\mu$ formation rate as well as hyperfine transition rate are decreased by increasing the ortho-deuterium concentration. This result is opposite to a calculation assuming the complete thermalization of $d\mu$ atoms, which predicts a slight increase of $dd\mu$ formation rate. We suspect that the solid-state effect plays an important role and a more detailed theory is necessary.

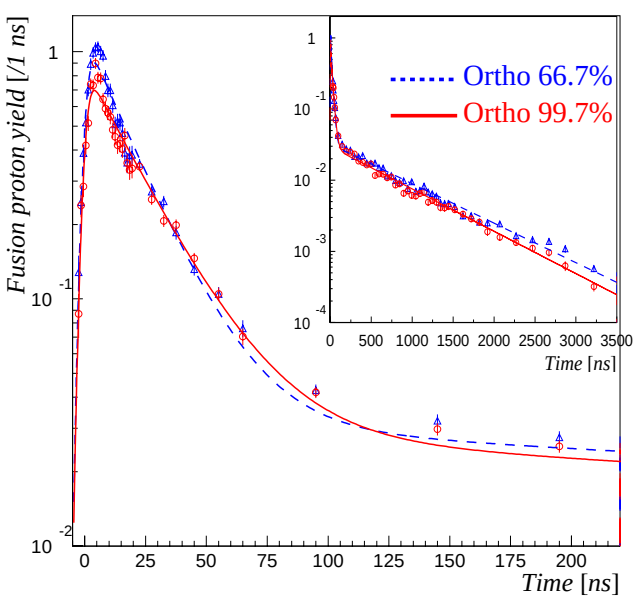

Fig. 74. Fusion proton time spectrum for normal deuterium (triangle data points and fitted dotted line) and that for ortho deuterium (circle points and solid line) are plotted. A significant difference was observed both in amplitude and decay rate of the fast component. The upper-right inset is for a different time range to show the slow component, which was used for the normalization.

Table X. Obtained value of the effective $dd\mu$ formation rate $\tilde{\lambda}_{\frac{3}{2}}$ and the hyperfine transition rate $\tilde{\lambda}_{\frac{3}{2}\frac{1}{2}}$ in normal D_2 and ortho D_2 and the relative effect due to ortho-para conversion.

	Normal D_2	Ortho D_2	Effect
$\tilde{\lambda}_{\frac{3}{2}}$	2.868(60)	2.131(43)	–26(3)%
$\tilde{\lambda}_{\frac{3}{2}\frac{1}{2}}$	36.14(84)	29.68(71)	–18(3)%

Table XI. Comparison of the $d\mu$ hyperfine-transition rate due to scattering [$\lambda_{d\mu}^{3/2\ 1/2\ \mathrm{scat}}$ (μs^{-1})] and the $d\mu$ hyperfine-transition rate via back decay rate [$\lambda_{d\mu}^{3/2\ 1/2\ \mathrm{back}}$ (μs^{-1})] between experiments (this work, Lauss *et al.* [Hyp. Int. **118**, 79 (1999); Voropaev *et al.*, Hyp. Int. **118**, 135 (1999)] and theories). Our experiment is for solid D_2 while others are for the liquid state.

	$\lambda_{d\mu}^{3/2\ 1/2\ \mathrm{scat}}$ (μs^{-1})	$\lambda_{d\mu}^{3/2\ 1/2\ \mathrm{back}}$ (μs^{-1})
This expt.	11.5 ± 4.2	24.7 ± 4.9
Lauss *et al.*	26.3 ± 3.0	11.0 ± 3.0
Voropaev *et al.*	23.6 ± 0.4	12.9 ± 0.4
Theories	∼36	∼14

Another interesting problem in dd-μCF is that there is a large discrepancy between theories and experiments concerning the $d\mu$ hyperfine-transition rate, to which two components are expected to contribute. Since one of the components (transition by back decay after $dd\mu$ molecule formation) is proportional to the measured effective $dd\mu$ formation rate with respect to the ortho-para conversion, while the other (transition due to scattering) is not dependent, we can use our data to separately determine the two components. Our result is shown in Table XI with previous experimental data obtained in the liquid state by completely different methods. It was confirmed that the scattering is much smaller than theoretical predictions.

Experiment 893
The hyperfine field of Rb in Fe, Ni and Co (LTNO at ISAC)
(P. Delheij, TRIUMF)

Principle

In the low temperature nuclear orientation (LTNO) set-up, a polarized nuclear ensemble is created by implanting the radioactive beam from the ISAC facility into a ferromagnetic target foil which is kept at a temperature near 10 mK. For these systems the polarization is determined by the factor μH/kT through the Maxwell Boltzmann distribution. Here, μ is the magnetic moment, H the hyperfine field, T the temperature and k the Boltzmann constant. This polarization produces an anisotropy in the emission of the decay

products which depends on nuclear structure properties like spins, multipole mixing and parity mixing. By raising the temperature the normalization (isotropic distribution) is measured. The normalized anisotropies determine the parameter values.

If two of the three parameters in μH/kT are known for the parent ground state, the third one can be determined. In this way (because μ and H are known) the temperature is determined by attaching a long lived source like ^{60}Co<u>Fe</u> to the cold finger that cools the target foil.

The product μH can be determined directly with rf irradiation (NMRON technique). As the frequency of the rf field is stepped the anisotropy of any subsequent transition is measured to detect the change of this anisotropy when the Larmor frequency is passed. This technique avoids the systematic errors that are due to the temperature determination. This improves the accuracy typically by an order of magnitude. Either the magnetic moment or the hyperfine field can be determined if the other quantity is known.

Development

At present the goal of this experiment is to resolve the difference between the experimental and calculated value for the hyperfine field of diluted Rb in Fe. In 2000 a calculation of the hyperfine field of dilute impurities in Fe of the elements from Rb to Xe was published [Cottenier and Haas, Phys. Rev. **B62**, 461 (2000)]. Compared to earlier calculations the lattice constant around the impurities was treated as variable. This improved agreement between experimental and calculated values by an order of magnitude to the few per cent level. The exceptions were Rb and Sr. For Rb a discrepancy of a factor –5 exists. An NMRON measurement with ^{79}Rb in the LTNO set-up at ISAC can resolve this issue (Expt. 893). For Sr a discrepancy of a factor +2 was removed this year in Japan [Nishimura *et al.*, Phys. Rev. **B68**, 012403 (2003)].

During the preparations for the on-line measurements a problem with the top loading mechanism on the mixing chamber was encountered. The rebuilding required a substantial disassembly of the set-up. Then on-line measurements with ^{79}Rb and ^{75}Ga showed polarization effects on the 15 per cent level. However, no NMRON signal could be observed.

After that ^{91}Rb was implanted to populate the isomeric state at 555 keV in ^{91}Y. The hyperfine field for this system is known [Hinfurtner *et al.*, Phys. Rev. Lett. **66**, 96 (1991)] and the resonance frequency is 310 MHz without an external magnetic field. As shown in Fig. 75, an effect of 200% was observed for the intensity ratio of the detectors perpendicular (D90+D270) and parallel (D0+D180) to the external magnetic field due to the polarization.

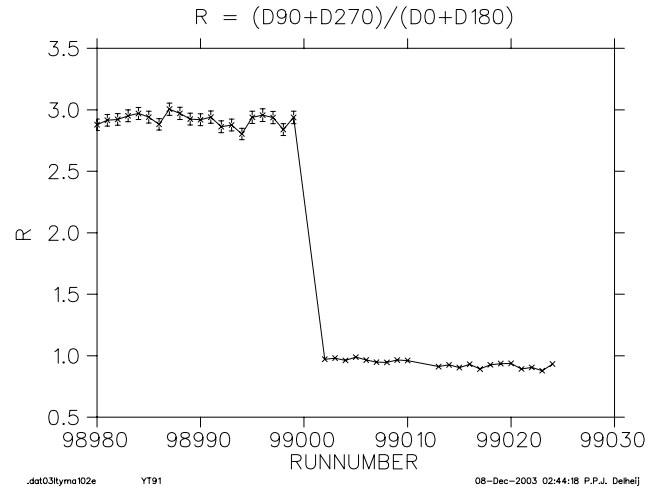

Fig. 75. Change of the intensity ratio R as the target foil is warmed up.

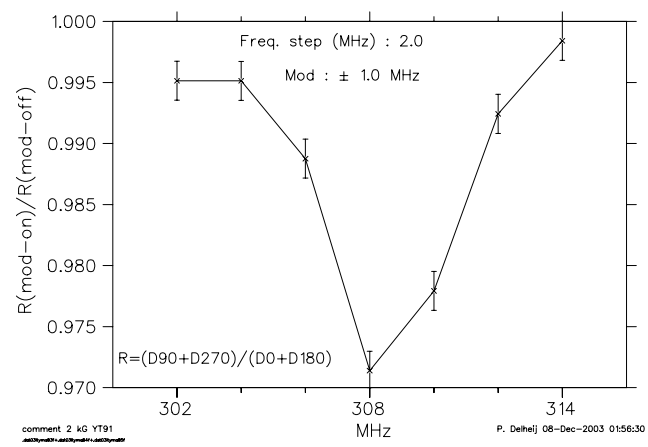

Fig. 76. NMRON resonance for ^{91}Rb**Fe** in an external magnetic field of 0.2 T. The ratio of R with the rf modulation on and the rf modulation off dips as the frequency is stepped through the resonance.

With this system a resonance was observed at 308 MHz as expected for the external field of 0.2 T (see Fig. 76). The rather small size of the resonance (a frequency integrated destruction of only 1/30 of the polarization signal) was a surprise, particularly in view of our earlier result for ^{60}Co**Fe** (see last year's TRIUMF Annual Report) when a polarization destruction efficiency of 1/3 was observed at 165 MHz, approximately a factor 10 better. With the small polarization signal from ^{91}Y it was still possible to measure the spin-lattice relaxation for the first time. The result of 10 ± 5 s is in good agreement with the semi-empirical relation in Shaw and Stone [Atomic Data and Nucl. Data Tables **42**, 339 (1989)]. This might suggest that the small NMRON effect is less likely related to the sample preparation than to the operation of the rf system. To address this problem a mock-up of the rf transmission system was being built at the end of the year. Furthermore, computer simulations are in progress.

Experiment 909
Isospin symmetry breaking in superallowed Fermi β-decays
(C.E. Svensson, Guelph)

Precision measurements of the ft values for superallowed $0^+ \rightarrow 0^+$ Fermi β-decays between isobaric analogue states provide demanding tests of the standard model description of electroweak interactions. To date, superallowed ft values have been determined at the $\pm 0.1\%$ level for nine nuclei between ^{10}C and ^{54}Co and, once corrected for small radiative and isospin symmetry-breaking effects, their consistency has confirmed the conserved vector current (CVC) hypothesis at the level of 3×10^{-4}. However, the value of V_{ud} derived by comparing these β-decay data with the purely leptonic muon decay, combined with present knowledge of V_{us} and V_{ub}, indicates a violation of the unitarity of the Cabibbo-Kobayashi-Maskawa (CKM) quark-mixing matrix at the 98% confidence level [Towner and Hardy, Phys. Rev. **C66**, 035501 (2002)]. Should this discrepancy be firmly established, it would indicate the need for new physics, either in terms of explicit quark effects in nuclear structure or an extension of the minimal electroweak standard model. Before a definitive conclusion can be reached, all uncertainties contributing to the unitarity test must be carefully scrutinized and, if possible, reduced. For V_{ud}, the dominant uncertainties are those associated with theoretical corrections to the ft values, and the search for systematic effects has focused on the nuclear-structure dependent δ_C corrections that account for the breaking of isospin symmetry by charge-dependent forces in the nucleus.

Experiment 909 involves a series of measurements with the 8π spectrometer and SCEPTAR β array aimed at constraining the above-mentioned isospin symmetry-breaking corrections in superallowed Fermi β-decays. This program will take advantage of the unique beams of radioactive ions available at ISAC to study particular decays in which the predicted δ_C corrections show the greatest model sensitivity. An initial focus of Expt. 909 will be on lifetime and branching ratio measurements for ^{34}Ar, with the aim of establishing the superallowed ft value at the $\pm 0.1\%$ level. The first objective will be to improve the current half-life precision by approximately one order of magnitude. These measurements will be carried out by collecting samples of ^{34}Ar at the centre of the 8π and following their decay for $\sim$30 half-lives by time-stamping γ-rays emitted from excited states in the daughter ^{34}Cl populated in Gamow-Teller decay branches of ^{34}Ar.

In anticipation of ^{34}Ar beams from the ISAC ECR ion source in 2004, tests of the experimental techniques to be employed in Expt. 909 were carried out with radioactive ^{26}Na beams. This isotope was chosen because

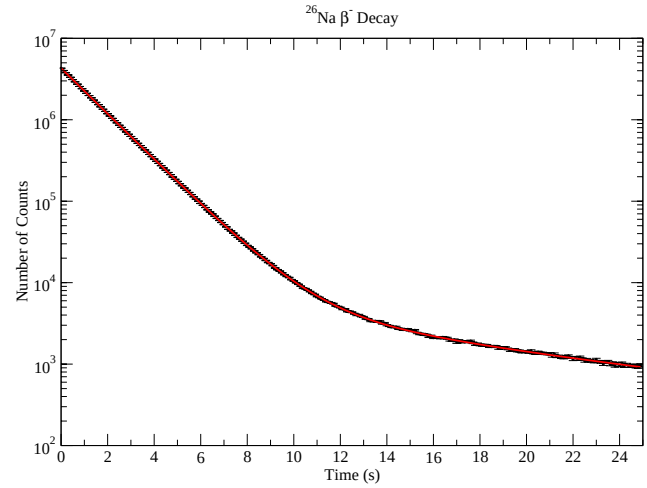

Fig. 77. Summed decay curve from β counting ^{26}Na samples with the 4π gas proportional counter at the ISAC GPS station. The second (longer lived) decay component results from a small ^{26m}Al contamination of the beam.

i) high yields were available from ISAC surface ion sources, ii) the half-life ($\sim$1.07 s) is similar to ^{34}Ar, iii) the daughter ^{26}Mg is stable, and iv) $\sim$99% of ^{26}Na β-decays are followed by the 1809 keV γ-ray transition in ^{26}Mg, facilitating tests of the γ-ray lifetime technique to be employed for ^{34}Ar. The first requirement was to determine a precise value for the ^{26}Na lifetime. To this end, a ^{26}Na beam was delivered in 2002 to the fast tape system at the ISAC GPS station and its lifetime determined to high precision by the well-established β counting technique with a 4π gas proportional counter. The analysis of these data (a sample of which is shown in Fig. 77) is now complete, and the ^{26}Na lifetime has been established at the $\pm 0.03\%$ level.

In June, ^{26}Na beam was delivered to the 8π spectrometer to commission SCEPTAR (the scintillating electron positron tagging array) and to continue the

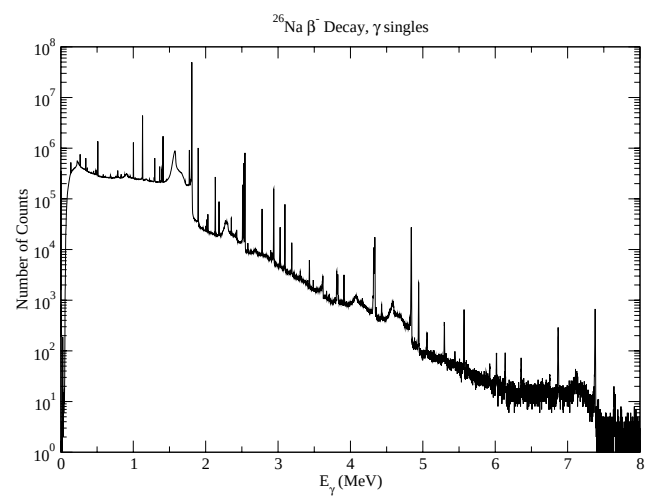

Fig. 78. γ-ray singles spectrum from ^{26}Na decay recorded with the 8π spectrometer at ISAC.

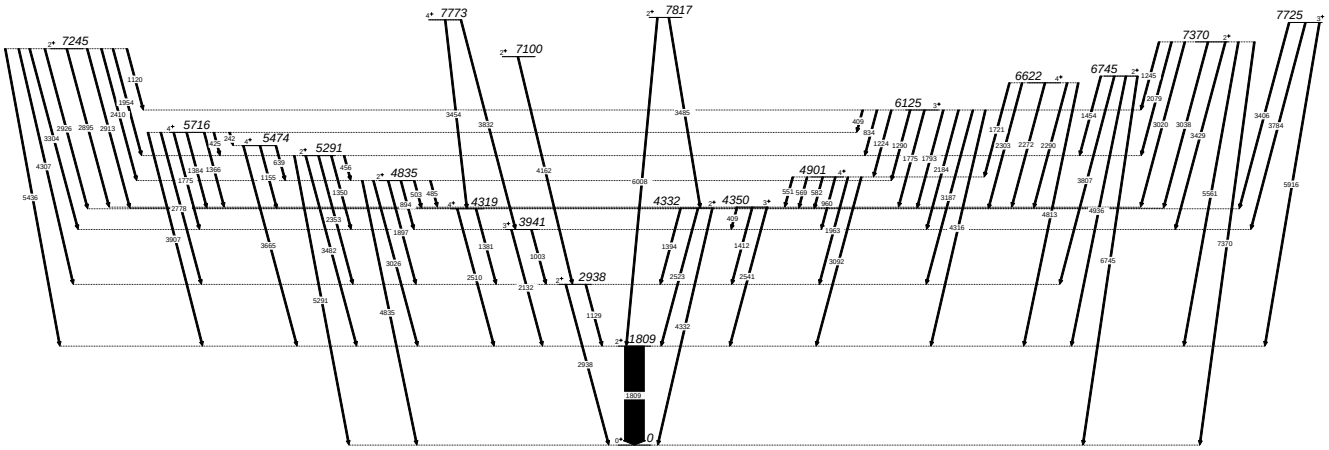

Fig. 79. γ-rays from the daughter nucleus ^{26}Mg identified with the 8π spectrometer following β-decay of ^{26}Na.

development of lifetime measurement techniques for Expt. 909. A γ-ray singles spectrum from ^{26}Na decay recorded in the 20 HPGe detectors of the 8π spectrometer is presented in Fig. 78. A total of 82 γ-ray transitions in the daughter ^{26}Mg were identified, with energies between 241 keV and 7.368 MeV and intensities ranging from 0.99 to below 10^{-5} per β-decay (see Fig. 79). Together with the above mentioned lifetime measurement and the previously known Q-value, these data have established precision ft values for 20 β-decay branches of ^{26}Na. The ^{26}Na beam also enabled further testing of the γ-ray lifetime technique to be employed for ^{34}Ar, and these data are currently being analyzed for comparison with the precise ^{26}Na half-life determined through β counting.

Following measurement of the ^{34}Ar lifetime, subsequent measurements with the 8π and SCEPTAR will focus on an improved determination of the ^{34}Ar superallowed branching ratio. Large, and model-dependent, isospin symmetry-breaking corrections are also predicted for the $A \geq 62$ odd-odd $N = Z$ nuclei. A program of precision lifetime measurements (Expt. 823) for these nuclei with the 4π gas proportional counter at the ISAC general purpose station is being led by G.C. Ball of TRIUMF. Future experiments with the 8π spectrometer and SCEPTAR will provide branching ratio measurements for these short-lived isotopes. Weak non-analogue Fermi decay branches that provide direct, and absolute, information on one component of the isospin symmetry breaking will also be measured. Initial measurements of ^{74}Rb decay by our collaboration with a single HPGe detector have identified a number of high-energy γ-rays from excited states in the daughter ^{74}Kr [Piechaczek *et al.*, Phys. Rev. **C67**, 051305(R) (2003)]. The high γ-γ efficiency of the 8π spectrometer will be used to clarify the coincidence relationships between these γ-rays and identify further γ-ray transitions following weak Gamow-Teller decay branches, with the aim of establishing the superallowed branching ratio at the $\pm 0.05\%$ level. With the continued development of ion source technology at ISAC, these superallowed and non-analogue Fermi β-decay branching ratio studies will be extended to include ^{38m}K, ^{62}Ga and ^{70}Br.

Experiment 920
Nuclear charge radii and moments of short lived neutron deficient lanthanum and other rare earth isotopes
(H.A. Schuessler, Texas A&M)

We had our first on-line run scheduled September 5–9. The plan was to measure HFS and isotope shifts of short lived $^{129-134}$La isotopes. In case of difficulties with lanthanum production, we were also ready to substitute short lived Pr isotopes for investigation. Initial field tests on a Ta foil target running at about 40 μA proton beam indicated that such experiments should be possible, even though more yield tests needed to be carried out to definitely confirm the required $\sim 5 \times 10^6$ ion/s for laser spectroscopy signals. Unfortunately shortly before our run started, the on-line ion source was destroyed, and nothing more could be done to pursue spectroscopy on either La or Pr. We hope that in a future ion source period our experiment will be scheduled closer to the beginning of the period to have a newer on-line ion source.

Since our experimental equipment was ready and needed to be tested, and since all the major collaborators were present, it was decided to try using the off-line plasma source (OLIS) with argon gas. We got excellent and fast support to arrange a stable beam run from the ISAC ion source management and the ion source operators.

Transitions accessible to laser dyes in the 550 nm region lie very high in Ar II and it was necessary to find transitions for which the lower level is metastable,

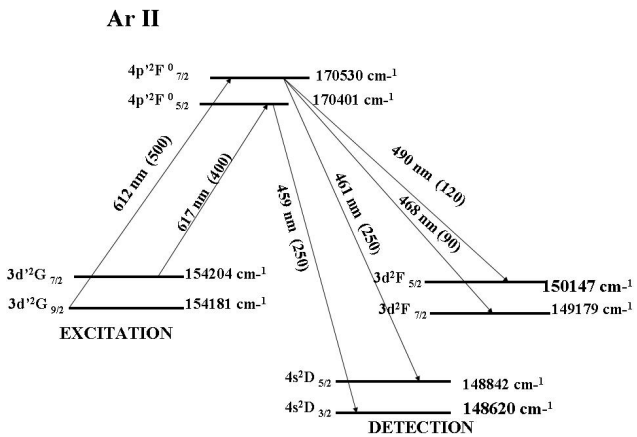

Fig. 80. Ar II level scheme of interest.

and populated by the plasma discharge of the source. The scheme used in our experiment is shown in Fig.80.

Laser radiation at $\lambda = 611$ nm and $\lambda = 617$ nm was employed for excitation and several lines between $\lambda =$ 459–490 nm for detection.

These excitation wavelengths lie on the border of the DCM dye range, so rather than change the dye in our laser (currently working with Rh110), we used Phil Levy's polarization beam line laser, which already operated with DCM.

We were successful in observing the laser spectroscopy signals even though the plasma ion source is not well suited for producing the required metastable states from which laser excitation starts. A signal from stable ^{40}Ar is shown in Fig. 81. It is hard to make a sensitivity estimate from this proof-of-principle experiment since it is unknown which minor fraction of the argon ion current is in the required metastable state (less than 10^{-4}). Also the signal line width is more than an order of magnitude broader than the lifetime limit due to the unfavourable conditions in the ion source plasma.

Nevertheless a milestone in our work was reached, since our experiment demonstrated that all our equipment is working and that we are ready for our first on-line experiment at ISAC.

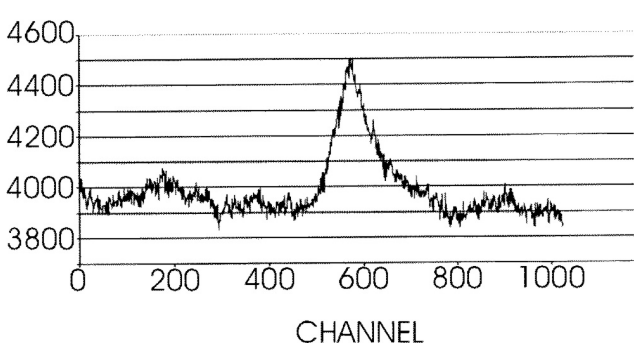

Fig. 81. Laser spectroscopy signal of ^{40}Ar.

Experiment 921
High-K isomers in the mass 180 region

(P.M. Walker, TRIUMF/Surrey, UK)

A program of high-K isomer studies has been initiated at TRIUMF-ISAC. In the first experiment, a radioactive source, prepared off-site, was measured with the 8π γ-ray spectrometer. Following this, measurements of $A \approx 180$ nuclides were made with the 8π spectrometer, in conjunction with the SCEPTAR electron detector array, on-line to the ISAC-I radioactive beam facility.

The motivation for these studies comes from the wish to understand the nuclear structure of high-K isomers, especially the transition rates of highly K-forbidden decays. The neutron-rich $A \approx 180$ nuclides provide a fertile testing ground for model predictions, which indicate the existence of an especially favoured region for the formation of high-K, multi-quasiparticle isomers. These may influence the r-process pathway of stellar nucleosynthesis. Furthermore, there is the prospect of exploiting isomers as novel energy-storage devices [Walker and Dracoulis, Nature **399**, 39 (1999)].

The spontaneous decay of 31-year ^{178m2}Hf

A preliminary description of this experiment was given in the 2002 TRIUMF Annual Report. γ-rays from a 15 kBq source of the 31-year, $K^\pi = 16^+$ isomer were measured for 42 days with the 20-detector 8π spectrometer. The γ-γ-coincidence events were analyzed to produce level-scheme information. In this way, sensitivity to transitions with intensities as low as one in 10^5 parent decays was achieved. Detailed results have been published [Smith *et al.*, Phys. Rev. **C68**, 031302(R) (2003)].

The vast majority of the isomer decay proceeds by electron conversion, and the principal findings from the new measurements consist of the first unambiguous identification of direct γ-ray emissions from the 31-year isomer itself. These are 310 keV, M4, and 587 keV, E5 transitions with intensities of 15 and 6 parts in 10^5, respectively. The high transition multipolarities set new boundaries for the operation of the K quantum number, broadly in line with expectations, i.e. their reduced hindrance factors are $f_\nu \sim 100$ (per degree of K forbiddenness).

In addition, the observation of a previously unknown E2 transition, between members of the two known $K^\pi = 8^-$ bands, has enabled the testing of a band-mixing model proposed by Emery *et al.* [KVI Annual Report, 1979] with consistent results.

It is notable that the M2 decay of the 4-s, $K^\pi = 8^-$ isomer was too weak to be identified (< 1 part in 10^5) with $f_\nu > 160$.

Search for new isomers in $A = 170 - 180$ nuclides

A K-isomer research program is now under way on-line to ISAC-I, to search for predicted isomers in neutron-rich nuclides. With a 30 μA beam of 500 MeV protons incident on a natural tantalum target connected to a surface ionizer, low-energy ions were extracted at 40 keV, mass separated, and transported to the 8π spectrometer. The latter has been supplemented with a large-solid-angle, 20-element array of plastic scintillators, SCEPTAR, for electron detection. The 40 keV ions were stopped at the centre of the 8π/SCEPTAR spectrometers in a remote-controlled tape, which periodically transported the accumulated activity to a lead-shielded location. In this way, short-lived isomers and β decays could be studied with minimum interference from long-lived isobars.

Preliminary results have been reported at the RNB-6 conference [Smith *et al.*, Nucl. Phys. A (in press)]. A significant aspect has been the observation of decays from a 3 ms, $1/2^+$ isomer in ^{179}Lu. While the isomer itself is well known, the short half-life had led to the expectation that it would not be observed with the present experimental arrangement. Therefore, its identification provides valuable evidence for the sensitivity to ms isomers.

Data analysis is in progress, with an emphasis in the present data on the search for new high-K isomers in ^{178}Lu and ^{179}Lu.

Experiment 927
(^{3}He,p) as an alternative to resonant elastic scattering

(F. Sarazin, Colorado School of Mines/TRIUMF; P. Walden, TRIUMF)

The carbon-nitrogen-oxygen (CNO) cycles are thought to be the main source of energy generation in novae and X-ray bursts in their ignition phase. Under certain extreme conditions of temperature and pressure, these cycles may be broken by so-called breakout reactions such as ^{15}O(α,γ)^{19}Ne(p,γ)^{20}Na or ^{18}Ne(α,p)^{21}Na(p,γ)^{22}Na, which link the CNO cycles to the rp-process, a long sequence of proton captures and β-decays. Precise knowledge of the structure of a few states above the relevant particle threshold in the compound nuclei is required to calculate the rate of the reactions involved in the breakout of the CNO cycles and in the subsequent rp-process.

In this context, resonant elastic scattering is a very valuable tool to identify astrophysically relevant states as demonstrated again recently at ISAC/TRIUMF [Ruiz *et al.*, Phys. Rev. **C65**, 042801R (2002)]. However, it is limited to low spin states and/or resonances of relatively large width. This technique also requires already having a fairly good knowledge of the compound nucleus level scheme, so that the beam energy could be tuned to match the reaction excitation energy to that of known resonances. Experimentally, it requires time-consuming frequent beam energy changes to map out the excitation function for every state. We proposed to use the (^{3}He,p) reaction in inverse kinematics at the TUDA scattering chamber at ISAC as an alternative to elastic scattering. For proton-rich nuclei this reaction has a high Q-value, which allows the population of a wide range of states with only one beam energy.

In early December, a first beam time period was allocated at ISAC/TRIUMF, mainly to test the method at ISAC energies (max 1.73 MeV per nucleon). At these energies, the deuteron transfer is expected to proceed mainly (but not exclusively) via a compound nucleus mechanism. Two stable beam tests ($^{20-21}$Ne(^{3}He,p)$^{22-23}$Na) and one radioactive beam test (^{20}Na(^{3}He,p)^{22}Mg) were performed.

Experimental set-up

The experimental set-up consisted of a 5 mm thick LN_2-cooled ^{3}He gas cell at a pressure of 500 mbar. The entry and exit foils were 1.3 mg/cm^2 Ti foil. The target was designed, built and already used for experiments or secondary beam production [Harss *et al.*, Rev. Sci. Instr. **71**, 380 (2000)] at Argonne National Laboratory. It was shipped from Argonne to TRIUMF for the experiment.

The clear advantage of such a cold target is that for at the same operating pressure, it contains almost 4 times more ^{3}He atoms/cm^2 than at room temperature. Therefore, it allows the target to be thinner, enabling better energy resolution.

A ΔE-E system, consisting of two stacked 300 μm LEDA detectors was placed, respectively, 8.1 cm (14 cm) for the ^{20}Ne(^{3}He,p)^{22}Na experiment (for the ^{20}Na(^{3}He,p)^{22}Mg and the ^{21}Ne(^{3}He,p)^{23}Na experiments) upstream from the target covering the [123°,147°] ([138°,160°]) range in the laboratory frame. A 6 μm thick mylar foil was placed in front of the first LEDA to stop the beam ion particles which had backscattered off the Ti foils.

^{20}Ne(^{3}He,p)^{22}Na*, Q $\sim$ 5.8 MeV

The ^{20}Ne(^{3}He,p)^{22}Na*, using direct kinematics, has already been studied at various energies, including 2.8 and 3 MeV [Meynadier *et al.*, Nucl. Phys. **A161**, 305 (1971)]. The main goal of this first experiment was therefore to test the experimental set-up and evaluate the resolution obtained in inverse kinematics. The ^{3}He target was operated at room temperature. A 10^9 pps 1.73 MeV per nucleon ^{20}Ne beam was used for this first test. After about 8 hours, proton peaks were clearly seen in every strip of the silicon array. A prelim-

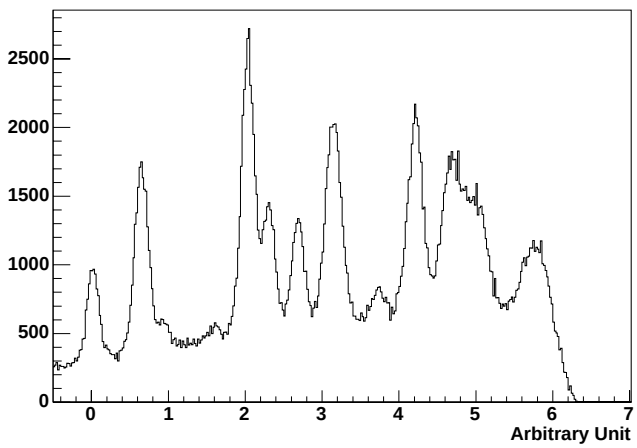

Fig. 82. Excitation function of ^{22}Na from the ^{20}Ne(^{3}He,p)^{22}Na reaction.

inary excitation function, summed over all the strips, was extracted (see Fig. 82). As observed in the direct reaction, a large number of excited states are present, which confirms the potential of the reaction to find new excited states, as it seems to populate all excited states which are angular momentum accessible. The analysis of the ΔE-E spectrum showed that only protons were recorded in the detectors.

^{20}Na(^{3}He,p)^{22}Mg*, Q $\sim$ 14.9 MeV

Following the initial success of the ^{20}Ne experiment, a 10^7 pps 1.73 MeV per nucleon ^{20}Na radioactive beam was used in the search of new states in ^{22}Mg. The precise knowledge of the level scheme of ^{22}Mg in the 5–7 MeV energy range is especially of importance for the ^{21}Na(p,γ) reaction, the rate of which is being investigated at the DRAGON facility. A very large background at low energy was observed in the detectors, due to the β-decay of the backscattered ^{20}Na implanted in the mylar foil. Another source of background was due to the β-delayed α-decay of ^{20}Na (20.5%). The energy of the alphas did not, however, overlap significantly with the energy region where the protons of interest were expected. After an initial 8 hour period, the ^{3}He target was cooled to LN_2 temperature. Although protons were clearly present from examining the ΔE-E scatter plot, no apparent structure could be seen in the accumulated energy spectrum. This suggested that the cross section for the ^{20}Na(^{3}He,p)^{22}Mg reaction was much lower than for the ^{20}Ne(^{3}He,p)^{22}Na reaction and it also suggested that the protons observed were coming from a separate distinct additional reaction. Currently, we speculate that the very significant loss of cross section is due to the larger Q-value of the reaction. A further investigation is in progress.

^{21}Ne(^{3}He,p)^{23}Na*, Q $\sim$ 11.4 MeV

In order to gather some evidence for our speculation, we switched back to stable beam, namely ^{21}Ne. The idea was to study a reaction with a somewhat lower Q-value with the advantage of the higher beam intensity offered by the use of stable beam (10^9 pps). As shown in Fig. 83, small peaks can be seen on the energy spectra. The peaks, however, sit on a much larger background than the one observed in the ^{20}Ne(^{3}He,p) data. The evident loss of cross section compared to the nearby ^{20}Ne(^{3}He,p) reaction seems to confirm the Q-value correlation with the cross section. The background was confirmed to be from a separate distinct reaction because a run without ^{3}He gas showed a similar background without the peaks (see Fig. 83).

The TUDA chamber was finally opened and the target foils examined. A large carbon build up was observed on both entry and exit foils. This carbon build up is likely to have occurred while the target was cooled and was therefore acting like a cold trap. The condensates were probably hydrocarbons which were carbonized by the ion beams. This built up as a function of time. The low background seen in our ^{20}Ne data was due to the fact that the build up had not yet occurred. As a last test, the target was replaced by a mylar foil to see if a reaction of the beam on the carbon build up was responsible for the background observed. A similar background was indeed observed.

Conclusions

Despite the apparent disappointing results of the radioactive beam experiment, much has been learned and improvements to the experimental set-up are being discussed. In particular, we are currently working towards the ^{18}Ne(^{3}He,p)^{20}Na experiment, the subject of the original (^{3}He,p) proposal, which has a Q-value (Q 6.1 MeV) comparable to our successful ^{20}Ne(^{3}He,p) test.

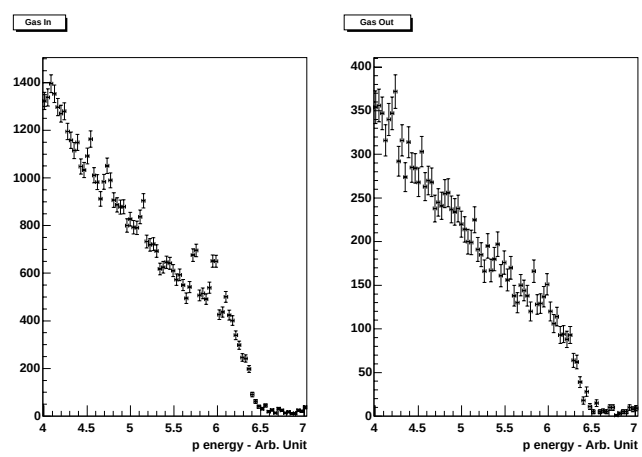

Fig. 83. Proton energy spectra obtained in the ^{21}Ne experiment. The figure on the left corresponds to runs with ^{3}He gas in the target. States in ^{23}Na can be seen although sitting on a large background. The figure on the right corresponds to runs without ^{3}He in the target, which shows that the background is due to protons unrelated to the (^{3}He,p) reaction.

Experiment 928
Level structure of ^{21}Mg: nuclear and astrophysical implications
(A. Murphy, Edinburgh)

Binary star systems are extremely interesting astrophysical phenomena due to their ability to undergo cataclysmic variability. The mechanism that drives these changes is thermonuclear runaway occurring in accreted layers of material transferred from a less evolved massive star on to the surface of its more evolved compact companion. Novae occur when the hydrogen rich outer layers of material from, for example, a red giant, are drawn off and deposited on the surface of a white dwarf companion. If the companion were instead a neutron star, the resulting detonation would occur in a much deeper gravitational potential, resulting in the hotter, faster event known as an X-ray burst. The criterion for the onset of the explosion is that the accretion rate is such that a degenerate layer builds up, which at some critical density then undergoes a thermonuclear runaway.

The rate of energy generation, and the amount of nucleosynthesis that develops, depends on the nuclear reactions that occur. A critical reaction path in novae and X-ray bursts may be breakout from the hot-CNO cycle to the rp-process and a key link in this chain is the ^{20}Na$(p,\gamma)^{21}$Mg reaction. A measurement of the ^{20}Na$(p,p)^{20}$Na reaction is able to determine many of the properties of the ^{21}Mg nucleus, and as the ^{20}Na$(p,\gamma)^{21}$Mg reaction rate is dominated by resonant contributions in these temperature regimes, such a measurement is highly important. This was the focus of Expt. 928 conducted at TRIUMF.

Accurate knowledge of the excited states of the ^{21}Mg nucleus are also of interest from a nuclear structure perspective. Properties may be compared to those of isobaric analogue states, allowing a study of the Thomas-Ehrman shifts to be made. Similarly, comparisons to predictions of recent shell model calculations will aid theoretical descriptions of proton-rich nuclei of similar masses. Finally, previous measurements of this and similar reactions have had to be made without the capabilities afforded by radioactive beam facilities such as TRIUMF. Consequently, indirect reaction techniques had to be applied, and conclusions drawn from complex model-dependent analyses of the reaction. Comparison of the data from this measurement with those of previous data sets will allow an assessment of these previous indirect techniques.

In order to determine the parameters of resonant states in ^{21}Mg, resonant elastic scattering of protons was employed. Experimentally, this consisted of impinging a radioactive ^{20}Na beam on to a hydrocarbon foil, and then detecting the recoil protons. The beam was generated by ISAC, using a primary silicon-carbide target with a driver beam of typically 20 μA of 500 MeV protons. Typical beam currents on target in the TUDA chamber were a few pA, and during the experiment beam energies of 1.25 MeV/u and 1.60 MeV/u were requested. Accurate confirmation of the beam energies was assured by making measurements with the Prague magnet and then cross checking with the DRAGON spectrometer. This consisted of sending the beam in to each device and focusing the beam on to a set of exit slits (after the first magnetic dipole in the case of DRAGON), and then measuring each independently calibrated field. For the higher beam energy, where the field of the DRAGON MD1 magnet was unable to sufficiently bend the beam, this required first introducing gas in to the DRAGON target volume to slow the beam. Measurements of the required magnetic field were performed with various pressures of gas, and an extrapolation to zero gas pressure made. In all cases, an agreement between the beam energy measured with the Prague magnet and with DRAGON of $\sim$1 keV/u was observed.

The target consisted of $\sim$795 μg/cm^2 of CH_2. Since the projectile loses a significant fraction of its energy in passing through such a thick target, the elastic reactions can occur over a wide range of energies, allowing an excitation function over a range of energies to be measured in a single experiment. For the lower beam energy, reactions can occur at $\sim$0.51–1.20 MeV in the centre-of-mass, and for the higher beam energy between $\sim$0.91–1.54 MeV, covering much of the astrophysically and structurally important resonances. Detection of the recoiling protons was achieved in two LEDA-design silicon detector arrays. These were placed downstream of the target at 19 and 62 cm.

Analysis of the data is ongoing. Various inconsistencies in calibration data have been resolved, and the data from the near detector are ready to be subjected to an R-matrix analysis. Progress on data from the farther detector is likewise expected. A multi-channel R-matrix code appropriate for the analysis of these data has been successfully developed at TRIUMF to support another experiment (Expt. 879) and is expected to be employed soon.

Experiment 929
Toward radon electric dipole moment measurements at ISAC
(T.E. Chupp, Michigan; C. Svensson, Guelph; J.A. Behr, M. Pearson, TRIUMF)

As a precursor to measurements of time-reversal violating electric dipole moments, Expt. 929 began tests of manipulating radioactive xenon beam in August. We demonstrated transfer of 40% of the ISAC beam into

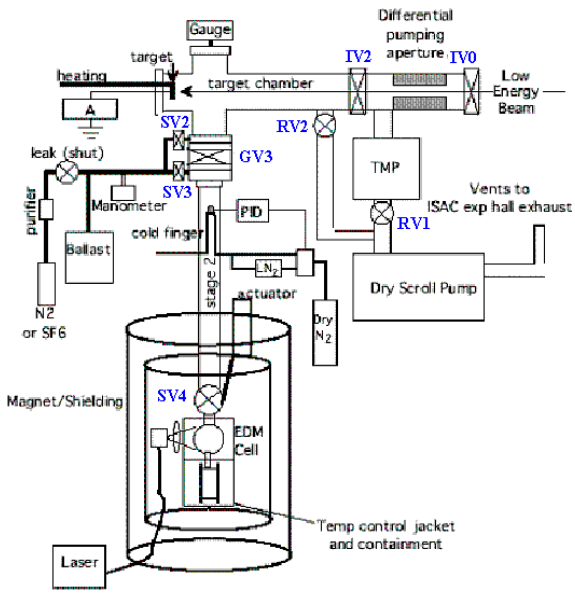

Fig. 84. Side view schematic of Expt. 929 test set-up at the GP2 station.

the form of xenon atoms in a mock-up of an eventual EDM cell.

The method is demonstrated in Fig. 84. We stop a ^{120}Cs beam from the ISAC surface source in a thin foil catcher. We irradiate for two half-lives of the ^{120}Xe daughter, isolate the system, and heat the catcher by direct current to release the Xe. We freeze it onto a cold finger at LN_2 temperature. Then we isolate this section, warm up the cold finger, and push the Xe efficiently into the cell with a burst of 1 atm of nitrogen buffer gas. The activity was monitored at all stages by Ge detectors. The cryogenic and gas push techniques are being written up for publication. Diffusion constants of xenon in platinum, tantalum, and zirconium foils were also measured and are shown in Fig. 85 and being prepared for publication. The control system, vacuum system, and diffusion measurements formed the senior thesis of Tim Warner of SFU.

These techniques should be applicable to radon atoms once they are available at ISAC.

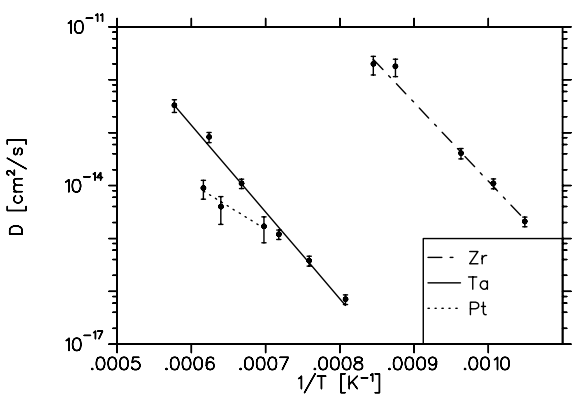

Fig. 85. Diffusion of Xe in Pt, Ta, and Zr foils.

Experiment 947
Evaluation of the competition beween single-step and multi-step γ decay in the ^{12}C(^{12}C,γ) reaction

(D. Jenkins, York)

Heavy ion radiative capture

Experiment 947 is intended to answer long-standing questions concerning the possibility of molecular-like configurations in nuclei. The ^{12}C+^{12}C system has long been regarded as the exemplar of the nuclear molecule hypothesis. Anomalous structures in the elastic and inelastic scattering of ^{12}C+^{12}C were explained in terms of the occurrence of short-lived molecular configurations. The heavy ion radiative capture reaction, ^{12}C(^{12}C,γ) affords another perspective on the molecular hypothesis. Sandorfi and Nathan [Phys. Rev. **C24**, 932 (1981)] found that this reaction was strongly resonant with a total capture cross section of less than 1 μb (see Fig. 86). They employed a large single-crystal sodium iodide detector to observe capture to the first few low-lying states in ^{24}Mg. This decay mechanism was attributed to a coupling to the GQR strength in ^{24}Mg. Due to pile-up of low-energy γ-rays in the NaI detector, it was not possible to answer the important question of whether a substantial proportion of the capture decay might be mediated through high-lying doorway states in ^{24}Mg. This is especially topical as these doorway states are likely to be highly deformed since they are intermediate between the molecular-like entry

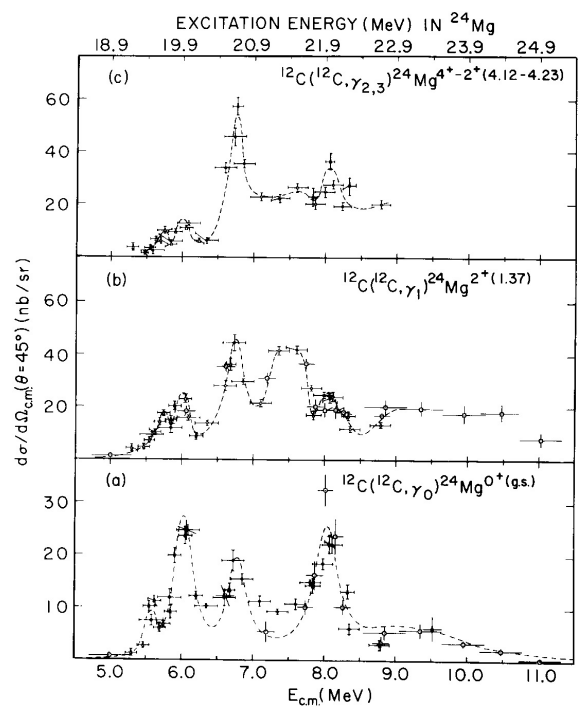

Fig. 86. Excitation functions for ^{12}C(^{12}C,γ) measured by Sandorfi and Nathan.

state and the well-deformed ground state of ^{24}Mg.

Ongoing research

We have reopened the issue of heavy ion radiative capture with a series of measurements using the Gammasphere array of HPGe detectors at Argonne National Laboratory. These measurements strongly suggest that multi-step decay is, indeed, the predominant mechanism and that the total capture cross section is significantly larger than was previously believed. These studies, however, were complicated by the very poor efficiency of the Gammasphere array for the high energy (10–20 MeV) γ-rays involved in the capture mechanism.

Role of DRAGON

The unique combination of the DRAGON separator and its associated BGO detector array allows us to explore the full phase space for the decay mechanism by detecting the high energy capture γ-rays in coincidence with ^{24}Mg fusion residues. In order to perform these measurements, a solid target mechanism was designed and built for installation at the target position of DRAGON. An initial week of data was taken in November, at a beam energy corresponding to the resonance previously observed at a centre-of-mass energy of 8.0 MeV (see Fig. 86). It was possible to cleanly separate and identify ^{24}Mg residues at the focal plane. Moreover, high energy γ-rays were detected in coincidence with these residues. It should be noted that the recoil kick imparted by the high energy γ-rays means that depending on the angle of emission, only a fraction of the residues make it into the acceptance of the separator. This effect is qualitatively understood and is presently being modelled using the Monte Carlo modelling package, GEANT. This will allow absolute cross sections for the different decay pathways to be obtained from the observed γ-ray coincidences.

Future plans

The initial measurements have been very promising and it is planned to run for a further two weeks in early 2004, when we hope to cover lower energy resonances in the ^{12}C+^{12}C system.

Experiment 948
Proton and neutron radiation effects in silicon-on-insulator and bulk-silicon devices

(J.R. Schwank, Sandia National Laboratories)

Introduction

The primary goal of these experiments was to investigate proton radiation-induced effects on silicon-on-insulator and bulk-silicon devices for space applications. The proton energy range available at TRIUMF ($\sim$20 to 500 MeV) is well matched to the energy spectrum of protons in space. The experiments were divided into four main tasks: 1) the investigation of proton-induced single-event effects in advanced SRAMs, 2) investigation of the effects of proton-induced displacement damage on the single-event latchup rate, 3) evaluation of TRIUMF's neutron source capability for simulating the terrestrial neutron environment, and 4) determination of the optimum laboratory radiation source for simulating the space environment.

Single-event effects

One of the most detrimental effects of the natural space environment on electronics is single-event effects (SEE). In memory circuits, information is stored at nodes in a circuit. If a high-energy heavy ion strikes a circuit node, it can create sufficient charge in a transistor to change the state of the node and cause false information to be stored. This type of failure is a non-destructive soft error and is known as a single-event upset (SEU). In addition to heavy ions, protons and neutrons can also cause single-event upset.

This year at TRIUMF, we performed several experiments investigating proton and neutron induced SEE in silicon-on-insulator and bulk-silicon ICs. Proton experiments were performed to investigate proton-induced SEE in advanced SRAMs. We also investigated the dependence of single-event upset cross section on angle of incidence by comparing front versus back-side exposure. Neutron experiments were performed to evaluate TRIUMF's newly developed neutron capability as a source for investigating the effects of terrestrial neutron exposure on commercial ICs. We also performed proton experiments to investigate the effects of proton-induced displacement damage and total-dose effects on the single-event latchup rate in SRAMs.

Space does not permit showing all of the test results. Two of the interesting studies are described here.

Evaluation of TRIUMF's neutron facility (TNF)

The TRIUMF neutron facility (TNF) comprises one of the neutron channels located at the high power beam dump. At this dump typically 100–150 μA of 450–500 MeV protons are stopped after passing through meson and isotope production targets. A track with a pulley system was installed in a vertical access channel to allow measurement instrumentation to be lowered to neutron beam level. Devices to be tested or activation foils are mounted on a trolley plate, which can be accurately placed in the beam.

To confirm the suitability of the TRIUMF neutron irradiation facility for terrestrial cosmic ray soft error rate (SER) characterization, 5 different SRAM types were irradiated that had previously been characterized at the Los Alamos National Laboratory Weapons Neutron Research (WNR) facility.

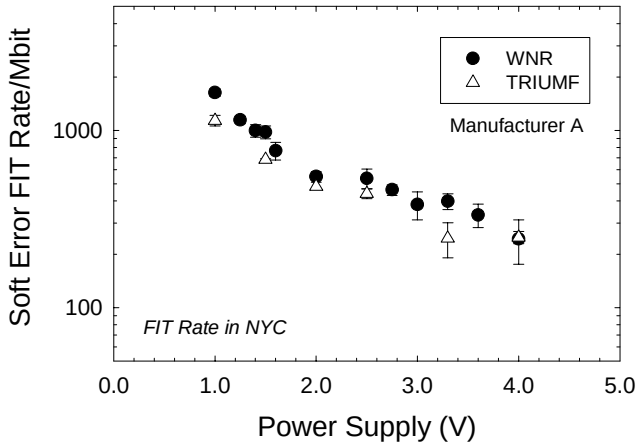

Fig. 87. Neutron-induced SER in 1.5/3.3 V 6T full CMOS 1 Mbit SRAMs from manufacturer A's 0.16 μm process as a function of power supply voltage. Ground-level FIT rates are shown for New York City.

Figure 87 shows the measured SER in 6T CMOS 1 Mbit SRAMs from manufacturer A's 0.16 μm process as a function of power supply voltage. The TRIUMF data are in reasonably good agreement with previous WNR tests, but appear to be systematically 10–30% lower than the SER calculated from the WNR data.

In contrast to the WNR neutron spectrum, the continuous neutron spectrum in the TNF includes a contribution from thermal neutrons. It has previously been shown that some ICs are sensitive to thermal neutrons, especially those whose construction incorporates boron-10. In Fig. 88, the neutron-induced SER in a 5 V 4 Mbit SRAM from a third manufacturer is plotted as a function of power supply voltage. Previous experiments have shown that this SRAM is sensitive to thermal neutrons. Data were taken at TRIUMF using both the unmoderated spectrum, and with a sheet of cadmium covering the SRAMs to remove all thermal neutrons. At low supply voltages, the unmoderated TRIUMF data lead to a calculated SER about a factor of two higher than with the cadmium sheet, indicating a significant enhancement in SER due to thermal neutrons at these voltages. In contrast, data taken with the cadmium sheet in place match the scaled WNR data at all voltages, indicating successful removal of the thermal neutron flux.

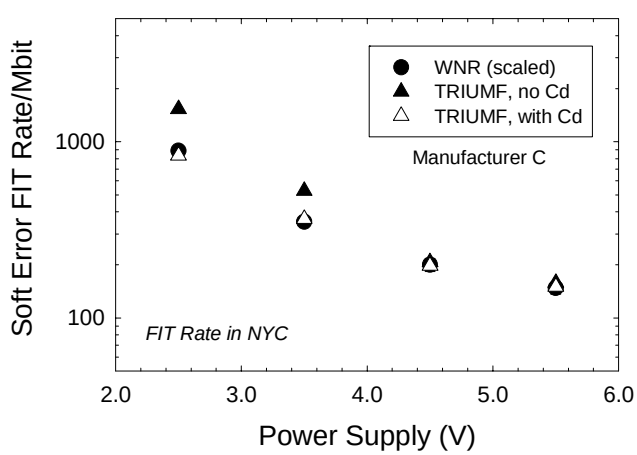

Fig. 88. Neutron-induced SER vs. power supply voltage in 5 V 6T TFT-load 4 Mbit SRAMs from manufacturer C. The WNR data were multiplied by 0.75 to match the TRIUMF data. Note increased SER at low power supply due to thermal neutron contribution in unmoderated TRIUMF spectrum.

Total dose hardness assurance

The energetic electrons and protons of the space environment will generate radiation-induced charge in the gate and field oxides of bulk-silicon and silicon-on-insulator (SOI) devices. This charge buildup can cause parametric and/or functional failure of ICs. Recent works have demonstrated that proton degradation is more accurately simulated by X-ray irradiation, over a wide range of proton energies. Similarly, Co-60 gamma degradation was also shown recently to match electron degradation. This raises concerns about what laboratory source is best for qualifying bulk-silicon and SOI devices for space environments.

The work that we performed this year at TRIUMF culminates a three-year effort to determine the optimum laboratory radiation sources for qualifying bulk-silicon and SOI devices for space environments.

The samples were irradiated with 10 keV X-rays, Co-60 γ-rays, 41.4 MeV protons, and 1 MeV electrons, in the ON bias configuration ($V_G = 5$ V). During total dose irradiation, radiation-induced positive charge builds up in the field oxide. This charge buildup can turn on the lateral parasitic transistor structure, revealed by an increase in leakage current (drain current at $V_G = 0$ V). The results are displayed in Fig. 89,

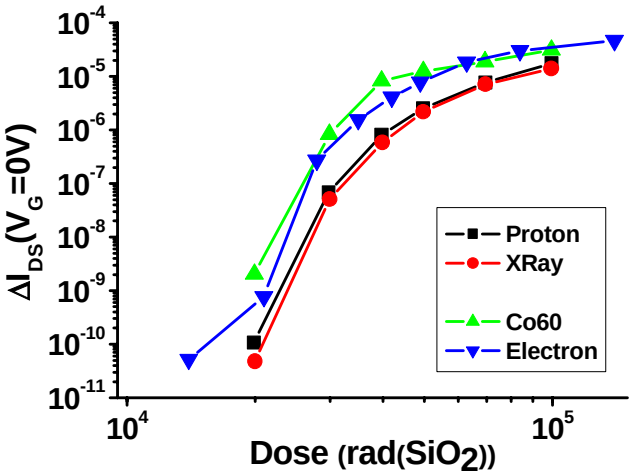

Fig. 89. Radiation-induced increase in leakage current (drain current at $V_G = 0$ V) versus total dose, for non-hardened bulk-Si transistors irradiated with 10 keV X-rays, 41.4 MeV protons, Co-60 γ-rays, and 1 MeV electrons. The transistors were irradiated with ON bias configuration.

where the increase in leakage current of the bulk-silicon transistors is plotted for the different radiation sources.

For the different technologies investigated here, the total dose degradation caused by protons with energies up to 200 MeV is well simulated by 10 keV X-ray irradiation, and the total dose degradation caused by 1 MeV electrons is well simulated by Co-60 γ-ray irradiation.

This work has been published in IEEE Trans. Nucl. Sci. **50**, 2310 (2003).

Experiment 952
A new measurement of ^{12}C(α,γ)^{16}O reaction
(L. Buchmann, TRIUMF)

The ^{12}C(α,γ)^{16}O reaction determines the ratio of oxygen to carbon in the universe, among other things. Yet it is one of the remaining reactions in nuclear astrophysics of high relevance which is rather poorly determined. The reason is that there are no compound states of natural parity in ^{16}O at the energies corresponding to quiescent helium burning. In fact, there is a complex mixture of ground state and cascade transitions of different types.

The difficulty in determining this cross section so far has been the complexity of extrapolation combined with the overall low cross sections. In measurements of the emanating γ-rays considerable backgrounds are also encountered. In Exp. 952 it has therefore been proposed to measure both recoil particles and γ-rays in coincidence with the DRAGON facility at TRIUMF. Given acceptance restrictions of DRAGON, we decided to measure the high energy region first, roughly defined as energies above the first 4^+ state at E = 10.36 MeV. At these energies the cross section of the cascade transition into the E = 6.9 MeV state, which is a subthreshold state important for determining the reaction rate, is directly proportional to the α strength of that 6.9 MeV state [Buchmann, Phys. Rev. **C64**, 022801(R) (2001)]. In addition, the transition to the ground state is most likely of pure $E2$ nature, contrary to lower energies, where the $E1$ transition is dominant.

We have made runs in April/May and November. We covered energies from 0.75 MeV/u to 1.5 MeV/u (E = 2.25–4.5 MeV). In summary, we made the following observations:

- The recoil spectra are free of background. As an example, Fig. 90 shows the single recoil and the coincidence γ spectrum of the 1.07 MeV/u 4^+ resonance.
- The ^{12}C beam current which can be delivered by using a carbon stripper is marginal (about 50 pnA), still big enough though to obtain events at the lowest measured energy. However, the data require information about angular distributions and fits to cascade data, i.e. acceptable statistical accuracy.
- The acceptance of DRAGON is challenged for the present configuration given the recoil angle involved in the ^{12}C(α,γ)^{16}O reaction. We found, however, sextupole polarities to be corrected and a more symmetric tune which, as tests have shown, delivers full transmission through DRAGON at higher energies.
- The angular recoil distribution for the ground state shows up very nicely in the energetic distribution of the recoil particles and thus delivers this crucial angular distribution with far better resolution than can be obtained from the BGO array of DRAGON.
- There is clear evidence for a cascade transition to the E_x = 6.05 MeV state in ^{16}O (see Fig. 91 for an example spectrum).
- Between the first and second 4^+ resonance cascade transitions are clearly dominant.

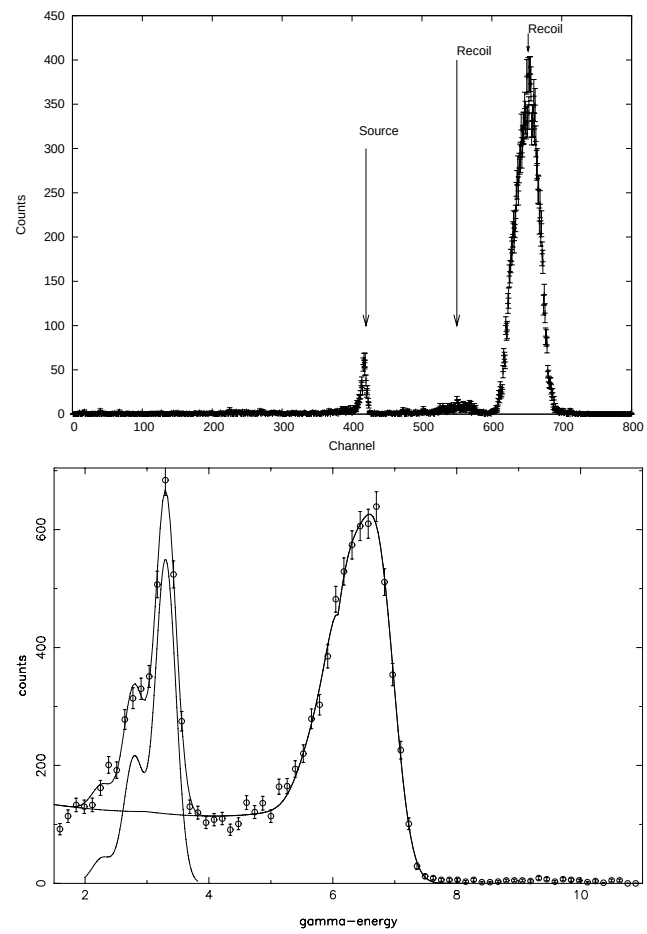

Fig. 90. Upper panel: Single recoil spectrum in E = 3.2 MeV resonance. Lower panel: γ spectrum gated by the recoil events of the upper panel. A fit to the cascade decay over the 6.9 MeV state is also shown.

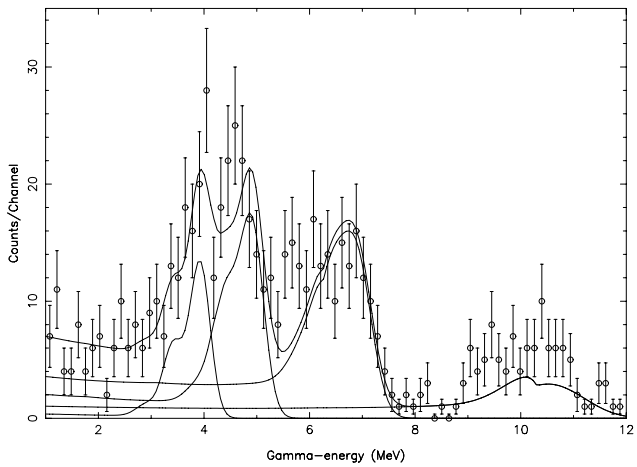

Fig. 91. Recoil gated γ-spectrum taken at 1.28 MeV/u and fit to its components. The primary transition to the 6.05 state is visible at 4.95 MeV.

Recently it has been demonstrated that the energy of the ISAC-DTL can be increased for a ^{12}C beam to 1.83 MeV/u. This will allow us to cover the E_x=12.440 MeV 1^- resonance which has a strong ground state $E1$ transition with its characteristic angular distribution centred around 90°. This will provide an acceptance test and a possible confirmation of our GEANT calculations of DRAGON which are in progress.

Experiment 955
Study of the β-decay of ^{32}Na
(F. Sarazin, Colorado School of Mines; G. Hackman, TRIUMF)

The structure of stable and long-lived nuclei is well understood in terms of the traditional magic numbers (2, 8, 20, 28, 50...) corresponding to large gaps in single-particle energy levels of nucleons in realistic mean-fields including a spin-orbit interaction. The evolution of shell closures far from stability is, however, a subject of much debate [Werner *et al.*, Phys. Lett. **B335**, 259 (1994); *ibid.*, Nucl. Phys. **A597**, 327 (1996)]. For example, a breaking of magicity has already been observed at the N = 20 shell closure, where an "island of inversion" in shell ordering has been shown to exist [Orr *et al.*, Phys. Lett. **B258**, 29 (1991); Warburton *et al.*, Phys. Rev. **C41**, 1147 (1990); Retamosa *et al.*, Phys. Rev. **C55**, 1266 (1997)]; more recently this has been seen at N = 28 for neutron-rich nuclei [Sarazin *et al.*, Phys. Rev. Lett. **84**, 5062 (2000)]. While understanding the apparent weakening or disappearance of the traditional shell closures far from stability is a challenge for nuclear structure, it also has very important implications in nuclear astrophysics, as it will significantly affect the path of the r-process. In this context, a proposal for this experiment was submitted to the EEC in 2002 to probe the shell structure with β- and β-delayed γ-spectroscopy at ISAC/TRIUMF. The first nucleus studied was ^{32}Na, which β-decays to ^{32}Mg, a key N = 20 nucleus. The main goal of this experiment was to resolve some discrepancies observed in the ^{32}Mg level scheme. Two beam time periods (August 17–20 and October 8–17) in 2003 were allocated for the study of the β-decay of ^{32}Na.

The ^{32}Na beam was extracted from a tantalum production target and implanted onto a moving tape at the centre of the 8π/SCEPTAR facility described in the Experimental Facilities section of this Annual Report. In the course of the experiment, the intensity of the proton beam impinging the production target was increased from 40 μA to 50 μA. An estimated 2 ^{32}Na atoms per second was delivered to the 8π. At this very low rate, the combination of the 8π, SCEPTAR and tape system has shown its potential to produce very clean spectra. Several time cycles of the tape system were used in order to remove, efficiently, the build-up of the long-lived daughters of ^{32}Na.

γ-ray energy spectra from the first period are shown in Fig. 92. A significant part of the beam time during this test period was spent on optimizing ISAC optics settings. No new γ-ray lines were seen during this period. However, it clearly demonstrated the potential of the experimental set-up for seeing transitions in nuclei produced with very low yield.

The main data set (October 8–17) is currently being analyzed. Spectra obtained on-line show some previously unreported lines in the ^{32}Na spectrum. However, their placement in a decay scheme requires a more thorough analysis. A preliminary spectrum is shown in Fig. 93. The identified lines are transitions known or believed to originate from the γ-decay of ^{32}Mg following the β-decay of ^{32}Na.

This collaboration includes scientists from TRIUMF, Colorado School of Mines, McMaster University, University of Guelph, Queen's University, Lawrence Livermore National Lab, Lawrence Berkeley National Lab, Georgia Institute of Technology, Louisiana State University, University of Surrey, and University of Vienna.

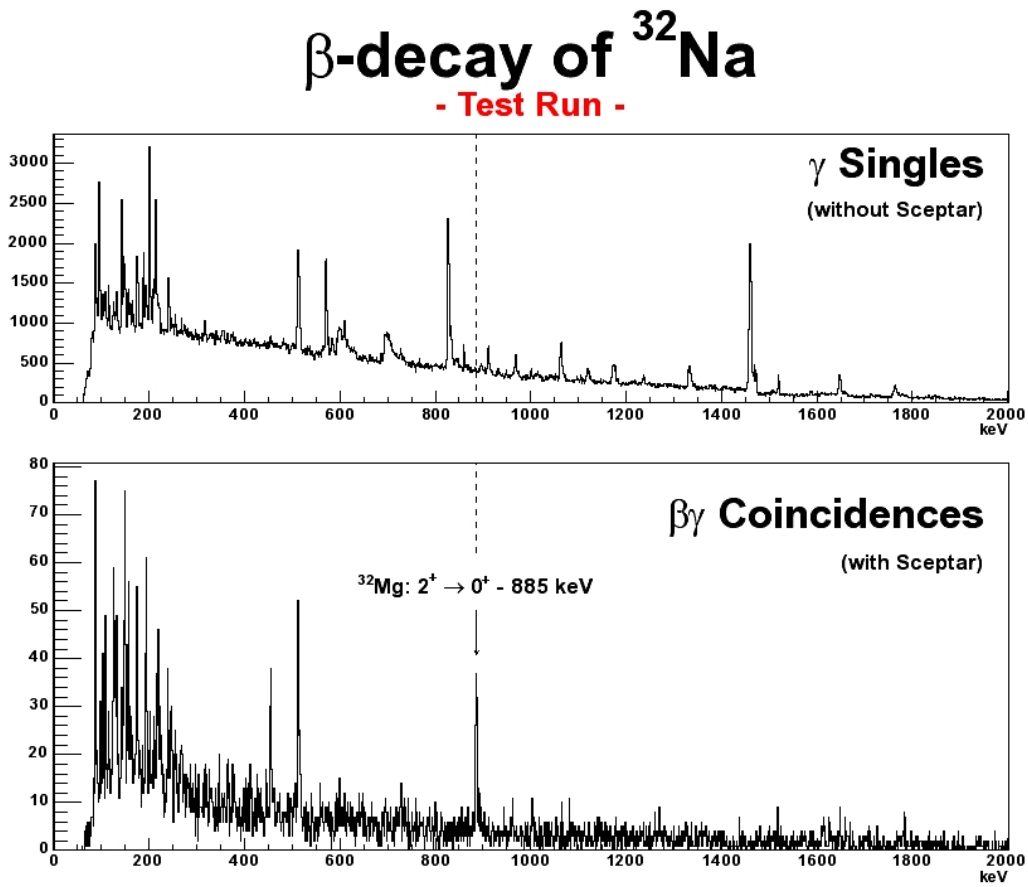

Fig. 92. Top: unconditional γ-ray spectrum; bottom: γ-ray spectrum in coincidence with βs detected in SCEPTAR, demonstrating the resolving power of the experimental set-up.

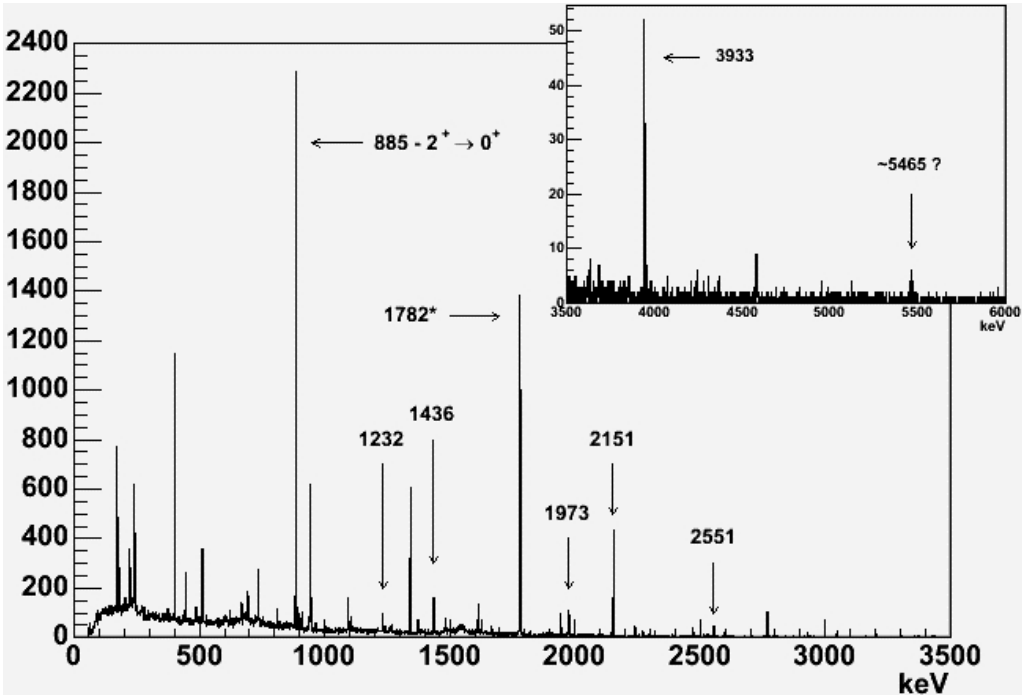

Fig. 93. (VERY PRELIMINARY) β-decay of ^{32}Na. The identified γ lines correspond to the decay of excited states of ^{32}Mg. The * sign indicates that the actual 1782 keV transition is part of a more pre-eminent transition coming from a contaminant. The ? sign indicates a possible new transition in ^{32}Mg.

Experiment 964
A study of the partial and total cross sections of the ^{8}Li$(\alpha, n)^{11}$B at astrophysically relevant energies
(A. Laird, York; P. Walden, TRIUMF)

The precise measurement of the ^{8}Li$(\alpha, n)^{11}$B cross section is an important measurement to know in the astrophysical sense. This reaction is deemed to play an important role in initiating r-process nucleosynthesis in core collapse supernovae, and in the production of light elements abundances in inhomogeneous big bang models (IBB). It is one of the few reactions that can play a key role in spanning the mass 8 gap and as such should be known and well determined. Cross section measurements to date have either large error bars or are conflicting.

The proposed experiment will measure the cross section directly in a large solid angle ion chamber which will be constructed. The future chamber has been designated with the name TACTIC (TRIUMF annular chamber for tracking and identification of charged particles). The experiment will be done with reversed kinematics using a ^{8}Li RIB beam from ISAC. Both the production of ^{11}B ions in the ground state and excited states would be identified. The excited states would be further selectively defined by a coincidence between the ion detection and the γ-ray picked off in an array of gamma detectors surrounding the chamber (the array will be initially borrowed from DRAGON).

The TACTIC concept is a specially designed cylindrical symmetrical ion chamber enclosing a full length cylindrical target with a larger diameter ion drift region. The dimensions of the chamber will be approximately 20 cm in length by 10 cm in radius. The size of the chamber and gas pressure used in TACTIC will be such that the ^{11}B ions will stop. The ion collectors will be mounted along the cylinder's outside radius to give "l" and "ϕ" coordinates. Drift time with respect to the ISAC accelerator rf will give the "r" coordinate. The path of the ion will thus be mapped out. The signal strength will be proportional to the dE/dx and will identify the ion type (e.g. ^{11}B or an elastically scattered α or ^{8}Li). The chamber as designed will not be just for one specific experiment. It can be used for other measurements. One experiment of significance that could use the TACTIC geometry is measurements of ^{12}C(^{12}C,α)^{20}Ne and ^{12}C(^{12}C,p)^{23}Na fusion which are key reactions for understanding supernova type Ia events.

We have been experimenting with GEM signal amplification technology and have aquired several samples of GEM material to this end. A planar GEM chamber is to be constructed and tested. A cylindrical GEM chamber will be manufactured for the next stage. A VME card has been acquired which has a 50 MHz sampling rate. The same card can be used for time and ADC extraction. Significant progress on the chamber is expected in 2004.

Experiment 967
Beta decay branching ratio of ^{21}Na
(S.J. Freedman, UC Berkeley-LBNL)

Our recent measurement of the β-ν correlation coefficient in the beta decay of laser trapped ^{21}Na, $a_{\beta\nu} = 0.5243 \pm 0.0092$, differs by 3.6 σ from the standard model prediction of $a_{\beta\nu} = 0.558 \pm 0.003$ [Scielzo *et al.*, submitted to Phys. Rev. Lett.]. The uncertainty in the decay branching ratio to the excited state of ^{21}Ne ($5/2^+$) is the largest systematic uncertainty in the measurement.

The current accepted value of the branching ratio is 0.0502(13). This is in agreement with shell model estimates of 0.05(1), but there are large disagreements among previous measurements (see Fig. 94). The resulting systematic uncertainty in the ^{21}Na experiment is 0.7% in $a_{\beta\nu}$. Reducing the uncertainty in the branching ratio by a factor of 3 to a relative uncertainty of 1% will allow us to determine the β-ν correlation more accurately.

All previous measurements of the branching ratio used the ratio of 350 keV γ-rays which tag ^{21}Ne ($3/2^+ \rightarrow 5/2^+$) to 511 keV γ-rays which tag all ^{21}Na $\rightarrow$ ^{21}Ne decays. They suffered from the presence of β^+ emitting contaminants. We are working on a different approach, taking advantage of recent developments in radioactive beams. The ISAC facility at TRIUMF is used to obtain a pure ^{21}Na beam with <0.1% contaminants. The technique counts individual accelerated ^{21}Na ions stopped in a thin scintillator and compares the particle number to the number of

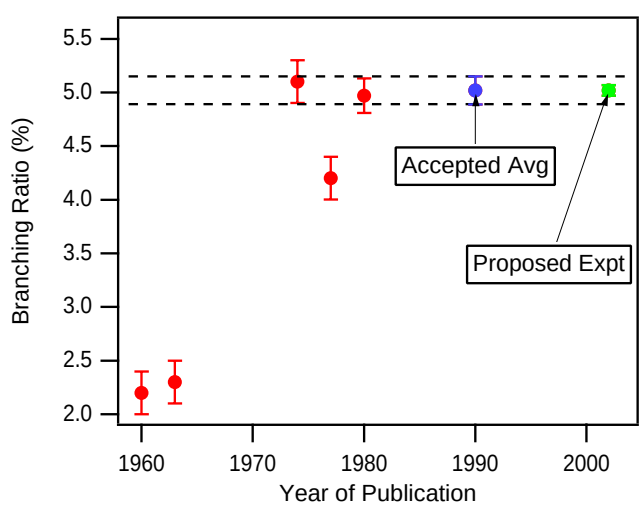

Fig. 94. Previous measurements of ^{21}Na decay branching ratio to the excited state of ^{21}Ne.

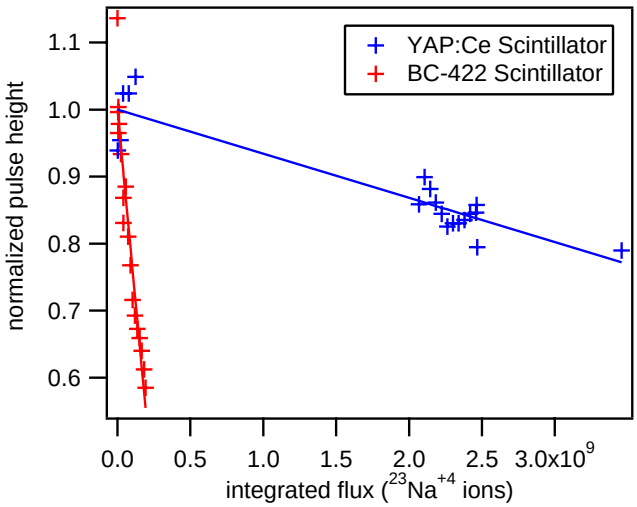

Fig. 95. Pulse height vs. number of incident ^{23}Na on YAP:Ce and BC-422.

350 keV γ-rays detected by a calibrated high purity Ge detector. The beam count rate of 10^5–10^6 ions/s is used to prevent pile-up. A total of 10^9 particles on target is required to reach the proposed sensitivity.

During the 2003 run, a plastic scintillator (BC-422) of 100 μm thickness was used. The rate of degradation of this scintillator due to radiation damage was unacceptably high. For the next run, we will use a YAP:Ce crystal scintillator which has been measured to have a higher radiation damage threshold by a factor of roughly 100 for γ-rays. A recent test at the LBNL 88 in. cyclotron using stable Na beam at similar energies of 1 MeV/u indicates that YAP:Ce is roughly 30 times more durable to heavy ion radiation damage than BC-422, and the damage will be limited for the dose required by this experiment (see Fig. 95).

Experiment 968
Ortho-para effect of muon catalyzed fusion in liquid deuterium; R&D of fusion neutron detection
(H. Imao, N. Kawamura, K. Nagamine, KEK)

The high resonant formation rate of ddμ in condensed deuterium has been one of the biggest problems in muon catalyzed fusion in pure deuterium (dd-μCF). In order to solve this problem, a detailed understanding of the behaviour of muonic atoms and muonic molecules in condensed deuterium is necessary. Especially, the study of the ortho-para effect on μCF in condensed deuterium can provide much information to reveal the effects in condensed matter. However, the experimental study of the orhto-para effect on dd-μCF was carried out only in a solid [Toyoda *et al.*, Phys. Rev. Lett. **90**, 243401 (2003)]. The experimental ortho-para effect shows the opposite tendency against recent theoretical predictions. A futher investigation on the ortho-para effect in a wide temperature range can throw light on μCF phenomena. The aim of Expt. 968 is the observation of the dependence of the molecular formation rate and the hyperfine transition rate on the ortho-para states of deuterium in liquid and solid. To reach this goal, we have to obtain the time distribution of fusion neutrons for each state. The R&D of the fusion neutron detection system was performed with liquid normal deuterium at 19 K in November.

The experiment was performed on beam line M9B at TRIUMF. Our experimental set-up consists of the target cell in the vacuum chamber, the muon beam counters, neutron detectors, electron counters, a continuous-flow liquid cryostat and a gas handling system (GHS). The schematic view of our experimental set-up is shown in Fig. 96. The target cell was a cylindrical copper (2 mm thick) container, 30 mm in diameter, 30 mm in length and with a volume of 20 cc filled with liquid deuterium. Deuterium target status was monitored by measuring temperature and vapour pressure. In this run, we controlled the temperature of the liquid deuterium target at 19 K. The target gas was prepared by GHS, which is connected to the target cell. We used only normal deuterium gas, and the ortho-para conversion system was not used in this run. A μ^- beam was injected into the liquid target through the three collimators, of which the inner diameters were ϕ50 mm, ϕ30 mm and ϕ25 mm, respectively.

The muon incoming signal was created by the coincidence of the signals of two muon beam counters (B1, B2). A 60 MeV/c μ^- beam was used in the November run. One of the other detector signals coincident with the muon beam makes an event trigger and opens a 10 μs gate for data-taking. In order to eliminate the pile-up, the following condition is required: no muon incoming 10 μs before the event trigger, no subsequent muon incoming during 10 μs event gate. This condition reduces the background and suppresses distortion of the time spectra due to pile-up.

Muon decay electrons were detected by four pairs of plastic scintillation counters (E1–E8) placed around the target in order to determine the muon's topping distribution. E1–E4 counters had a ϕ5.5 cm

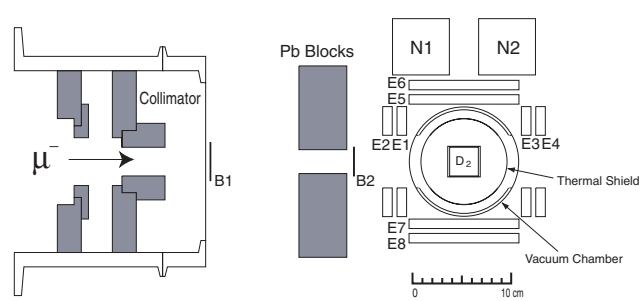

Fig. 96. Cross-sectional view of the experimental set-up in the November run.

hole at the centre for the muon entry. The timing and pulse height of coincidence signal from each pair of counters were recorded. As a neutron detector, $\phi 2$ in. $\times$ L2 in. NE-213 viewed by a photo-multiplier (Hamamatsu H1161) was used. NE-213 was chosen for its pulse shape discrimination properties. We placed two neutron detectors (N1, N2) at 10 cm from the target perpendicular to the μ^- beam. Charge-veto for neutron detection was not necessary because of the perpendicular position. For discrimination between gammas and neutrons, a pulse shape analyzer (Ortec PSA552) and a delay line amplifier (Ortec DLA460) were adopted. The time difference of the output signals from the DLA module, which reflects the pulse shape, was recorded. The energy scale of the neutron detector was calibrated by the Compton edges of two gamma sources (^{60}Co and ^{137}Cs).

The method for analysis of neutron data is essentially the same as Knowles' method [Knowles *et al.*, Phys. Rev. **A56**, 1970 (1997)]. The neutron events consist of fusion neutrons, n_f, capture neutrons, n_c, and neutrons from ambient background, n_z. In order to obtain the fusion neutron spectra, the pulse-shape discrimination gate, the pulse-height cut, and the delayed electron coincidence condition (del_e condition) with the efficiency ϵ_e were demanded. The pulse height window was chosen as 0.4–0.7 MeV electron energy scale (Fig. 97). The del_e condition was satisfied if the muon decay electron was detected between 0.2 and 5.0 μs after the time of a candidate of fusion event. The time window efficiency includes the detector solid angle, Ω_e, as given by

$$\epsilon_e = \Omega_e \lambda_0 \int_{0.2\ \mu s}^{5\ \mu s} d\tau e^{-\lambda_0 \tau}.$$

The raw neutron spectra, n_r, and del_e spectra, n_{del_e} are given by

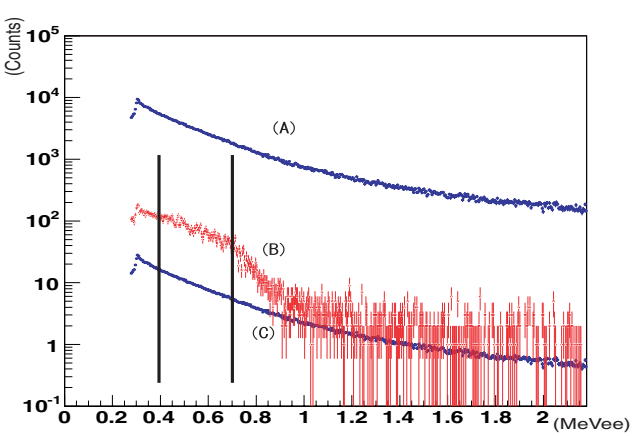

Fig. 97. Pulse height spectra without (A) and with del_e condition (B) and accidental neutron spectra (C) in the deuterium target run. A pulse height cut was chosen, selecting events between the solid vertical lines.

$$n_r = n_f + n_c + n_z,$$

$$n_{del\_e} = \epsilon_e n_f + \epsilon_a n_r + \left(\Omega_e \lambda_\circ \int_{t+0.2\ \mu s}^{t+5.0\ \mu s} d\tau\, \Theta(\tau - t_0) e^{-\lambda_\circ(\tau - t_0)} \right) n_z\ ,$$

where ϵ_a is accidental efficiency. The del_e condition strongly suppressed capture neutron background. As a result of these demands, the overall background was reduced to 10% for the fusion neutron measurement. Remaining background consists mainly of capture neutrons due to muon stops in the target cell.

Figure 98 is typical fitting results of neutron time spectra. The resonant ddμ formation rate and hyperfine transition rate are determined to be $\tilde{\lambda}_{3/2}$ = 2.6±0.1(stat.)±0.2(syst.) and $\tilde{\lambda}_{3/21/2}$ = 32.0±1.3(stat.)±0.3(syst.), which are consistent with other recent measurements [Demin *et al.*, Hyp. Int. **101/102**, 13 (1996)]. The muon loss rate by muon transfer process to impurities in the deuterium target was negligible in this run. This fact shows that some frozen impurities are deposited at the bottom in the liquid state target, and thus suppress the muon transfer process to the impurities. In the analysis, the empirically-based non-resonant molecular formation rate was used; $\lambda_{1/2}$ = 0.044±0.005 [Scrinzi *et al.*, Phys. Rev. **A47**, 4691 (1993)]. In order to determine the absolute value of molecular formation rates, the calculations for the neutron detection efficiency and the muon stopping number in the deuterium target are performed.

Measurement of time distribution of fusion neutrons was carried out in liquid deuterium at 19 K. The results show that our neutron detection system can observe a few per cent difference of $\tilde{\lambda}_{3/2}$ and also $\tilde{\lambda}_{3/21/2}$ between ortho-rich and normal deuterium within our requested beam time. Toward the ortho-para experiment in August, 2004, many studies of ortho-para conversion are being promoted.

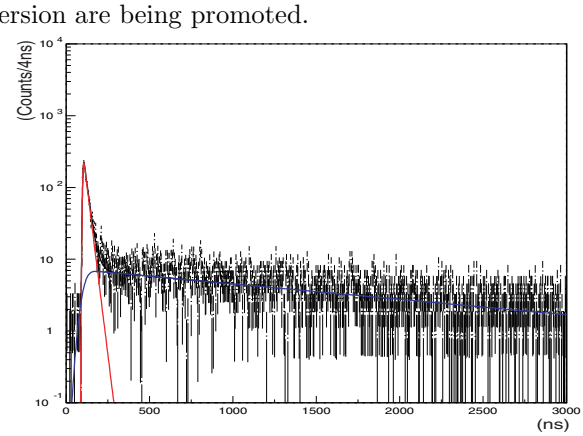

Fig. 98. Typical fitting results of time distribution of fusion neutrons with the accidental background subtracted.

Halo neutrons and the β-decay of ^{11}Li

(F. Sarazin, Colorado School of Mines/TRIUMF)

The structure of ^{11}Li, a ^{9}Li core surrounded by two distant neutrons (the so-called halo), has been the subject of intense studies. In particular, the β-decay of ^{11}Li is expected to shed light on how the weak interaction affects (and is affected by) the two neutrons composing the halo.

In August, 2002, the β-decay of ^{11}Li was investigated at TRIUMF-ISAC with the 8π spectrometer, an array of 20 Compton-suppressed germanium detectors. ^{11}Li was produced by bombarding a 22 g/cm^2 Ta foil with a 500 MeV proton beam. A pure 30.4 keV ^{11}Li beam of about a thousand ions per second was extracted by surface ionization from the target and implanted into a 0.2 mm thick Al foil at the centre of the γ-detector array. A total of 8.1 M γ singles and γ-γ coincidence events were collected over a 2.5 day period (see TRIUMF 2002 Annual Report).

Most of the β-decay strength is observed to proceed through unbound states in ^{11}Be, which subsequently decay by one-neutron emission to ^{10}Be. This results in the observation of a γ-spectrum dominated by the decay of the excited states in ^{10}Be. As shown in Fig. 99, these transitions exhibit characteristic Doppler-broadened lineshapes.

A Monte Carlo simulation has been developed to analyze the complex shape of the γ-lines observed in this experiment. The lineshape of a given γ-peak mainly depends on the energies, widths and relative intensities of all the neutron branches feeding, directly or indirectly, the state from which the transition arises, and on the lifetimes of the excited states in ^{10}Be involved before the transition occurs due to the slowing down of the recoils. The lineshape of the peaks can also

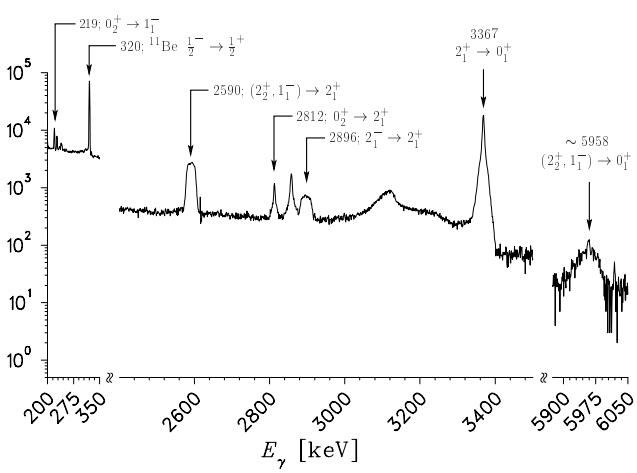

Fig. 99. Compton suppressed γ-spectrum following the β-decay of ^{11}Li. Only the relevant parts that contain the γ transitions observed in ^{10}Be and in ^{11}Be are shown (room background subtracted).

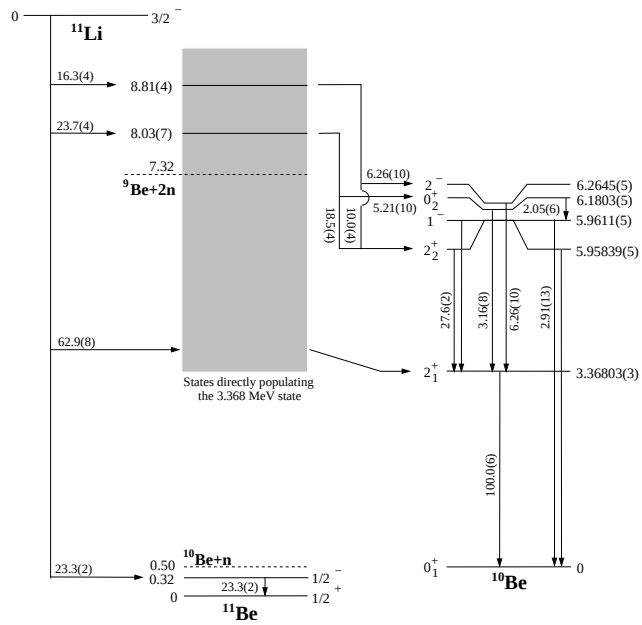

Fig. 100. Decay scheme of ^{11}Li deduced from this work. The energies of the two first excited states in ^{10}Be are the published values. All transitions are labelled with γ-ray intensities, normalized to the 3367 keV transition (100).

be affected by the angular correlation between the recoil and the γ-ray. The detailed β-decay scheme of ^{11}Li obtained from this experiment is shown in Fig. 100.

In this report, we present the conclusions of the lineshape analysis. A more detailed description of the procedure is presented in the upcoming publication [Sarazin *et al.* (submitted to Phys. Rev. C)]. The lineshape analysis of the 2896 keV transition originating from the 2^- state and of the 2812 keV transition originating from the second 0^+ state is fairly straightforward as no angular correlation between the recoil and the γ-ray is expected. This arises from the fact that the 2^- state is believed to be fed mainly by a ℓ=0 neutron, whereas the γ-ray emission from a 0^+ state is naturally isotropic. The remaining free parameters are the energy of the given transition, the energy of the neutron that gives rise to the observed Doppler broadening and the half-life of the state of origin. We find that the lineshape of the 2896 keV transition is best described by a neutron originating from the 8.81(4) MeV state in ^{11}Be and a half-life for the 2^- state of 85(6) fs, whereas the lineshape of the 2812 keV transition is best described by a neutron originating from the 8.03(7) MeV state in ^{11}Be and a half-life for the 0^+ state of 871^{+75}_{-70} fs. No need was found to add any other neutron branch to fit the experimental lineshapes of both these transitions. The analysis unambiguously confirms the existence of the 8.03 MeV state suggested once [Aoi *et al.*, Nucl. Phys. **A616**, 181c (1997)], but not confirmed. It also shows that the uncertainties in the energy determination of the states in ^{11}Be in this experiment are,

remarkably, as small as those obtained from neutron spectroscopy experiments.

The analysis of the transitions originating from the $(1^-,2_2^+)$ doublet states is more complex as it involves the indirect feeding from the 0^+ state and the feeding of the 2_2^+ state implies a ℓ=1 neutron inducing possible angular correlation effect. We find that the lineshapes of the 2590 keV and of the 5958 keV transitions are a composite of, at least, 3 different contributions. Beside the indirect contribution of the 0^+ state to the lineshape, we show that two different neutron branches, from the 8.03 MeV and the 8.81 MeV states in ^{11}Be, feeding the 2_2^+ state are required to obtain the best fit of both transitions. Although it is not possible to rule out a (small) direct neutron feeding of the 1^- state, the best fits are obtained without the need to include one. A limit on the half-life of the 2_2^+ state was determined to be $30<T_{1/2}<160$ fs. It is not possible to get a better determination with the present data because of the strong correlation between the half-life and the angular correlation parameter A_2.

The best fits for the four discussed transitions are shown in Fig. 101.

It has been suggested that if the β-decay of a halo nucleus takes place within its core, then it is possible for the halo wave function to retain its features after the β-decay, even though the core may now have a rather different structure. In this work, we show that two possible halo-like (1n) configurations in ^{10}Be, namely the 2^- and 2_2^+ excited states, are fed by the β-delayed neutron emission of ^{11}Li through the 8.81 MeV excited state in ^{11}Be. This excited state is strongly populated by 2n-transfer reaction and has been unambiguously shown recently to be the main excited state involved in the β-delayed two-neutron emission of ^{11}Li [Marques, private communication (2003)]. This strongly suggests that this state has a large overlap with a ^{9}Be+n+n configuration and that the β-decay of ^{11}Li to the 8.81 MeV state in ^{11}Be is likely to occur in the ^{9}Li core, leaving the two original halo neutrons of ^{11}Li undisturbed. The neutron emission path from this state is found to be consistent with the emission of one of the two halo neutrons, the surviving neutron giving the extended configuration suggested for the 2^- and 2_2^+ states in ^{10}Be.

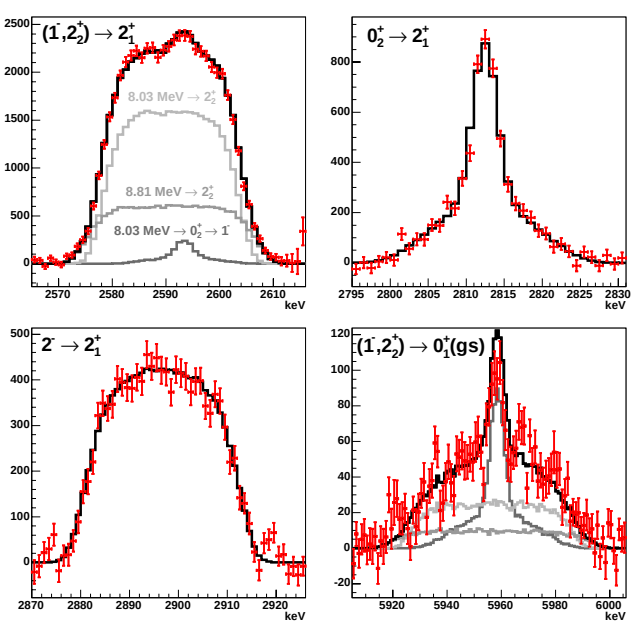

Fig. 101. Comparison between the experimental data and the best-fit obtained by the Monte Carlo simulation (black line). For the transitions involving the $(1^-,2_2^+)$ doublet, a breakdown of the 3 contributions discussed in the text is also shown.

LANSCE Experiment NPDGamma Measurement of the parity-violating gamma asymmetry A_γ in the capture of polarized cold neutrons by para-hydrogen, $\vec{n}+p\rightarrow d+\gamma$

(S.A. Page, W.D. Ramsay, Manitoba)

Introduction

In this experiment at the Los Alamos Neutron Science Center (LANSCE), a beam of polarized cold neutrons is directed on a liquid hydrogen target where neutrons are captured via the $\vec{n}p\rightarrow d\gamma$ reaction. The γ-rays produced are expected to be emitted slightly more in the direction opposite to the neutron spin. Such an asymmetry is parity violating and is a signature of the weak nuclear force. The capture reaction is dominated by the long range part of the nuclear force, and the parity violating up-down asymmetry $A_\gamma\approx -0.11 f_\pi$ provides a clean measure of the weak pion-nucleon coupling, f_π. (Some authors quote $H_\pi = f_\pi\frac{g_\pi}{\sqrt{32}}$, where g_π is the strong pion-nucleon coupling.) Despite several decades of intense experimental and theoretical effort, the strength of f_π is still a mystery. The most precise limit on f_π alone is believed to be from measurements of circularly polarized γ-rays from a parity mixed doublet in ^{18}F. These results, however, indicate a coupling constant consistent with zero, in contrast to a relatively large value implied by measurements of the anapole moment of ^{133}Cs via atomic parity violation. The np system is the only two nucleon system that is sensitive to the weak meson-nucleon coupling f_π^1 and, unlike the ^{18}F and ^{133}Cs results, can provide a clean measurement free of nuclear structure uncertainties. The best published $\vec{n}p\rightarrow d\gamma$ result, from a measurement at ILL Grenoble, is $A_\gamma=(6\pm 21)\times 10^{-8}$, which is not accurate enough to impose a significant constraint. Advances in techniques for producing high intensity beams of polarized, cold neutrons now make possible for the first time a measurement of A_γ and hence f_π^1 to within 10% of model predictions.

The $\vec{n}p \to d\gamma$ collaboration involves 13 institutions, with Canadian collaborators from the University of Manitoba, and infrastucture support from TRIUMF. The authors of this report, S.A. Page and W.D. Ramsay, have taken responsibility for precision monitoring of the neutron beam flux, and have designed a new current mode beam monitor that was tested successfully in the fall of 2001 at LANSCE. Three additional beam monitors based on this new design have now been constructed for the experiment. In 2002, we expanded our role, with vital infrastructure support from TRIUMF, to include design and construction of an integrated stand for the gamma detector array and liquid hydrogen target with remote position control for calibration of the effective detector alignment *in situ*. This procedure requires that the entire one-tonne detector array be moved accurately in the vertical and horizontal directions by up to ±5 mm. The required stand and motion control system was designed at TRIUMF, constructed at the Manitoba and TRIUMF shops, and is now undergoing final testing at Los Alamos. TRIUMF has also designed custom VME modules that permit the gain of each of 48 detector channels to be adjusted under computer control. One prototype is at Los Alamos for testing and 6 more will be fabricated at TRIUMF in 2004. We have engaged an M.Sc. student from the University of Manitoba who will do his thesis work on the commissioning run in 2003–4. A TRIUMF Co-op student has contributed to aspects of the detector package assembly, and a University of Manitoba NSERC USRA award holder worked on magnetic shielding and preparations for the new experimental cave during the summer of 2003. The Canadian group will also work on commissioning of the apparatus and diagnosis and minimization of systematic errors. The experimental cave is due to be completed in January, 2004, followed by a commissioning run early in 2004 and a first phase of data taking at LANSCE in late 2004.

Apparatus

The basic requirements of the experiment are an intense source of polarized cold neutrons, a liquid parahydrogen target, a high-efficiency, large solid angle γ-ray detector, and a means of reversing the spin of the neutron beam with minimal effect on other beam properties. At LANSCE, the neutron beam is produced by an 800 MeV proton beam pulsed at 20 Hz impinging on a tungsten spallation target; MeV neutrons emerging from the target are cooled in a liquid hydrogen moderator and transported via a supermirror guide to the experimental apparatus (Fig. 102), where they emerge with a time of flight distribution indicated in Fig. 103. The supermirror guide enhances the total neutron flux in the desired energy range (0–15 meV) by about a factor of 3 with respect to the Maxwellian distribution of neutrons emerging from the moderator. The pulsed beam enables the neutron energies to be determined from their times of flight.

Neutrons are polarized in the vertical direction by selective transmission through a polarized ^{3}He gas cell which acts as a spin filter, producing the energy dependent polarization spectrum indicated in Fig. 103 (top). The neutron beam intensity is measured with a current mode ^{3}He ionization chamber (Fig. 103, bottom) mounted on the end of the neutron guide. The transmission of the ^{3}He polarizer cell is measured with a similar device mounted immediately downstream, to provide an on-line measurement of its polarization and hence that of the neutron beam. A resonant rf spin flipper reverses the neutron spin every beam pulse according to a $+--+-++-$ reversal pattern, cancelling

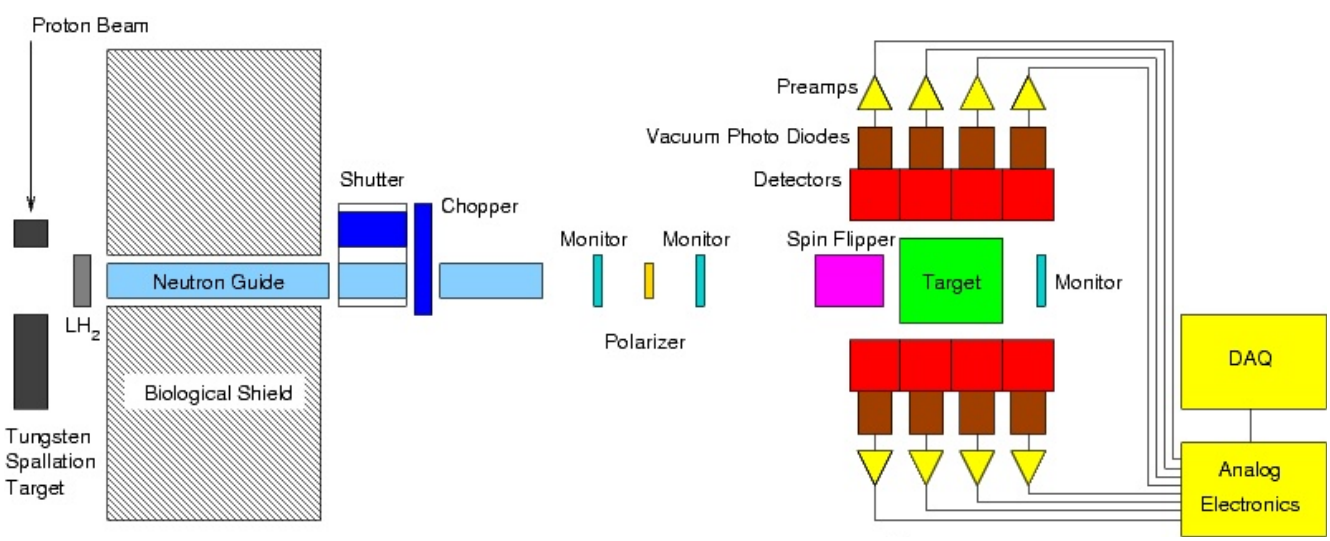

Fig. 102. $np \to d\gamma$ experimental apparatus at LANSCE.

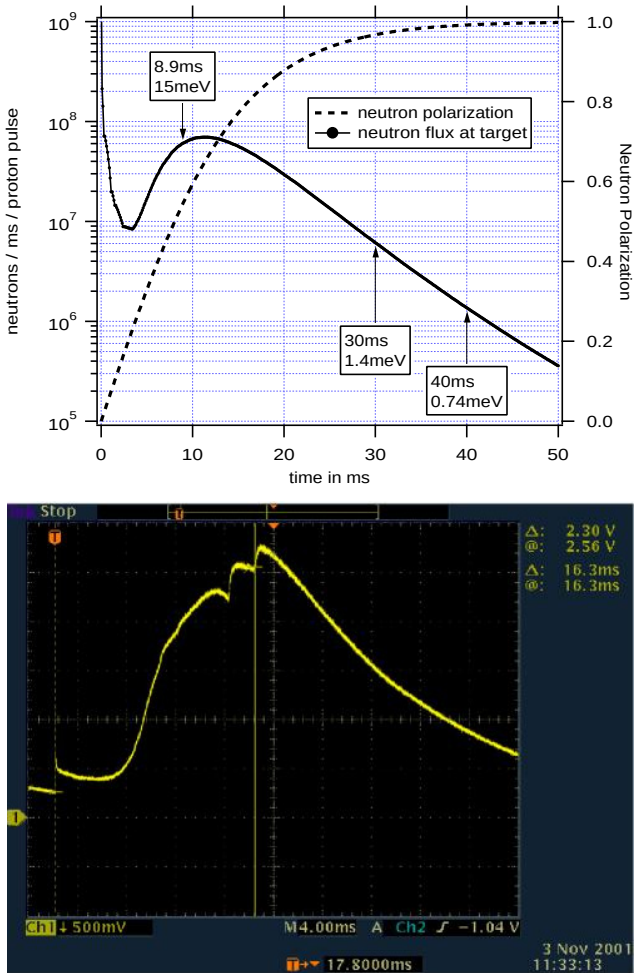

Fig. 103. Top: Predicted cold neutron beam flux and polarization. Bottom: neutron time-of-flight distribution measured by a dc coupled ^{3}He ionization monitor (frame overlap, the 1/v dependence of the capture cross section, and Bragg edges of Al beam windows account for the difference between top and bottom figures).

systematic drifts to second order. A uniform vertical guide field, $B_\circ = 10$ G, preserves the neutron beam polarization as it is transported to the liquid hydrogen target; field uniformity at or below the 1 mG/cm level is essential for optimum performance of the ^{3}He polarizer cell, the rf spin flipper, and to avoid systematic errors due to the Stern-Gerlach effect.

It is important that the ortho-hydrogen fraction in the target be kept low ($\sim$0.05%). Low energy neutrons depolarize rapidly in ortho-hydrogen, while those below 15 meV retain their polarization in a para-hydrogen target. To monitor the ortho-hydrogen content, a third beam monitor positioned downstream of the target will provide on-line monitoring of the target transmission and hence a measure of the ortho:para ratio, since the neutron cross sections for the two species are markedly different.

The 2.2 MeV γ-rays from neutron capture in the target are detected with an array of 48, (15 cm)^3 CsI(Tl) crystals read out in current mode by vacuum photodiodes coupled via low noise I-V preamplifiers to transient digitizers. The time-of-flight information from the CsI detectors allows the γ-ray asymmetry A_γ to be deduced as a function of incident neutron energy; A_γ should be constant, but the experimental asymmetry $\varepsilon = P_n A_\gamma$ will reflect the energy dependence of the beam polarization from Fig. 103. A beam chopper eliminates frame overlap and provides for a beam-off background measurement at the end of each pulse, allowing us to measure the contribution of γ-ray asymmetries from beta decays of polarized nuclei produced by interactions of the beam with materials upstream of the hydrogen target. The expected NPDGamma asymmetry is $A_\gamma = -5 \times 10^{-8}$ based on the best available theoretical predictions, and we ultimately aim to measure A_γ to $\pm 1 \times 10^{-8}$ or better with systematic errors less than 5×10^{-10}.

Experimental errors

The statistical uncertainty in the measurement of A_γ is ultimately determined by counting statistics, set by the beam intensity, the detector solid angle, and the counting time. The γ-ray detectors and low noise preamplifiers have been designed to ensure that sources of instrumental noise are small compared to this limit. An exhaustive Monte Carlo study of systematic errors has been ongoing since the preparation of a major DOE proposal for the experiment in 1998. Care has been taken to identify all possible sources of error, to minimize the sensitivity of the apparatus, and to work out a program of ancillary measurements to quantify individual error sources. The conclusion of these studies is that it should be possible, with sufficient beam flux, to measure A_γ to $\pm 0.5 \times 10^{-8}$ with systematic errors no larger than 10% of the statistical error quoted above.

Systematic errors arising from interactions of the neutron spin are potentially the most serious for the experiment, including a number of reactions that take place in the hydrogen target in parallel with the $np \rightarrow d\gamma$ reaction. One particular class of systematic errors can arise from admixtures of small parity allowed left-right scattering asymmetries into the up-down angular distribution via a misalignment of the detector symmetry axis with respect to the neutron spin direction. To keep these false asymmetry contributions at or below the 5 $\times 10^{-10}$ level, we require a means of determining the detector alignment with respect to the neutron spin direction to 20 mr or better. This will be accomplished by scanning the detector array in x and y by a few mm with the target in place and measuring the effective γ yield in each detector as a function of the array position. As mentioned in the introduction, the motion control system to accomplish this was designed

at TRIUMF and built in the Manitoba and TRIUMF shops.

Current status and future outlook

Since the NPDGamma proposal was written and the apparatus funded by the DOE and NSF commencing in 1999, the upgraded spallation neutron facility at LANSCE has been brought on line, and a new neutron guide has been constructed for the experiment. Unfortunately, the present schedule is about a year and a half delayed, due in large part to a conflict that arose when the facility installed a large, unshielded, superconducting magnet on a neighbouring beam line that imposed enormous technical challenges in the design of magnetic shielding for our experiment. This issue is being addressed with the support of LANL management, but a technical solution has not yet been found that would allow both beam lines to run concurrently.

In the course of developing the experiment, the collaboration has dedicated several test runs to characterizing the apparatus and the neutron flux at LANSCE. In the 2000 test run [Mitchell *et al.*, Nucl. Instrum. Methods A (in press) nucl-ex/040109], we mounted a 10% model of the full apparatus, and measured parity violating (PV) asymmetries with Cl, La and Cd targets. We demonstrated that the model apparatus reached the error limit imposed by neutron counting statistics (Fig. 104). In the 2002 test run [Seo *et al.*, Nucl. Instrum. Methods (in press)], we measured the brightness of the new flight path 12 moderator and confirmed that the first 12 m of the new neutron guide performed according to design.

We have determined that the physics asymmetry A_γ can be measured at LANSCE with the full NPDGamma apparatus to $\pm 4 \times 10^{-4}$ per pulse with 120 μA proton beam on the spallation target. Our test measurements have shown that expectations of the available neutron flux from the upgraded LANSCE facility (as advertised prior to the upgrade) were too optimistic by almost a factor of 4, with roughly equal contributions from reduced moderator brightness and reduced production beam current. An additional factor of 2 in running time for NPDGamma has effectively been lost due to the magnetic interference problem noted above.

In this context, the collaboration has carefully considered its options for commissioning and running the experiment at LANSCE in the near term. The experimental cave is scheduled to become available at the end of January, 2004. We will install and commission all elements of the apparatus (Fig. 105) with the exception of the target during the period January–March, 2004, when we anticipate approximately 8 weeks of beam to be available for the experiment. Once commissioned, the apparatus will be used to measure parity-violating asymmetries from cryostat materials and calibration targets, which are needed to understand backgrounds and possible systematic errors in the NPDGamma measurements. The liquid hydrogen target will be installed during the 2004 shutdown beginning in March.

We plan for a 1000 hour data run in calendar year 2004–05, which would result in a statistics-limited measurement of A_γ to $\pm 5 \times 10^{-8}$, or $\pm 100\%$ of the theoretical prediction based on the value of f_π as estimated by DDH. This measurement would be a factor of 4 better than the previous best published result $A_\gamma = (6 \pm 21) \times 10^{-8}$. While this would be a significant achievement, it falls short of our goals of either measuring or setting a meaningful upper limit on the weak-pion nucleon coupling that is currently known to be less than 30% of the best existing theoretical estimates. The compelling

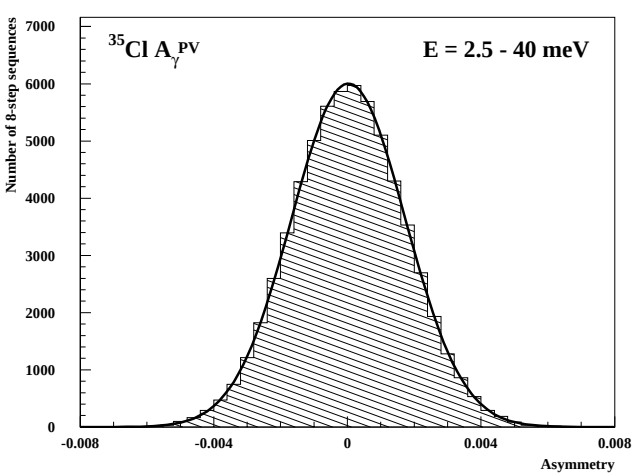

Fig. 104. Histogram of asymmetry values ($A_\gamma = (-29.1 \pm 6.7) \times 10^{-6}$) from test run on Cl [Mitchell *et al., op. cit.*] used to validate our model of statistical errors for the full experiment.

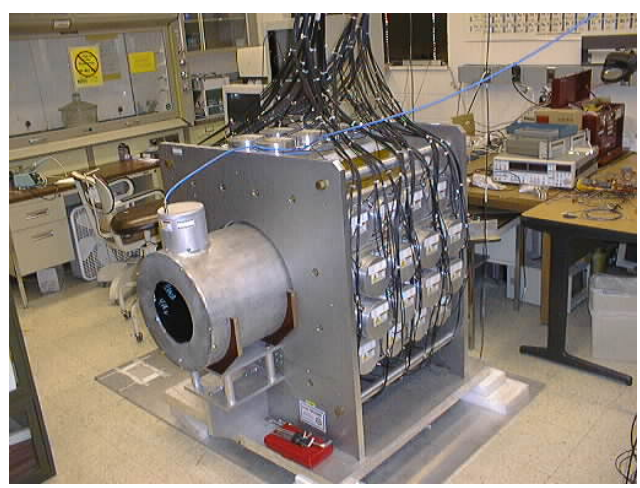

Fig. 105. Complete CsI detector array and spin flipper at Los Alamos mounted in the upper half of the detector position control stand designed by TRIUMF and built by the Canadian group.

physics case for a precise NPDGamma result merited recognition in the 2002 NSAC Long Range Plan for Nuclear Science (US), and the scientific priority of fundamental physics studies with cold neutrons has been confirmed with the approval of a new dedicated beam line for this work at the Spallation Neutron Source (SNS), currently under construction.

While the collaboration intends to pursue related measurements in the future at the SNS, we strongly prefer to complete the NPDGamma precision measurements on a much earlier timescale. We have informed the DOE of our desire to move the experiment to a new beam line at the Oak Ridge facility, HFIR, to pursue a much higher-statistics measurement than is currently possible at LANSCE. Conservative estimates indicate that HFIR could provide an order of magnitude higher neutron flux in the energy range of interest, and in addition the available running time per calendar year would be higher by a factor of 2–5. The new "CG"4 beam line suitable for NPDGamma could be ready as early as mid-2005, and only a modest capital investment would be required to adapt the experiment to the new facility.

Collaborators (spokesman is underlined): C.S. Blessinger, M. Gericke, G. Hansen, M.B. Leuschner, G.L. Morgan, H. Nann, W.M. Snow (Indiana University); J.D. Bowman, G.E. Hogan, J.N. Knudson, S.K. Lamoreaux, G.S. Mitchell, C.L. Morris, S.I. Penttila, W.S. Wilburn, V.W. Yuan (Los Alamos National Laboratory); R.D. Carlini (Thomas Jefferson National Accelerator Facility); T.E. Chupp, K.P. Coulter, R.C. Welsh, J. Zerger (University of Michigan); M.S. Dewey, T.R. Gentile, D.R. Rich, F.E. Wietfeldt (National Institute of Standards and Technology); T. Case, S.J. Freedman, B. Lauss (University of California, Berkeley); S. Ishimoto, Y. Masuda, K. Morimoto (KEK National Laboratory, Japan); G.L. Jones (Hamilton College); F.W. Hersman, V.R. Pomeroy (University of New Hampshire); R.C. Gillis, S.A. Page, W.D. Ramsay (University of Manitoba); E.I. Sharapov (Joint Institute for Nuclear Research, Dubna); T.B. Smith (University of Dayton); D. Desai, G.L. Greene (University of Tennessee).